

**MINERALIZATION FOR CO₂ SEQUESTRATION USING OLIVINE
SORBENT IN THE PRESENCE OF WATER VAPOR**

A Dissertation
Presented to
The Academic Faculty

by

Soonchul Kwon

In Partial Fulfillment
of the Requirements for the Degree
Doctor of Philosophy in Environmental Engineering
School of Civil and Environmental Engineering

Georgia Institute of Technology

May 2011

COPYRIGHT © 2011 BY Soonchul Kwon

**MINERALIZATION FOR CO₂ SEQUESTRATION USING OLIVINE
SORBENT IN THE PRESENCE OF WATER VAPOR**

Approved by:

Dr. Armistead G. Russell, CO-Advisor
School of Civil and Environmental
Engineering
Georgia Institute of Technology

Dr. Maohong Fan, CO-Advisor
School of Civil and Environmental
Engineering
Georgia Institute of Technology

Dr. James A. Mulholland
School of Civil and Environmental
Engineering
Georgia Institute of Technology

Dr. Costas Tsouris
School of Civil and Environmental
Engineering
Georgia Institute of Technology

Dr. Greg Huey
School of Earth and Atmospheric
Sciences
Georgia Institute of Technology

Date Approved: January 07, 2011

To my wife, sons, and family

ACKNOWLEDGEMENTS

I would like to thank the many people who have provided their enormous support during my studies at Georgia Institute of Technology. I sincerely appreciate the guidance of my advisors, Professors Armistead (Ted) Russell and Maohong Fan. Their mentorships has created and maintained an atmosphere that provided not only enormous research opportunities with insightful guidance and knowledge about CO₂ capture and storage, but also a great personal interaction, and I am honored to have been a part of the research group. The author is really grateful for the suggestions and the advice of the committee members—Dr. James Mulholland, Dr. Costas Tsouris, and Dr. Greg Huey—for their time and input. Outside of Atlanta, I would like extend my gratitude to Dr. Herbert DaCosta of Caterpillar’s Product Development Center of Excellence who supported and helped me start in this field. I would like to give special appreciation to Dr. Seung Soon Jang for helping me conduct the quantum study associated with the CO₂ sorption technology. I would also appreciate the helps of people in the Laboratory for Atmospheric Modeling, Diagnostics and Analysis (LAMDA) at Georgia Tech for their many helps. I have had the pleasure of working with other LAMDA members, including my officemates Jorge and Siv, and also Dr. Sangil Lee, Dr. Jaemeen Baek, Dr. Burcak Kaynak, Dr. K.J. Liao, Gretchen, and so many others. I appreciate all the Korean students at our school for their interactions, helps and, friendships. Moreover, I also appreciate the faculty and staff of the School of Civil and Environmental Engineering at Georgia Tech. Foremost, I would be lost without the support and encouragement of my family, and the unbelievable patience and love of my wife Myunghwa Jung for making me capable enough to accomplish this study.

TABLE OF CONTENTS

ACKNOWLEDGEMENTS	IV
LIST OF TABLES	VIII
LIST OF FIGURES	IX
SUMMARY	XII
CHAPTER 1. INTRODUCTION	1
1.1 Statement of Problems	1
1.2 Structure and Scope of the Thesis.....	6
CHAPTER 2. CO₂ ADSORPTION: A REVIEW	8
2.1 Carbon Dioxide.....	8
2.2 An overview of CO ₂ Capture and Storage (CCS).....	9
2.2.1 CO ₂ separation	9
2.2.2 CO ₂ capture technologies.....	14
2.2.3 CO ₂ transportation	17
2.2.4 CO ₂ sequestration (storage)	18
2.3 CO ₂ Adsorption.....	21
2.3.1 Sorption based CO ₂ separation processes	22
1) Physical adsorption	25
2) Chemical adsorption	30
2.3.2 Adsorption for CO ₂ capture	31
1) Zeolites.....	33
2) Activated carbon	46
3) Amines	51
4) Organic/Inorganic Hybrid Materials.....	57
5) Lithium zirconate	63

6)	Sodium based sorbent	67
7)	Hydrotalcite-like compounds (HTlcs)	70
2.4	CO ₂ Sequestration by Mineral Carbonation	73
2.4.1	Overview of mineral carbonation	73
2.4.2	Mineral carbonation: A DFT quantum study	75
2.4.3	Kinetics of surface Mg ₂ SiO ₄ carbonation	76
2.4.4	Mineral selection	80
2.4.5	Mineral availability in the United States	82
2.4.6	The Process of mineral carbonation	84
1)	Pre-treatments	85
2)	Carbonation processes	86
3)	Final products	89
2.5	The Cost of CO ₂ Capture and Storage	90
2.5.1	General cost of CCS	90
2.5.2	Mineral carbonation: energy penalties and costs	93
2.6	Summary of CO ₂ Adsorption and Capture Development Strategies	95
CHAPTER 3. REACTION KINETICS OF MG₂SIO₄ BASED CO₂ SORPTION		97
3.1	Introduction	98
3.2	Experimental methods	100
3.2.1	Materials	100
3.2.2	Experimental apparatus	101
3.2.3	Operating procedures	103
3.3	Results and discussion	104
3.3.1	Determination of the temperature range for kinetic study	104
3.3.2	Multiple carbonation– regeneration cycles	107
3.3.3	Sorption kinetics	108
CHAPTER 4. MINERAL CARBONATION USING NATURAL OLIVINE SORBENT		
IN THE PRESENCE OF WATER VAPOR		115
4.1	Introduction	116
4.2	Experimental section	118
4.2.1	Materials	118
4.2.2	Experimental apparatus	119
4.2.3	Operation procedure	120

4.3	Results and discussion	121
4.3.1	Characterization of olivine materials	121
4.3.2	Thermodynamics of olivine carbonation	125
4.3.3	Effect of the temperature on CO ₂ separation	129
4.3.4	Regeneration of spent sorbent.....	134
4.3.5	Effect of residence time	135
4.3.6	Effect of initial concentration	137
4.3.7	Water sensitivity	138
4.3.8	Effect of SO ₂ and NO	140
4.4	Conclusion	141
 CHAPTER 5. DENSITY FUNCTIONAL THEORY (DFT) STUDY OF CO₂		
ADSORPTION ON THE CALCIUM OXIDE (100) SURFACE		143
5.1	Introduction.....	144
5.2	Computation details	147
5.3	Results and discussion	149
5.3.1	Single CO ₂ adsorption on CaO	149
1)	Adsorption Energy and Geometry	149
2)	Charge Reorganization.....	153
3)	Effect of Surface Coverage	154
5.3.2	Multiple CO ₂ adsorption on CaO.....	155
1)	Formation of Monolayer	155
2)	Charge Reorganization.....	158
3)	Formation of Multilayer.....	160
5.4	Conclusion	162
 CHAPTER 6. SUMMARY AND FUTURE STUDIES		163
6.1	Summary of this study	163
6.2	Recommendations for Future Study	167
6.2.1	The investigation of molecular CO ₂ adsorption on the Mg-based silicate mineral surface	167
6.2.2	The process development of the large scale reactor for mineralization.....	168
 VITA.....		181

LIST OF TABLES

TABLE 1. Physical properties of different solid sorbents	32
TABLE 2. CO ₂ capture capacities of different solid sorbents	33
TABLE 3. Langmuir Isotherm Parameters for CO ₂ and N ₂	37
TABLE 4. Capacity cost and capital cost of CO ₂ capture with zeolite 13X	43
TABLE 5. Typical values of forward rate constant for CO ₂ -amine reactions	54
TABLE 6. CO ₂ adsorption capacities on Mg-Al-CO ₃ Layered double oxide (LDO) dependent on temperatures at 100kPa	73
TABLE 7. Adsorption properties of single molecular CO ₂ on the (2×2) MgO (100) surface	76
TABLE 8. The milling parameters and physicochemical properties of olivine samples	78
TABLE 9. BET analyses of CaO/Al ₂ CO ₃ sorbent before carbonation and after 20 cyclic carbonations	80
TABLE 10. Annual CO ₂ emissions and minimum mineral requirement with region	83
TABLE 11. Estimated costs of CO ₂ capture, transport, and geological storage.	91
TABLE 12. Energy losses for mineral carbonation process	93
TABLE 13. The required quantities of minerals for CO ₂ sequestration.....	94
TABLE 14. Reaction order and activation energy of the carbonation in the presence of steam as a function of different flow rates. Uncertainty results from 5 time multiple tests.	114
TABLE 15. The chemical composition of the olivine sample.....	122
TABLE 16. The capture capacities of mineral carbonation as a function of the initial CO ₂ concentration.....	138
TABLE 17. Olivine carbonation processes for CO ₂ sequestration as a function of water vapor concentration.....	139
TABLE 18. Effect of SO ₂ concentration for olivine carbonation processes	141
TABLE 19. Effect of NO concentration for olivine carbonation processes	141
TABLE 20. The geometry and energy of the single CO ₂ adsorption on CaO (100) surface	150
TABLE 21. Adsorption energy (E _a) of CO ₂ on CaO (100) surface.....	155

LIST OF FIGURES

Figure 1. Anthropogenic emission sources of greenhouse gases worldwide in 2006.	2
Figure 2. Worldwide carbon dioxide emissions from fossil fuel combustion as a function of usage sectors and fuel type in 2007	3
Figure 3. Schematic diagram of general carbon capture and storage	9
Figure 4. Schematic diagram of a pre-combustion plant (IGCC power plant).....	11
Figure 5. Schematic diagram of a post combustion plant (conventional power plant).....	12
Figure 6. Schematic diagram of an oxy-fuel power plant.....	13
Figure 7. Schematic diagram of the CO ₂ capture plant (adsorption process) for post combustion and the actual picture of the pilot plant in Japan	22
Figure 8. Schematic diagram of Pressure Swing Adsorption system.	25
Figure 9. Operation steps of Pressure and Vacuum Swing Adsorption system.....	26
Figure 10. Vacuum Swing Adsorption (VSA) system.....	29
Figure 11. Temperature Swing Adsorption (TSA) System.	30
Figure 12. Evaluation of zeolite 13X on the basis of isotherm, purity and recovery.	35
Figure 13. The adsorption equilibrium and kinetic separation factor for a TSA process with zeolite β	39
Figure 14. Vacuum Swing Adsorption for CO ₂ +air, H ₂ O + air and CO ₂ / H ₂ O + air in zeolite 13X at 30°C.	41
Figure 15. CO ₂ Vacuum Swing Adsorption (VSA) on zeolite 13X	44
Figure 16. Evaluation of activated carbon on the basis of isotherm, purity and recovery.....	47
Figure 17. Equilibrium isotherms of a double layer PSA system for multi-gas components. 49	49
Figure 18. The effect of layer length on a double layer PSA system for multi-gas components	51
Figure 19. Breakthrough profiles of carbon dioxide on amine modified SBA-15	56
Figure 20. Schematic structure of various amines modified SBA-15.	58
Figure 21. Different crystal structures of MOFs at room temperature. For each MOF, the framework formula, pore size, surface area are shown.	61
Figure 22. Comparison of GCMC simulations and experimental adsorption isotherms for CO ₂ in IRMOF-1.....	62
Figure 23. Schematic diagram of the proposed mechanism for CO ₂ adsorption on Li ₂ ZrO ₃ . 64	64
Figure 24. Schematic diagram of the proposed mechanism for CO ₂ desorption on Li ₂ ZrO ₃ . 66	66
Figure 25. The Temperature Swing Adsorption System on sodium-based solid sorbent.....	68
Figure 26. Carbon dioxide adsorption on Hydrotalcite-like compounds (HTlcs).	71
Figure 27. Adsorption and desorption on nano CaO/Al ₂ CO ₃ sorbent.	79
Figure 28. Bulk size of olivine and serpentine mineral.	81
Figure 29. Ultramafic mineral carbonation regions	82
Figure 30. Mineral quarry in Pittsburgh, PA	83
Figure 31. Schematic diagram of carbonation for CO ₂ sequestration	84
Figure 32. Process flow diagram of the direct carbonation using magnesium-based minerals	86
Figure 33. Process diagram of the indirect carbonation using serpentine.	88
Figure 34. Olivine deposit for mine reclamation in Twin Sisters, WA	90

Figure 35. Cost of electricity generation (2007 US\$/Mwh) as a function of the CO ₂ emission rate (t CO ₂ /Mwh) for new power plants burning bituminous coal or natural gas.	91
Figure 36. Schematic diagram of experimental apparatus for CO ₂ adsorption.....	101
Figure 37. Picture of experimental set-up.....	101
Figure 38. Picture of olivine adsorbent inside quartz wool tube.	102
Figure 39. XRD patterns of the Mg ₂ SiO ₄ carbonation products.....	104
Figure 40. Total and 90 % breakthrough CO ₂ capture capacities as a function of temperature.	106
Figure 41. Cyclic CO ₂ adsorption processes at different temperatures.	107
Figure 42. CO ₂ carbonation and regeneration profiles in the presence of steam as a function of temperature.	109
Figure 43. Determination of the reaction order at 200°C for Mg ₂ SiO ₄ carbonation with CO ₂ in the presence of steam.....	110
Figure 44. Determination of the apparent activation energy, E_a for Mg ₂ SiO ₄ carbonation with CO ₂ in the presence of steam.....	113
Figure 45. Pore size distribution for olivine after carbonation/regeneration.	121
Figure 46. SEM images of (a) Fresh olivine sample, (b) After olivine carbonation in the absence of water vapor at 200°C, (c) After olivine carbonation without the presence of water vapor at 200°C, and (d) EDS spectra of the fresh olivine sample.	123
Figure 47. XRD patterns of the fresh (a) and (b) carbonated product samples with 10% vol CO ₂ , ~8.3% vol H ₂ O at 200°C.....	124
Figure 48. Thermodynamic properties of olivine carbonation reaction. (a) Enthalpy change, (b) Entropy, and (c) Gibbs free energy change	126
Figure 49. Gibbs free energy change as a function of extent of carbonation at T=473 K (a); Carbonation pressure of Mg ₂ SiO ₄ -MgCO ₃ -CO ₂ equilibrium (b).	128
Figure 50. CO ₂ carbonation and regeneration profile with water vapor (a) and without water vapor (b) as a function of temperature.....	130
Figure 51. CO ₂ capture capacities without and with water vapor dependent on the temperature.	132
Figure 52. Cyclic CO ₂ adsorption and desorption processes in the different temperatures .	134
Figure 53. CO ₂ capture capacities as a function of residence time.....	136
Figure 54. Structure of CaO crystal: (a) unit cell; (b) (100) unit surface; (c) (100) 2×2 surface. The green ball and the red ball denote calcium and oxygen, respectively.	146
Figure 55. Coverage (θ) as a function of CO ₂ adsorption energy.....	148
Figure 56. Geometries of the single CO ₂ molecule on the (2×2) CaO (100) surface: (a) before geometry optimization; (b) after geometry optimization.....	151
Figure 57. Charge reorganization of (a) the CaO (100) surface and (b) the CO ₂ molecule..	152
Figure 58. Change of CO ₂ adsorption energy as a function of surface coverage (θ).	154
Figure 59. Optimized geometries of (a) single CO ₂ molecule and (b) a pair of CO ₂ molecules on the (1×1) CaO (100) surface.	156
Figure 60. Optimized geometry of the eight CO ₂ molecules on the (2×2) CaO (100) surface: (a) non-uniform adsorption; (b) uniform adsorption.	157
Figure 61. Charge reorganization of (a) the CaO (100) surface and (b) four CO ₂ molecules.	159

Figure 62. Optimized geometries of the multilayer CO₂ adsorption on the (2×2) CaO (100) surface: (a) bilayer; (b) trilayer. Note that the numbers at oxygen atoms of CO₂ molecules are the atomic charges (unit: e)..... 161

SUMMARY

Mineralization has the potential to capture CO₂. In nature, mineralization is the chemical weathering of alkaline-earth minerals in which stable carbonate minerals are formed, which leads to the removal of CO₂ from the atmosphere. The adsorptive carbonation reaction of olivine [(Mg,Fe)₂SiO₄], consisting mainly of pure magnesium silicate (Mg₂SiO₄), a main constituent of the Earth's crust, was carried out to estimate its potential application in the separation of CO₂ with the presence of water vapor in combustion plumes.

This thesis first presents a review of the literature pertaining to various CO₂ capture technologies and the evaluation of their performance. The review mainly describes the application of CO₂ adsorption on various solid sorbents that capture CO₂, including mineral carbonation. In addition, it includes the selection of minerals and the mineralization processes. Following the review, this thesis presents an experimental set-up and analyses in this study. It also describes the experimental apparatus and procedures used to acquire information about CO₂ capture capacities.

Experiments were mainly performed on pure Mg₂SiO₄ carbonation to determine the reaction properties, temperature effects, and cyclic adsorption, and to evaluate a reaction kinetics model. Based on the changes in the CO₂ concentration with sorption time, a kinetic model of the reaction between Mg₂SiO₄ and CO₂ was developed. The reaction order with respect to CO₂ was approximately 1. Based on the changes in the reaction rates with temperature in the range of 150°C to 200°C, the activation energy derived for the Arrhenius equation of Mg₂SiO₄-based carbonation process is 76.2 ± 4.8 kJ/mol.

To evaluate the application of natural olivine for CO₂ sequestration, experiments were conducted on natural olivine mineralization in the presence/absence of water vapor

under various conditions of temperature, concentration, and space time. Based on calculations, the olivine carbonation reaction is thermodynamically favorable. Water vapor was found to play an important role in accelerating the carbonation rate, and experimental results revealed that carbon dioxide can combine with olivine minerals to form highly stable surface carbonates.

To investigate the molecular reaction mechanism and adsorption configuration of CO₂ adsorption on the metal oxide surface, we performed a quantum chemistry calculation of multiple CO₂ adsorption on a CaO (100) surface due to higher reactivity for CO₂ adsorption than MgO. In the formation of a monolayer, CO₂ molecules were chemi-sorbed due to the charge reorganization between the CaO surface and CO₂ molecules. The adsorbed CO₂ molecules got together rather than distributing uniformly over the CaO surface. The second layer adsorption can take place at ambient condition and characterized as the physi-sorption.

Consequently, this study helps lay the groundwork for the chemical mechanism of mineral carbonation of olivine with carbon dioxide in the presence of water vapor and provides the relevant information for the real application of the olivine based CO₂ separation.

CHAPTER 1 INTRODUCTION

1.1 Statement of Problems

In the coming decades, it is expected that the energy demand and consumption of energy increase. The growing demand is expected to lead to a need for an increased use of various fossil fuels by an average of 1.7% per year until 2030. Average annual growth in consumption is estimated to be 1.4% for coal, 1.6% for oil, and 2.4% for natural gas [1]. These anthropogenic activities are expected to raise greenhouse gas emissions more than 70% between 2000 and 2030, amounting to 38 billion tons of energy-related carbon dioxide (CO₂) emissions worldwide in 2030, resulting in global climate change [1]. About 40% of the total CO₂ emissions are currently released due to the generation of electricity from sources employing fossil fuel energy, with an additional fraction coming from other industrial uses. Therefore, a reduction in CO₂ emissions from the energy and/or process industry is a primary environmental goal.

CO₂ is naturally released from the respiration of animals, plants, and microorganisms, and is released by volcanic eruptions and hot springs [2]. However, human activities, primarily the combustion of fossil fuels that account for more than 80% of worldwide energy consumption, contribute to the growth in global CO₂ emissions. The generation of electricity is the largest source of total CO₂ emissions, accounting for about 41% of the total (Figures 1 and 2). The total annual amount of worldwide anthropogenic carbon emissions is 7.6 G tons, with 5.4 G tons of the total being released due to fuel combustion [2]. About 60% of the emitted carbon remains in the atmosphere while the remaining 40% ends up in oceans and forests, and on rocks [2]. CO₂ emissions have been increasing at a rate of about 3.3% per year

since 2000 (in the 1990s, 1.3% per year) and is ascribed to human activities [3]. Since carbon dioxide is considered the most significant component of greenhouse gas emissions, the reduction of CO₂ has been the focus of the efforts to mitigate climate change [4].

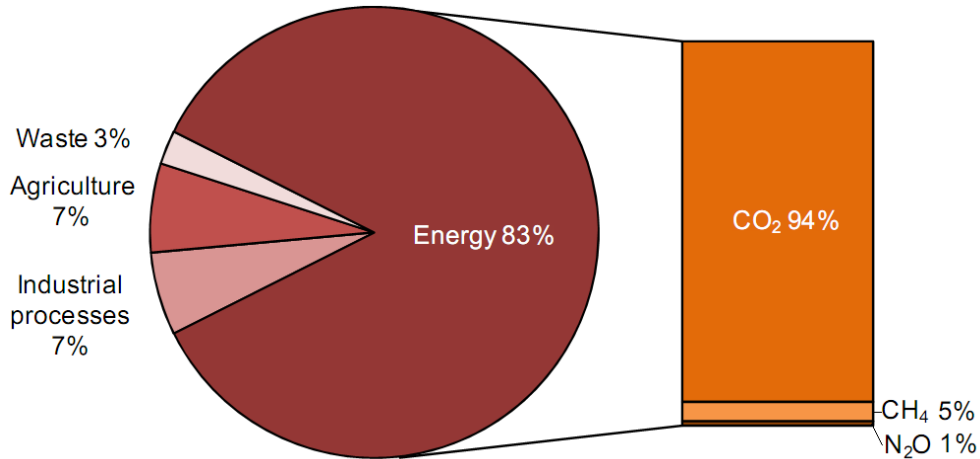


Figure1. Anthropogenic emission sources of greenhouse gases worldwide in 2006 [5, 6].

For power plants, fossil fuels are still the major energy sources, and currently affordable and available amounts of fossil fuels are large enough to meet the world's current demands. In a fossil-fuel-fired power plant, which is generally considered a point emission source, typical power plant flue gases contain 8-12% CO₂, 8-10% water vapor, and smaller concentrations of other pollutant species such as SO_x and NO_x balanced with about 90% N₂ [7, 8]; thus, the separation of CO₂ from the captured flue gas is essential to avoid having to deal with a large amount of N₂ and to attain a high purity CO₂ which could be used in other applications such as oil recovery.

CO₂ separation and sequestration from flue gases of power plants can play a very important role in reducing global CO₂ emissions. To reduce CO₂ emissions, three technical options are available as follows: (1) decreasing energy consumption and increasing the

efficiency of energy usage, (2) developing renewable energy sources and non-fossil fuels such as hydrogen, and (3) developing capture and sequestration technologies to separate and sequester CO₂. Of the general options for power production, carbon capture and sequestration (CCS) has the potential to contribute to the reduction of global emissions sooner and faster than the development of renewable energy sources in order to prevent CO₂ emission into the atmosphere [3]. CCS involves capturing and separating carbon dioxide in flue gases, transporting (e.g., piping and shipping), and storing the separated CO₂ into geological reservoirs.

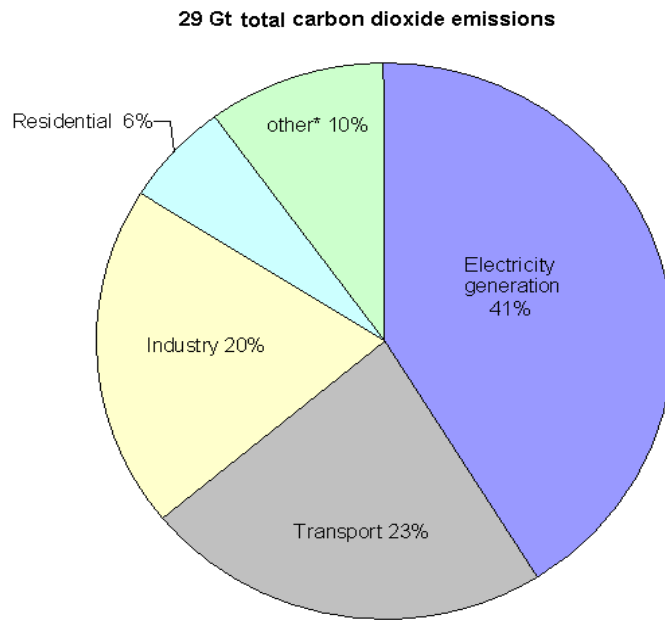


Figure 2. Worldwide carbon dioxide emissions from fossil fuel combustion as a function of usage sectors and fuel type in 2007 [2, 6].*Other contains commercial/public services and agriculture/forestry.

CCS has already been used by the oil and gas industry. For example, in the United States, the enhanced oil recovery industry captures about 8.5MtC [9]. However, the major concern with the use of separation methods for CCS at very large scales are the increased energy consumption and costs resulting from the separation process (e.g., absorption and adsorption) to initiate CO₂ desorption. Furthermore, the low separation efficiency of current CCS methods necessitates alternative or improved CO₂ separation methods that have lower energy demands, higher CO₂ capture capacity, and higher regeneration capacity [9]. CO₂ capture capacity is defined as the amount of CO₂ captured per unit mass of adsorbent used (e.g., g CO₂/g sorbent) and regeneration capacity denotes how much capture capacity is recovered after multi-cycle sorption.

Among the various separation processes, adsorption is a potential method of CO₂ separation due to its simple operation and low cost [3, 10-12]. For an adsorption processes to be effective, adsorbents should have the following characteristics: (1) high selectivity and adsorption capacity for CO₂, (2) fast adsorption and desorption rates, (3) high stability to be cycled multiple times, (4) low attrition rate, (5) low energy requirements for the regeneration of CO₂ after adsorption, and (6) scalability to megaton/year CO₂ capture rates. In addition, for practical power plant applications, a rapid adsorption rate of CO₂ is highly desirable along with high adsorption efficiencies during the multi-cycle adsorption/desorption process, leading to the use of less adsorbent material, and fewer required control devices.

The adsorption capabilities of sorbents depend on various physical and chemical properties of the flue gas and sorbent, including the CO₂ concentration, temperature, pressure, affinity of sorbent to CO₂, surface area, pore size, and structure of sorbents. Because of this, the improvement of processes and adsorbents requires a process level understanding of

dependence on these variables [13-15]. In addition, many sorbents are not effective for capturing CO₂ in the presence of water vapor, making them less attractive for use in such applications. Thus, there is also a need for materials with enhanced CO₂ sorption capacities in the presence of gas streams containing water vapor, which would make them useful in real-world applications such as in coal-fired power plants.

Of the CO₂ sorption methods, adsorption on minerals (mineralization) has become a promising technology for CO₂ sequestration because minerals can react with CO₂ and form stable carbonates, leading to permanent CO₂ sequestration. This mineral carbonation is essentially the process of chemical weathering by alkaline earth minerals. In order to apply such mineral carbonation to CO₂ capture, we identify potentially attractive reaction approaches and evaluate the associated reaction rates.

In this study, we chose olivine ((Mg, Fe)₂SiO₄) for carbonation in the presence of water vapor because olivine is one of the most abundant natural minerals and water vapor contained in a flue gas mixture can accelerate the carbonation rate [16, 17]. In addition, it produces environmentally-friendly stable carbonates for mine reclamation or soil amendments [18]. The reaction of olivine with CO₂ in the presence of water vapor is shown in Eq. 1:



In spite of its exothermic and thermodynamically favorable properties, mineralization is an inherently slow reaction in nature. Mineralization is not a feasible system without additional treatment [18-20]. Therefore, to accelerate the carbonation rate, many pretreatment processes such as magnetic separation, heat treatment, various acid treatments, and HCl

extraction have been developed. However, these methods are all energy intensive, resulting in an increased energy penalty of about 40% for the electricity output of a power plant [18, 19, 21]. Thus, the development of an efficient process that would allow the commercial application of these sorbents requires a significant increase in the reaction rate of the natural mineral carbonation process.

1.2 Structure and Scope of the Thesis

The primary objective of this research is to provide relevant information useful to develop a technically feasible CO₂ sequestration system using cost-effective solid adsorbents that are suitable for retrofit of current and inclusion in future fossil fuel power plants. To achieve this goal, this study focuses on (1) sequestering CO₂ using mineral carbonation in the presence of water vapor, (2) evaluating the reaction kinetics and thermodynamics of olivine carbonation, and (3) identifying approaches to improvement of the carbonation reaction rate.

This thesis first provides an overview of various CO₂ capture technologies including those based on mineralization processes. As a part of the review, the general information of CO₂ mineralization is discussed. Then the experimental results of olivine based CO₂ carbonation are discussed. To investigate the molecular reaction mechanism of CO₂ adsorption on the metal oxide surface, a quantum mechanical calculation of CO₂ adsorption on the CaO (100) surface was carried out.

The chapters of the thesis are organized as follows. Chapter 2 presents a literature review on carbon capture and storage focusing on CO₂ adsorption using solid sorbents, and analyzes/examines the principle of mineral carbon dioxide sequestration. This chapter

includes the selection of minerals, the procedures of the separation system, and the economical and environmental aspects of the mineralization processes. Chapter 3 discusses the results of pure Mg_2SiO_4 carbonation in which the reaction characteristics, temperature effects, and cyclic adsorption are studied. In addition, a kinetic model of the reaction between pure Mg_2SiO_4 and CO_2 was developed. Kinetic parameters such as the reaction order, and the apparent activation energy in the empirical Arrhenius form of the pure magnesium silicate reaction with CO_2 were derived from the relationship between temperatures and the corresponding reaction rate coefficients. Chapter 4 describes natural olivine mineralization in the presence/absence of water vapor under different temperatures, concentrations, and residence times. The study evaluated thermodynamic parameters of olivine carbonation process and the role of water vapor. The limiting factors for CO_2 adsorption on olivine were determined based on varying various parameters, including space time. Chapter 5 uses a quantum computation of CO_2 adsorption on the CaO surface to evaluate the molecular carbonation mechanism and to determine CO_2 molecular reactivity on the (100) CaO surface using first-principles methods. This study investigated the electronic and adsorption properties of the CO_2 -CaO system. Chapter 6 presents the conclusions of this study and recommendations for future research.

CHAPTER 2

CO₂ ADSORPTION: A REVIEW

2.1 Carbon Dioxide

Carbon dioxide consists of two oxygen atoms covalently double bonded to a single carbon atom. CO₂ has no electrical dipole, and is non-flammable. Carbon dioxide (CO₂) is colorless and odorless at low concentrations (<400ppm). Concentrations above 5,000 ppm are unhealthy and those above about 50,000 ppm cause intoxication and asphyxiation of animals life [22].

Above 194.7K, carbon dioxide directly transforms from a solid phase to a gas phase through sublimation. Liquid carbon dioxide forms only at pressures above 5.16 bar; the critical point is 73.8 bar at 304.18K; the triple point of carbon dioxide is about 5.18 bar at 216.55K [23].

In nature, plants, animals, fungi, and microorganisms produce carbon dioxide for respiration and plants consume CO₂ to produce glucose for plant growth and development during photosynthesis. Moreover, carbon dioxide is emitted at low levels (1/150th of anthropogenic emissions) from volcanoes, hot springs, and geysers. These natural sources are mostly equilibrated by natural physical and biological sinks such as the dissolution of CO₂ in sea water and photosynthesis.

Anthropogenically generated CO₂ is formed by the combustion of fossil fuels for heating, electrical power generation, and other chemical processes such as cement production. However, these anthropogenic CO₂ emissions, which are estimated to be about 3% of annual

natural emissions, break the equilibrium of CO₂ emissions and sinks, CO₂ has been accumulating in the atmosphere, leading to the current CO₂ concentration that is 30% higher than existed prior to non-industrial periods [24].

2.2 An overview of CO₂ Capture and Storage (CCS)

2.2.1 CO₂ separation

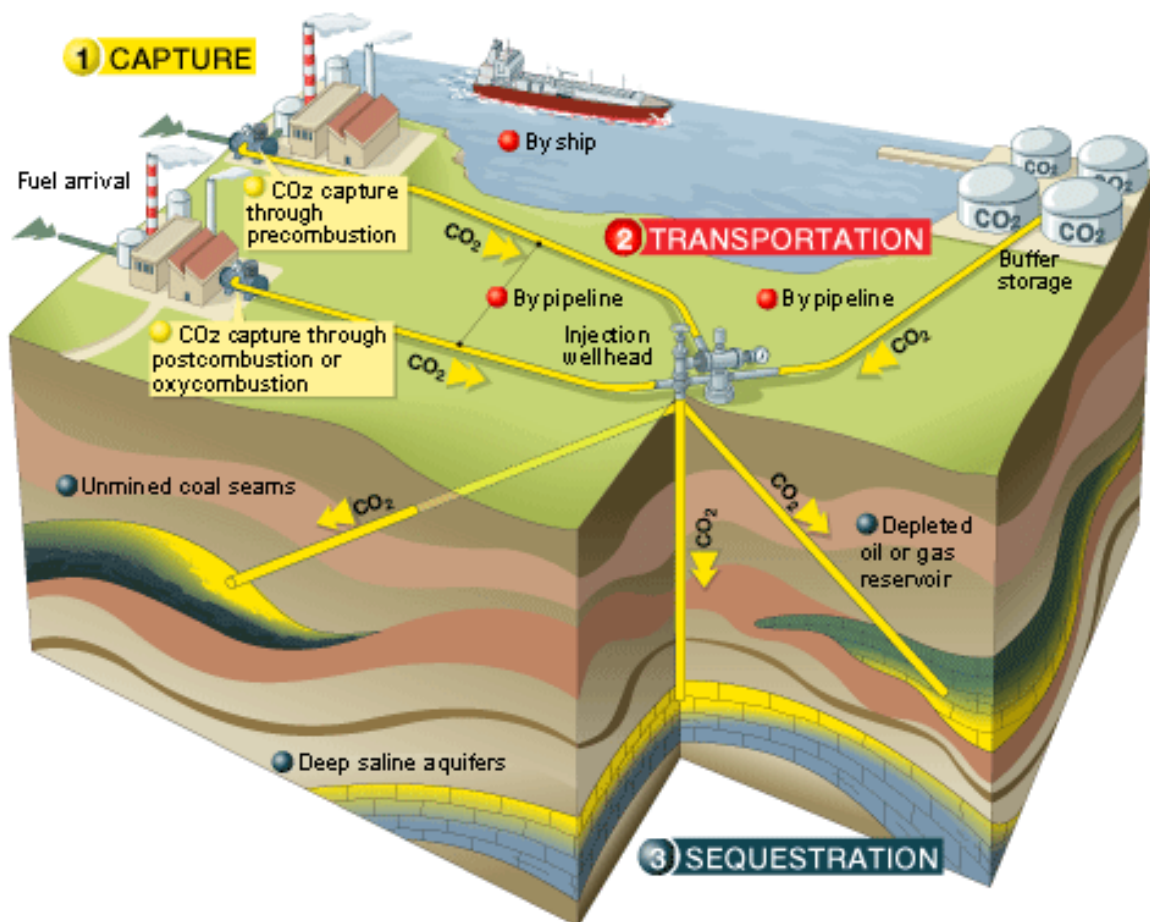


Figure 3. Schematic diagram of general carbon capture and storage [25].

The purpose of carbon capture and sequestration (CCS) is the reduction of carbon dioxide emissions to the atmosphere. Due to limited underground storage capacity, the CO₂ should be separated from a flue gas mixture because most of the flue gas is N₂ and mixture gas sequestration causes higher storage cost. As shown in Figure 3, carbon capture and storage works, essentially, by capturing carbon dioxide emissions as they are produced by large point sources such as large fossil fuel, biomass energy, and industrial facilities, transporting separated CO₂ using an intermediate mode to a storage site, and then storing it underground via various transportation systems so that CO₂ cannot interact with the atmosphere or exacerbate the greenhouse effects. The first step in direct sequestration is to accumulate concentrated CO₂ gas for transport and storage. Typically, CO₂ from large-scale industrial facilities or power plants is conventionally captured in three different processes: (1) pre-combustion, which is designed to remove CO₂ from gas mixture produced typically by gasification prior to its combustion; (2) post-combustion, which separates the diluted CO₂ emitted due to the combustion of fossil fuels or biomass; and (3) oxy-fuel combustion, which uses pure oxygen instead of air for combustion, producing flue gases that consist mostly of CO₂ and water from which the CO₂ is more readily separated. A new approach, chemical looping combustion, is under development. Each of these options is discussed below.

1) Pre-combustion

Gasification of the fossil fuel with oxygen and the subsequent treatment of the gas produced generate a synthesis gas (syngas: a gas mixture of H₂ and CO₂) through the water-gas shift process. After coal gasification and before combustion takes place, CO₂ is removed from the released gas mixture after water-shift reaction (Figure 4). The CO₂ is separated from

the gas stream and the hydrogen is used for combined-cycle power generation. Since syngas is used as a fuel in a gas turbine which produces electricity similar to a conventional combined-cycle plant, this process is called as integrated gasification combined-cycle (IGCC). Heat is recovered from both the gasification process and the exhaust steam in a gas turbine. And then the steam is employed to create additional electrical power in steam turbines [26]. The energy cost of IGCC without CCS is \$56/MW-hr while that with CCS is \$79/MW-hr[27].

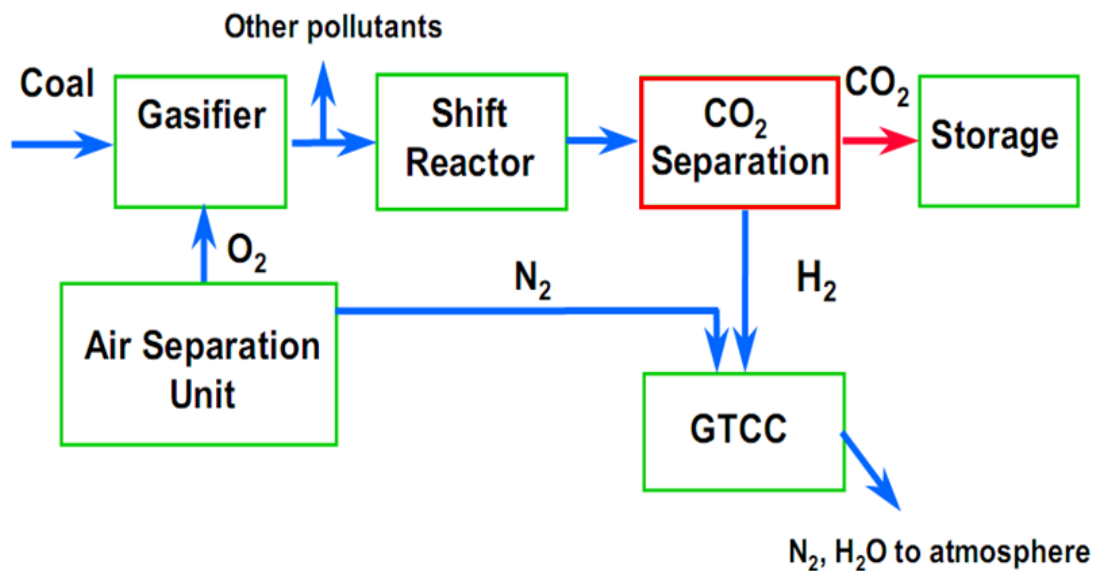


Figure 4. Schematic diagram of a pre-combustion plant (IGCC power plant). IGCC and GTCC denotes Integrated Gasification Combined Cycle and Gas-fired Turbine Combined-Cycle, respectively [28].

2) Post-combustion

Post-combustion is a power plant that uses fossil fuels such as coal, natural gas, or petroleum to generate electrical power and releases flue gas mixture to atmosphere, mainly consisting of nitrogen, carbon dioxide, water vapor, and oxygen. In post-combustion, CO₂ separation is to extract CO₂ from the flue gas mixture, which typically follows a pre-treatment process designed to remove other pollutants such as SO₂ and NO_x as shown in Figure 5. The energy cost of post-combustion system without CCS is \$52/MW-hr while that with CCS is \$92/MW-hr [27].

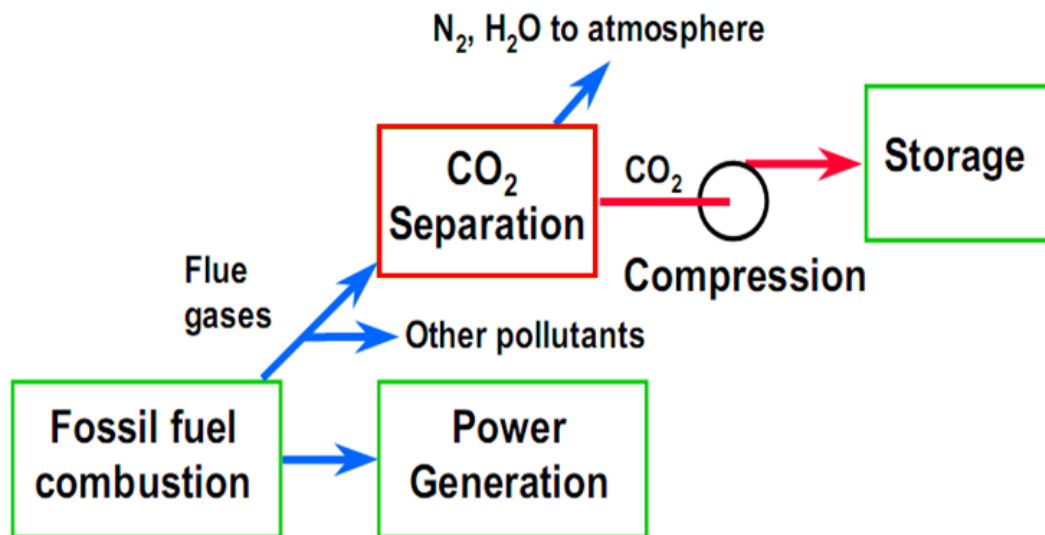


Figure 5. Schematic diagram of a post combustion plant (conventional power plant) [28].

3) Oxy-combustion

Oxy-fuel combustion is one of options to reduce CO₂ from the flue gas mixture. In the oxy-combustion process, instead of being combusted in air, the fossil fuel is combusted in pure oxygen, releasing flue gases that consist mostly of CO₂ and water, part of which is then re-circulated. After water vapor is removed through a condensation process, the concentrated CO₂ stream can be compressed and stored (Figure 6). In oxy-fuel system, fuel consumption can decrease, and higher flame temperatures are possible since N₂ of air is not included in the feed gas stream.

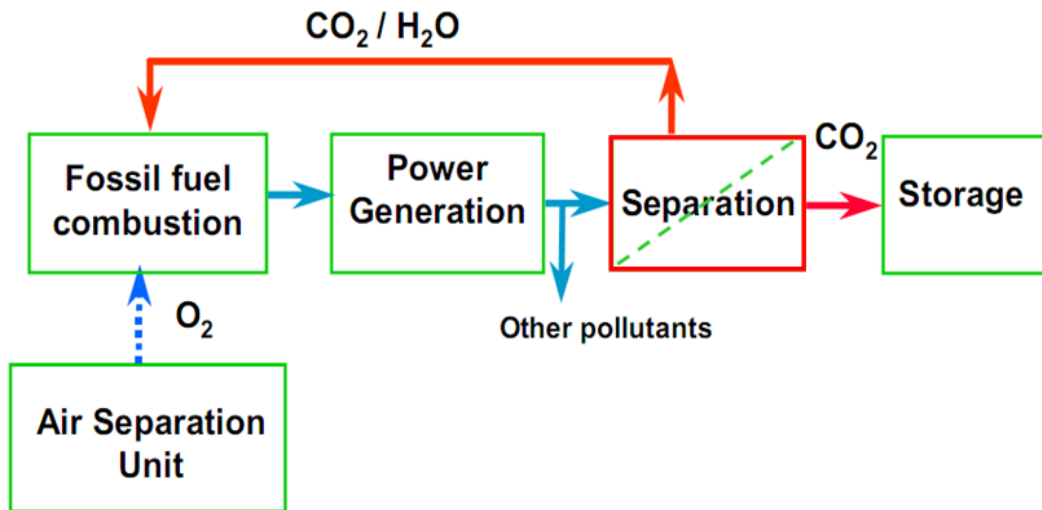


Figure 6. Schematic diagram of an oxy-fuel power plant [28].

As an alternate method, chemical looping combustion (CLC) is still being developed. Chemical looping employs a metal oxide as a solid oxygen carrier. Metal oxide particles react with a solid, a liquid, or a gas fuel in a fluidized bed reactor, releasing solid metal

particles, and a gas stream mixture of CO₂ and water vapor. The water vapor is removed through condensation, leaving relatively pure CO₂, which can then be sequestered.

2.2.2 CO₂ capture technologies

The major technologies used for capturing CO₂ from a flue gas mixture are (1) absorption, (2) adsorption, (3) membrane system, and (4) cryogenic processing [26, 29].

1) Absorption

Separation takes place with a solvent that absorbs the CO₂ from the gas and afterwards discharges it, liberating a nearly pure CO₂ stream. Absorption depends on a solvent's chemical property which highly tends to dissolve solutes over solvents. For scrubbing CO₂ from the flue gas of power plant, CO₂ absorption is preceded by the dissolution of CO₂ in a liquid solvent. Chemical absorption is the most conventional method for the separation of CO₂ from exhaust gases when carbon dioxide levels are at a low concentration (5-15% vol) in a gaseous stream at atmospheric pressure.

The CO₂ capture process using chemical absorption includes two steps [29]:

- The absorption of CO₂ by chemical solvents at a low temperature (40°C to 65°C).
- The recovery of CO₂ from chemical solvents by using low-grade heat (a temperature in the range of 100°C to 150°C).

2) Adsorption

For absorption (a homogeneous process), CO₂ is dissolved into the solvent, but for adsorption (a heterogeneous process), the CO₂ molecules are bound/trapped or physi-sorbed on the surface of the adsorbent due to the interaction between the sorbent and the adsorbate molecules. Different adsorption methods are described as follows [29]:

- In pressure swing adsorption (PSA) process, the gas mixture passes through a packed bed of adsorbents at an elevated pressure as the adsorption of the CO₂ gas approaches equilibrium conditions at the bed exit. Then, the bed is regenerated by stopping the inlet gas mixture and reducing the pressure, and CO₂ is released to move towards the new equilibrium conditions.
- In temperature swing adsorption (TSA), adsorption takes place at the appropriate temperature for the chemical sorbent to react with CO₂, and the adsorbent is regenerated by raising its temperature.
- Electric swing adsorption (ESA) includes a TSA cycle with an electrothermal desorption step. The adsorbent particles are heated directly through an electric current passing through them.

3) Membrane system

Membranes are conventionally used to separate one gas from mixed gases. In this case, separation results from the target gas molecules permeating a porous or semi-porous structure more easily than other gases. This process is based on the selectivity of polymeric membranes to interact with the particular molecules. Either solution-diffusion or absorption-

diffusion mechanisms lead to the diffusion of CO₂ across the membrane [26]. Porous ceramic and metallic membranes are selective to allow CO₂ molecules to pass through the pores of the membrane, which functions as a molecular sieve. This process works by the differences in physical or chemical interactions between the gases and the membrane materials cause one component to pass through the membrane faster than others.

4) Cryogenic fractionation

Cryogenic separation involves compressing the gas stream, after which the compressed gas is cooled to a temperature low enough to allow the formation of a liquid mixture which can be separated by distillation [29]. This process requires the removal of other components from the flue gas stream except N₂ and CO₂ before cooling. After compression and cooling, the remaining gas is introduced to a cryogenic chamber, which allows the CO₂ to liquefy. When the temperature is below 194.64K and the pressure is above 7.4 atm, CO₂ condenses, but N₂ remains in the gas phase [30]. The N₂ gas leaves through an outlet at the top of the chamber, but the highly concentrated liquid CO₂ can be separated at the bottom of the chamber. The resulting liquid CO₂ may then be removed for disposal. This process has the following characteristics [29]:

- It is suitable to high CO₂-concentration (typically >90%) gases.
- It requires compression and refrigeration, and therefore has a high energy demand.
- To avoid blockages, some gas species such as H₂O (g) and NO_x have to be removed before the gas stream is cooled down.

- It is most applicable to high-pressure gases in pre-combustion capture processes or oxygen-fired combustion.

2.2.3 CO₂ transportation

Following separation, CO₂ is compressed to increase its density and make it easier and cheaper to transport. In the end, CO₂ has to be transported to suitable storage sites through various options of overland transport. Feasible methods include truck, train, ship, and pipeline [31]. The cost-effective mode of transport can depend on the locations of capture and storage, distance from source to storage, and the quantities of CO₂ which should be transported, but the quantity to be transported is the most important factor [32].

Transports by truck, train, and ship, similar to the transportation modes for liquefied petroleum gas (LPG), are applicable options for small to medium volumes of CO₂ over very long distances. The CO₂ is remained in liquid phase on the saturation line by a pressure higher than atmospheric pressure and a temperature lower than the ambient temperature in semi-pressurized modes, which are designed for a working pressure of 5 bar to 7 bar at -52°C [32].

For large volumes of CO₂, pipeline is the most practical option for overland transport because on the order of 2 million to 3 million metric tons (Mt) per year of CO₂ are required to be transported from a single fossil fuel power plant [32]. Pipelines are currently the most common approach to transporting large amounts of compressed CO₂ over long distances because they are the cheapest type of transport. CO₂ pipelines operate at ambient temperature and at a pressure of more than 74 bar (the supercritical phase of CO₂), with primary

compressor units placed where CO₂ is injected, and booster compressors located as needed further along the pipeline [31]. For example, approximately 5,800 km of CO₂ pipelines in the United States transported CO₂ to oil production fields, where the CO₂ was injected in older fields to extract extra oil in 2008 [32].

2.2.4 CO₂ sequestration (storage)

Various sequestration methods have been considered for CO₂ storage. Carbon dioxide sequestration involves the injection of CO₂ into various formations: (1) geological storage, providing that the CO₂ is injected deep underground where it is hydrodynamically isolated; (2) ocean storage, where the CO₂ is injected deep into the ocean below approximately 3,000 meter depths; and (3) mineral carbonation through which CO₂ is reacted with minerals to form stable carbonates [32-34]. The last option is a near permanent storage method because carbonates are stable over millions of years compared to the hundreds to thousands of years of stability anticipated for other sequestration methods [34]. Each of the options is discussed below. However, the main drawback of these storage methods, besides their limited applicability, is the temporary nature of the storage.

1) Geological storage (geo-sequestration)

In this option, supercritical CO₂ is directly injected underground into the geological formations in oil/natural gas fields and in saline formations. The most practical isolation methods have been discussed as storage regions [32].

- *Use for oil recovery.* CO₂ is frequently injected into declining oil fields to increase oil recovery. This option is attractive because the geology of hydrocarbon reservoirs is generally well understood and because storage costs may be partly or totally compensated by the sale of the additional oil recovered. However, geographic distribution and capacity is limited.
- *Saline formations step.* A saline formation is a deep underground rock formation composed of stable materials which contain highly saline fluids. This kind of formation has highly mineralized brines which have a relatively high affinity for CO₂. Saline aquifers may store chemical waste. The main advantage of saline storage sites is the amount of available storage regions and the low cost of the storage, but these sites are still relatively poorly understood regarding their properties and characteristics compared to oil fields; thus, additional research is required.

The IPCC report states that CO₂ could be isolated for millions of years in optimized managed geological storage sites, and the sites are likely to retain over 99% of the injected CO₂ over 1,000 years [32]. Furthermore, about 6,000 square miles of suitable rock formations in the U.S. have been mapped and they could be used to store 500 years worth of U.S. CO₂ emissions.

2) Ocean storage

Another possible option of the disposal of CO₂ is storing it in the deep oceans. The ocean is the largest reservoir for carbon and the largest part being in the form of deep

carbonate sediments. The captured CO₂ would be injected into the deep ocean through pipeline. Various methods have been proposed including [32, 33]:

- CO₂ can be directly deposited onto the sea floor at depths greater than 3,000 m to form a lake of liquid CO₂ on the seabed.
- CO₂ can be converted to bicarbonates with the use of limestone.
- CO₂ can be stored in solid clathrate hydrates structures, which already exist on the ocean floor, implying permanent CO₂ storage.

The likely environmental impact of oceanic storage is not well understood, but it is generally considered to have negative effects because large concentrations of CO₂ could kill ocean organisms and because dissolved CO₂ would eventually interact with the atmosphere due to a leakage issue. Moreover, carbonates of CO₂ as H₂CO₃ also cause an increase in the acidity of ocean water. Ocean sequestration of bicarbonate would reduce the pH effects and enhance the retention of CO₂ in the ocean, but this would likely increase overall cost while leading to other environmental issues (e.g., from mining limestone).

3) Mineral storage (mineralization)

Mineralization is the process of the formation of stable carbonates by reaction of CO₂ with alkaline metal oxides (typically Mg and Ca-based minerals). The process of mineralization is stable over geological time scales, and it results in near permanent CO₂ fixation.

Minerals exist abundantly enough to be used to capture the large quantities carbon dioxide emitted from fossil fuel combustion systems [26, 34, 35]. In particular, magnesium-

based silicate minerals are very attractive because they occur in large deposits, and Mg-rich mixture minerals have a large MgO content, between 35% and 45% by weight, implying that more CO₂ can react with MgO to form carbonates. By contrast, calcium silicates rarely have more than 12% to 15% of CaO by weight. Thus, magnesium silicates appear more attractive for CO₂ capture [35, 36].

The reaction between CO₂ and metal oxides forms magnesium carbonate (MgCO₃) and calcium carbonate (CaCO₃) because the reaction is exothermic, providing a thermodynamically favorable reaction. This reaction occurs naturally (e.g., the weathering of rock) [35, 36]. Thus, this carbonation reaction does not require additional energy input, and can actually produce some heat. However, the carbonation process occurs extremely slowly under ambient temperatures and pressures, and its reaction must be significantly accelerated for the feasible capture and storage of CO₂ from anthropogenic sources. The reaction rate of carbonation can be improved through a pre-treatment. The details of mineral carbonation will be discussed later.

2.3 CO₂ Adsorption

A common drawback of methods for CO₂ capture and sequestration is their high energy consumption. This necessitates alternative CO₂ separation methods with higher CO₂ adsorption capacity, higher regeneration capacity, and lower energy demand [37, 38]. Among the various processes, adsorption has attracted attention because of its simple operation, low corrosiveness, and overall low cost [3, 10-12]. In addition, molecular sieves and molecular baskets of solid adsorbents are environmentally friendly. Figure 7 shows the schematic diagram of a post-combustion CO₂ capture pilot plant and the actual appearance of the pilot

plant in Japan.



Figure7. Schematic diagram of the CO₂ capture plant (adsorption process) for post combustion and the actual picture of the pilot plant in Japan [39].

For feasible application, CO₂ adsorption from the flue gas mixture of power plants requires rapid adsorption rate, which reduces adsorption/desorption multi-cycle times and the required quantity of adsorbent. This section provides an overview of the currently studied CO₂ adsorption technologies with various solid adsorbents and an evaluation of their performances in the literature. Potential future trends and strategies for CO₂ separation are also described.

2.3.1 Sorption based CO₂ separation processes

High-potential adsorbents usually have high sorption capacity, fast adsorption and desorption rates, high cyclic stability, and a low attrition rate. The adsorption capabilities of

sorbents depend on many factors such as the exposed CO₂ concentration, temperature, affinity of the sorbent to CO₂, sorption site density, and surface area, pore size and the structure of sorbents [13-15]. Two types of sorption processes are typically employed for CO₂ capture, aqueous (absorption) and dry (adsorption), which have different CO₂ sorption characteristics. Absorption is sorption from one substance into another substance of a different state (i.e., bulk reaction) whereas adsorption means sorption to a surface of another phase (i.e., surface reaction). In aqueous absorption process, CO₂ is dissolved into the solvent. In the dry adsorption process CO₂ is either chemisorbed to the sorbent by strong chemical bonds or physisorbed to the sorbent by weaker intermolecular bonds. These sorption processes result from the interaction between sorbents and CO₂ molecules [40]. While this chapter focuses on sorption using a solid adsorbent, aqueous processes are briefly discussed first.

In aqueous processes, the concentrated CO₂ solution is transported to a regeneration column where the CO₂ is separated from the solution by precipitation or degasification. The solvent is then regenerated and recycled to another inlet of flue gas. This approach can lead to high capital and operating costs because of (1) a high energy consumption for the solvent regeneration, (2) a high rate of corrosion of the process equipment, (3) a fast rate of evaporation causing solvent losses, and (4) a high rate of degradation in the presence of oxygen [37, 38, 41]. In addition, aqueous sorption processes require additional pretreatments such as electrostatic precipitation to remove particulates and flue gas desulfurization to remove the acidic species, since many solvents are degraded by reactive compounds such as fly ash, SO_x, and NO_x [42]. The aqueous system will require high pressures due to the temperature limitations and low CO₂ solubility in water. Additional chemicals such as

hydrochloric acid and acetic acid are needed in the dewatering stage to improve the aqueous processes, adding to the process costs and may result in corrosion [42].

Dry sorption processes without using a solvent shows a simple design and operation due to (1) the simple processes and (2) small pressure changes for physical adsorption [3, 10, 37, 38]. Two principal modes of adsorption, physical and chemical, are discussed below for the evaluation of the CO₂ sorption activity with respect to the separation type [9, 10].

The physical adsorption (physisorption) of molecules involves relatively weak intermolecular forces such as dispersion, dipolar, or Van der Waal interactions between the adsorbent surface and the adsorbate. These intermolecular interactions are weak due to the relatively small energy required; being on the order of magnitude of the enthalpy of condensation. Physisorption does not provide a large redistribution of electron densities at either the adsorbent surface or the adsorbate. Sorption energy can be absorbed as lattice vibrations and dissipated as thermal motion. The physisorption enthalpy of adsorption is typically on the order of 20 kJ/mol [43]. In terms of kinetics, physisorption rates are relatively fast because this is not associated with the barriers of activation energy. The required energy of regeneration of CO₂ from the physisorbed state is typically low, which makes it attractive. However in some cases, mass-transfer controlled processes could inhibit Van der Waal interactions. The two applicable options of physisorption, pressure and vacuum swing adsorption, are discussed below.

1) Physical adsorption

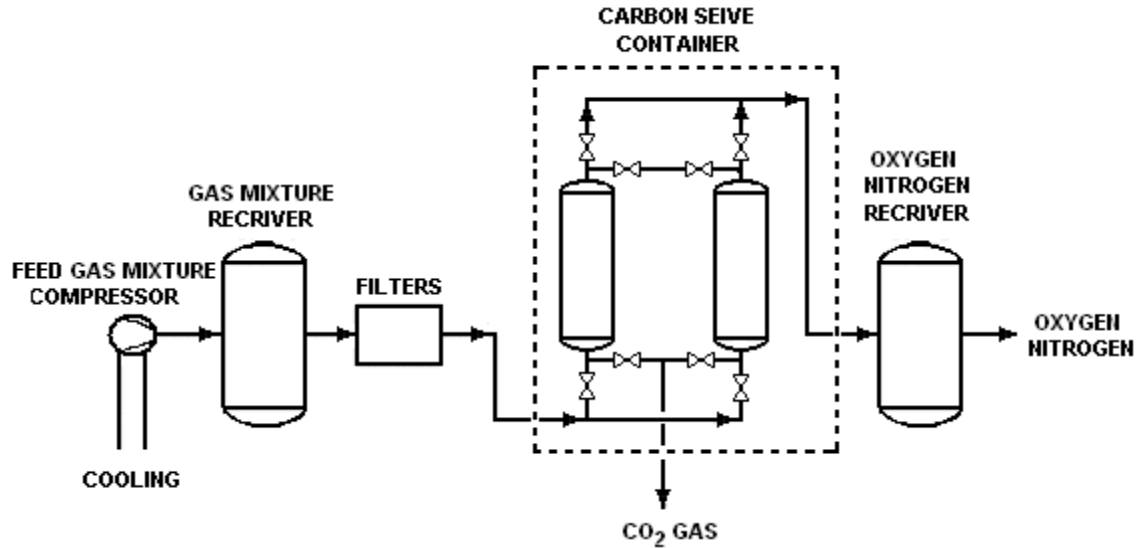
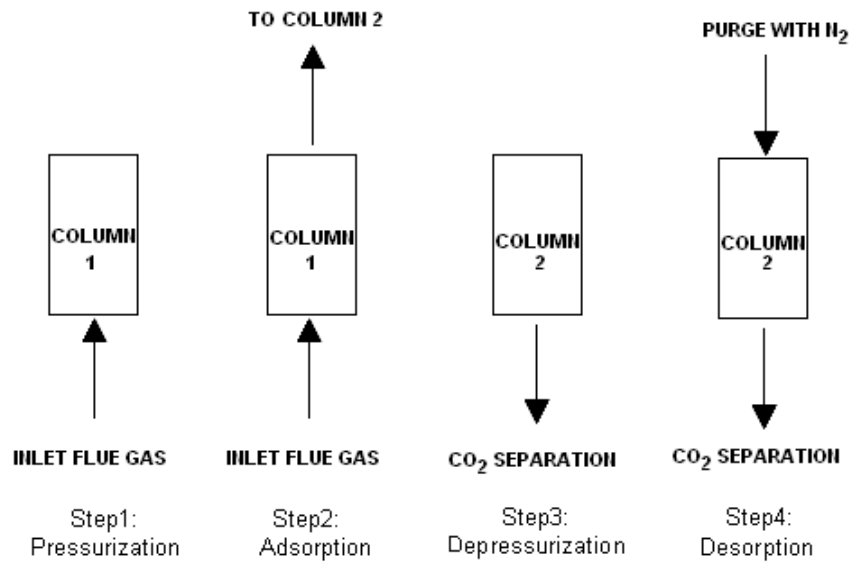
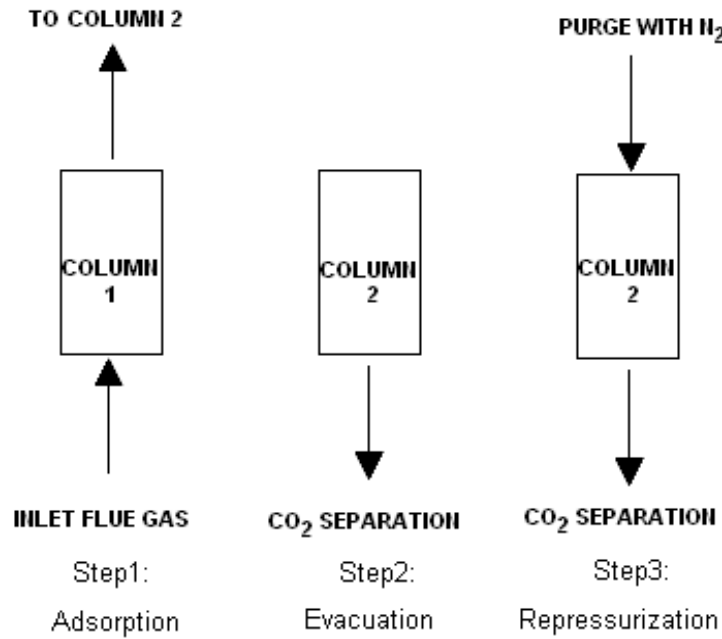


Figure 8.Schematic diagram of Pressure Swing Adsorption system [44, 45].

Pressure Swing Adsorption. Pressure swing adsorption (PSA) has been applied for the separation of contaminants from gas mixtures such as carbon dioxide capture in ammonia production and hydrogen purification [8, 15, 45-59]. Figure 8 is a conceptual diagram of a PSA system. In the PSA process, gas species can be separated from a gas mixture at high pressure and low temperature by passing the flow through a reactor containing the sorbent. The pressure is then reduced, resulting in the relatively easy release of CO₂ from the adsorbent surface because electrons are not shared between adsorbent and adsorbate [57].



(a) Pressure Swing Adsorption system



(b) Vacuum Swing Adsorption system

Figure 9. Operation steps of Pressure and Vacuum Swing Adsorption system [7, 15].

Figure 9a provides a conceptual illustration of the PSA operation procedure. First, flue gas is introduced into the first column with a sorbent and is pressurized, resulting in CO₂ adsorption to the sorbent. The applied pressure is transferred to column 2. After column 2 is pressurized, column 1 is depressurized to 1atm and CO₂ is separated from the gas mixture. The inlet CO₂ gas stream is stopped and N₂ is only introduced to desorb CO₂ from the sorbent after depressurization. Finally, the cycle continues switching modes from the adsorption column to the desorption column.

System factors and operating conditions are determined to optimize the PSA process. The rate-limiting mechanism of the PSA system is either the selectivity of equilibrium thermodynamics or reaction kinetics. Thermodynamic equilibrium selectivity depends on the different gas concentrations at the equilibrium state of the gas mixture for separation processes. For PSA using equilibrium selectivity, strongly adsorptive gas components remain in the adsorbent column whereas weakly adsorbed species are discharged in high pressure gas streams. Kinetic selectivity is based on having different diffusion rates of gas molecules in the non-equilibrium system. Faster diffusing gas species go to the sorbent column, while slower diffusing gases flow out. Thus, the gas specific diffusion rate determines the selectivity.

Operating processes have evolved to improve the efficiency of PSA separations. One example is to optimize the bed size and sorbent usage by using different sorbents such as activated carbon and zeolite, which have strong CO₂ affinity, within the layered sorbent bed. The activated carbon sorbents are placed ahead of zeolite sorbents [48]. In first layered column, activated carbon mainly adsorbs CO₂ species while the zeolites in the second layered column capture the residual CO₂ components. This approach was introduced in the 1970's,

but it was not well suited for industrial facilities due to low sorption capacity of adsorbents and unstable operating controls [14].

Pressure swing adsorption has three major drawbacks. Firstly, the short cycle-times lead to high losses of feed gas in the bed after venting out in the depressurization step [60]. In addition, the short cycle-times can cause a rate change in the inlet flow leading to an unstable pressure in the column during the operation. Secondly, PSA processes typically add impurities to the other gas species at low pressures and these species will be adsorbed on the surface more strongly than carbon dioxide. Thirdly, PSA processes may not be cost-effective for CO₂ recovery from flue gas streams. The cost of CO₂ recovery is lowered as the CO₂ concentration in the flue gas is increased. Separation chambers operate at high pressure (thousands of kPa) and PSA process cannot directly separate CO₂ at low pressure (<~10kPa) due to the low CO₂ partial pressure. A compression process is required to produce high pressures in this system, but this requires significant energy. In spite of these drawbacks, PSA still plays a significant role in the separation system due to its low cost and simple operation [8, 57].

Vacuum Swing Adsorption. Vacuum swing adsorption (VSA), a modification of the PSA process, has been developed to improve the regeneration efficiency with lower power consumption and an easier operation procedure than those of the PSA processes [3, 7, 61-64]. The VSA system operates at low absolute pressures (<150 kPa), depending on the nature of the gas species and affinity to the sorbents [28].

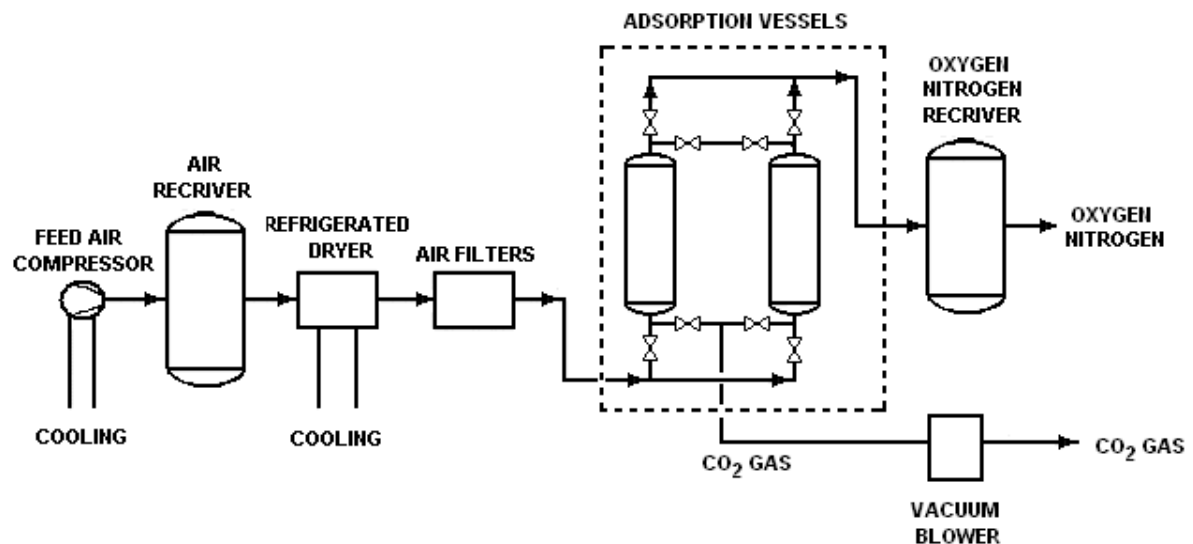


Figure 10. Vacuum Swing Adsorption (VSA) system [7].

Figure 10 shows a typical apparatus for a vacuum swing adsorption system in which the inlet is slightly compressed (<150 kPa). VSA is comprised of double adsorbent-packed reactors for adsorption and desorption and a vacuum pump for recovering CO_2 . Figure 9b shows a three-step vacuum swing adsorption cycle as follows: (1) adsorption of the inlet gas as it flows from bottom to top of a column at a fixed rate, (2) evacuation and removing adsorbed components, and (3) re-pressurization to atmospheric pressure with waste gas [7]. The VSA cycle is similar to the PSA cycle except for the absence of the high pressurization step that makes it both simpler and more cost-effective.

2) Chemical adsorption

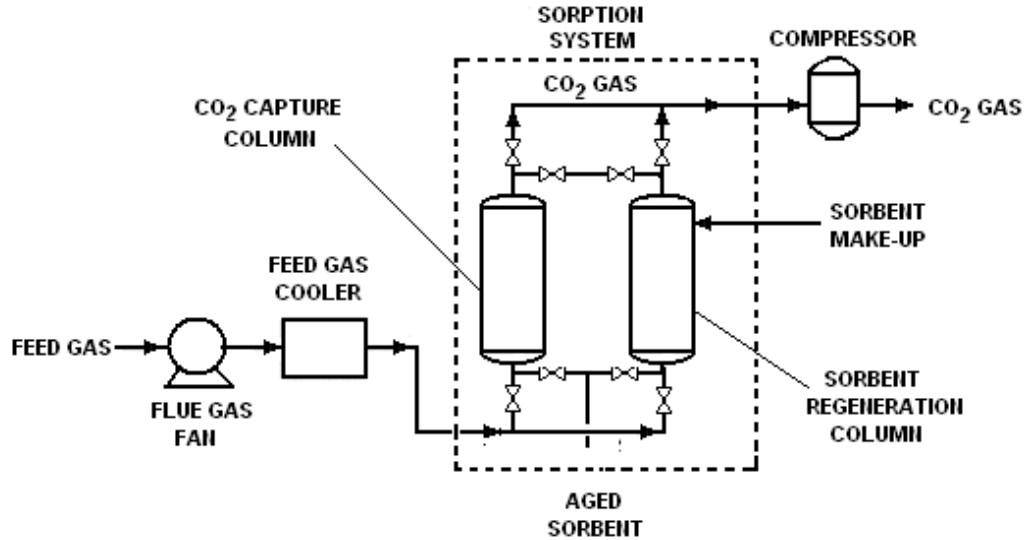


Figure 11. Temperature Swing Adsorption (TSA) System [65].

Chemical adsorption (or chemisorption) on solid materials is achieved by substantial sharing of electrons between the surface of the adsorbent and adsorbate to create a strong bond such as a covalent or ionic bond [66]. As carbon dioxide molecules are adsorbed onto the surface of the adsorbent through valence bonds, a monolayer of carbon dioxide is formed. Chemical adsorption may not be fully reversible and can require a high energy input to break the surface bonds for regeneration. The chemisorption energy between the gas molecules and adsorbents is equivalent to the energy change in the chemical reaction between an adsorbent and an adsorbate. Energy changes can vary significantly depending on the bond strength. Adsorption rates involve overcoming activation energy barriers. If the activation energy is sufficiently high, near equilibrium conditions may be obtained slowly [66].

TSA is an isobaric process in which the adsorption process takes place at low temperatures and desorption of the adsorbed gas components occurs at temperatures higher

than those temperatures where adsorption occurs. The solid sorbents for adsorption in TSA processes are usually composed of alkali and/or alkaline-earth metals. Desorption of adsorbed CO₂ can be accomplished by calcination [14, 16, 19, 37, 38, 51, 59, 65, 67-107], and has the advantage of being environmentally friendly [4]. A schematic diagram of a typical temperature swing adsorption system is illustrated in Figure 11. Following the cooling of the gas mixture, mixture containing CO₂ enters the reactor, and the CO₂ is adsorbed. When the adsorbent is heated, the adsorbed CO₂ is desorbed. During the desorption step, the sorbent is regenerated to be used again. However, during cyclic usage of the same sorbents, the chemical natures of the sorbents can be modified by reaction or surface dissociation so the original sorbents cannot be fully regenerated after desorption [66]. For the optimum condition (i.e., cost-effective maintenance and operation) of the system, TSA system should have a high sorption affinity, a strong sorbent structure, and improvement of processes is required for cost-effective maintenance and operation.

2.3.2 Adsorption for CO₂ capture

Several different kinds of sorbents have been used for physical and chemical adsorption of CO₂, e.g., amines, zeolites, potassium carbonate, lithium zirconate, sodium carbonate, and alkali-earth minerals. The potential adsorbents must have: (1) high selectivity and high adsorption capacity, (2) adequate adsorption/desorption kinetics, (3) stable cyclic adsorption capacity, (4) mechanical durability to maintain reasonable performance after extended cyclic exposure to high-pressures or high temperatures, and (5) low energy demand for regeneration of pure CO₂ [98].

TABLE 1. Physical properties of different solid sorbents

Solid Sorbent	Bulk density (kg/m ³)	BET surface area (m ² /g)	Pore volume (ml/g)	Reference
Tertiary Amine (DBU)	-	369	1.1	[77]
Aminated SBA-15	-	200~230	0.72	[83]
Zeolite 13X	689	726	0.25	[57]
Zeolite /Activated carbon	500	620	0.19	[57]
Li ₂ ZrO ₃	-	5	0.02	[51]
Activated Carbon	860	1300	0.6-0.8	[8], [108]
Hydrotalcites (HTlc)	440	271	0.55	[71]
Mg-Al-CO ₃ HTlc	-	184	0.31	[98]
Serpentine	2500	330	0.23	[18]
Metal–Organic Frameworks (MOFs)	-	345~2833	-	[109]

For carbon capture by adsorption, two of the most important physical properties of solid sorbents is BET (Brunauer, Emmett, and Teller) surface area and pore volume. BET surface areas and pore volumes of different adsorbents dramatically vary from 5 m²/g to 1,300 m²/g, and from 0.02 mL/g to 1.1 mL/g, respectively (Table 1). However, chemical properties are also relevant. Lithium zirconate, for instance, has relatively low BET surface area (5 m²/g) and pore volume (0.02 mL/g), but its capture capacity is among the highest (0.29 g CO₂/g sorbent) (Table 2). Typically, CO₂ sorption capacities of conventional solid sorbents are on the order of ~0.1 g CO₂/g sorbent. In order to reach the high capture capacity of ~0.15 g CO₂/g sorbent, several studies have modified well-known sorbents to improve their capture capacities, Improvement typically results from increasing surface areas and CO₂ affinity as well as modifying their properties of the covalently tethered sorbents [14, 77, 78, 110].

TABLE 2. CO₂ capture capacities of different solid sorbents

Solid Sorbent	Capacity (g CO ₂ /g sorbent)	Gas composition	References
SBA-HA ¹	0.09	15% CO ₂ , 85% N ₂ with 20mL/min rate of H ₂ O	[77]
Aminated SBA-15 ²	0.07~0.18	10% CO ₂ , 88% He with ~2% H ₂ O	[83]
Tertiary Amine (DBU)	0.13	10% CO ₂ , 88% He with ~2% H ₂ O	[14]
K-Li ₂ ZrO ₃ / Li ₂ ZrO ₃	0.22~0.29	10% CO ₂ , 90% N ₂	[51]
MCM-41 ³	0.09	15% CO ₂ , 85% N ₂ , 4% O ₂	[111]
K-promoted HTlc ⁴	0.44	15% CO ₂ , 75% N ₂ with 10% H ₂ O	[46]
Hydrotalcites (HTlc)	0.04	11% CO ₂ , 89% N ₂	[71]
Mg-Al-CO ₃ HTlc	0.02	20% CO ₂ , 80% N ₂	[98]
Zeolite 13X	0.22	15% CO ₂ , 85% N ₂	[57]
Zeolite/Activated carbon	0.22	15% CO ₂ , 85% N ₂	[57]
Activated Carbon	0.18	17% CO ₂ , 79% N ₂ , 4% O ₂	[8]
Basic alumina	0.03	100% CO ₂	[70]
Metal–Organic Frameworks (MOFs)	1.47~1.5	-	[109, 110]

¹SBA-HA denotes Santa Barbara Amorphous type of Hyperbranched mesoporous Aminosilica; ²SBA-15 a type of mesoporous silica (Santa Barbara Amorphous type material); ³MCM-41 a type of mesoporous silica (Mobil Crystalline of Materials, or MCM-41); ⁴K-HTlc potassium modified HTlc.

1) Zeolites

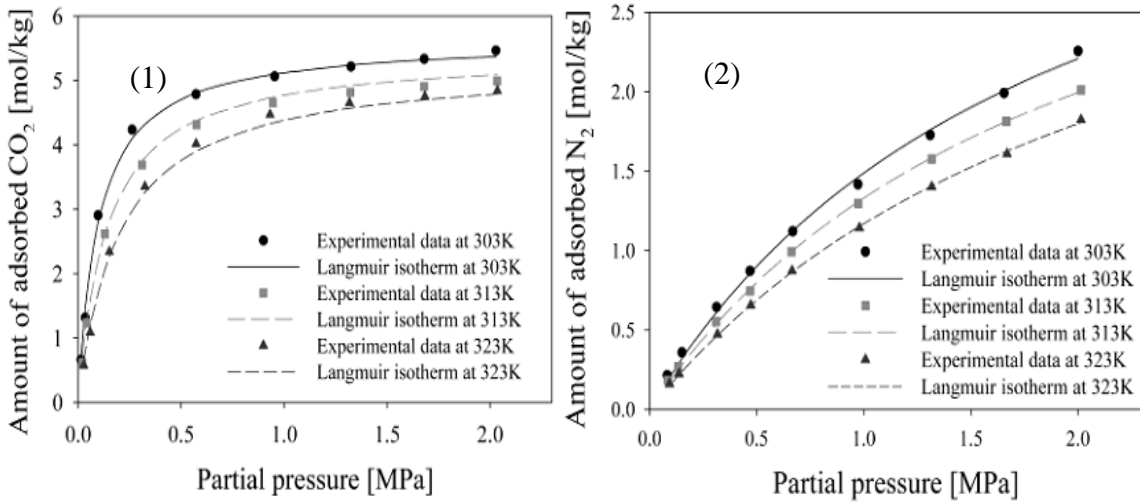
In nature, the reaction of volcanic rocks, ash, and water forms zeolites, a class of regularly arrayed porous crystalline aluminosilicates of TO₄ tetrahedra (where T = Si or Al). Aluminum or silicon atoms in the supported silicate cause negative framework charges, leading to exchangeable cations such as alkali cations in the pore space [57]. Zeolites have

high selectivity and capacity for CO₂ adsorption due to their unique porous characteristics of molecular-sized holes and pores of their framework which functions as molecular sieves. Zeolites not only can be artificially synthesized, but are also inexpensive and environmentally friendly because of their natural existence. They are also attractive in physical sorption, because they maintain a stable structure even after sorption [7, 15, 48, 50, 57, 62, 65, 67, 73, 82, 87, 90]. These characteristics place zeolites among the top of the sieve adsorbents.

Different types of zeolites have been utilized in various adsorption methods such as PSA [8, 15, 45, 47, 48, 50, 53, 55-58, 67], VSA [7, 61, 62], and TSA [65, 82, 85, 87, 90] with varying selectivity for CO₂ over other gases such as CH₄, CO, and N₂. For instance, the selectivity of CO₂ over N₂ on zeolites in PSA is ~48% whereas in TSA and VSA it is ~90% and ~81%, respectively [45, 82, 112], though zeolite adsorption reactivity is affected by temperature and pressure. Thus, the investigation of zeolite sorbents is primarily for TSA and VSA processes. However, zeolite-based PSA is still used to separate gas mixtures due to its cost-effectiveness and operational simplicity.

Among the various types of zeolites, 13X and 5A have high CO₂ capture capacities, due in part to their highly regular pore structure and large surface area [87]. The kinetics of CO₂ adsorption on zeolites leads to the reaction reaching near equilibrium within a few minutes, through the reaction is significantly faster in the initial adsorption period. The characteristics of zeolites can be evaluated by analyzing their selectivity, adsorption equilibrium, adsorption kinetics, and the effect of water.

Selectivity of zeolites.



(a) Adsorption Isotherm of CO₂ (1) and N₂ (2) [57]

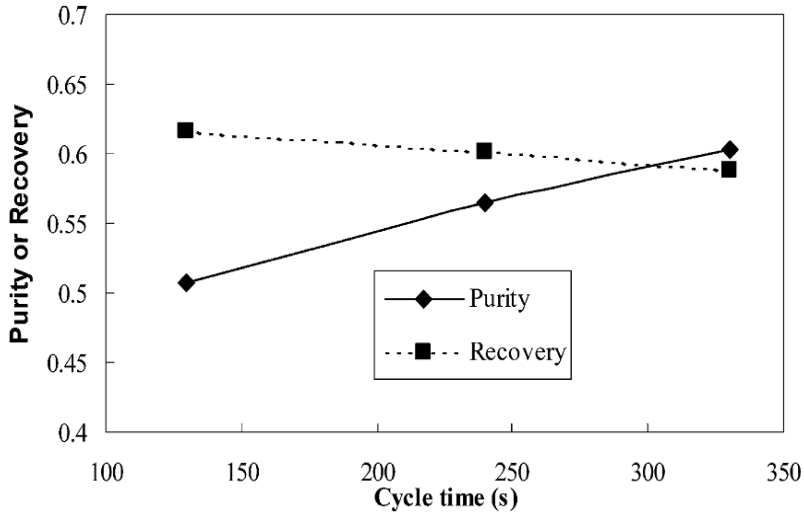


Figure 12. Evaluation of zeolite 13X on the basis of isotherm, purity and recovery.

One important property for capturing CO₂ effectively is a sorbent's selectivity for CO₂ over other gases, particularly for species with a smaller molecular volume such as N₂. Evaluating the sorbent selectivity for CO₂ over N₂ requires the development of the

equilibrium adsorption isotherms for CO₂ and N₂ gases on the adsorbent using experimental data and Langmuir isotherm models (Figure 12). The adsorption isotherms for CO₂ and N₂ on zeolite 13X were measured in the pressure range of 0 atm to 2.0 atm and the temperature range of 30°C to 50°C [45]. Measurements revealed that the amount of adsorbed CO₂ on zeolite 13X was four times larger than it was for N₂ in most over the temperature range, showing that zeolite 13X has a higher selectivity for CO₂ than N₂.

Adsorption isotherms are modeled by the Langmuir isotherm and the Langmuir-Freundlich isotherm. For the parameters of the equations, Langmuir isotherm parameter (b_i) and saturation amount adsorbed component (q_{si}) are functions of temperature as follows:

$$b_i = b_{io} \exp(b_1/T) \quad q_{si} = a_{i,1} + a_{i,2}/T \quad (2)$$

where b_i denotes the Langmuir isotherm parameter (1/mmHg), q_{si} saturation amount adsorbed of i th component (mol/g).

Langmuir isotherm equation is formulated as:

$$q_i = \frac{q_{si} b_i p_i}{1 + b_i p_i} \quad (3)$$

and the Langmuir-Freundlich isotherm:

$$q_i = \frac{q_{si} b_i p_i^{1/n}}{1 + b_i p_i^{1/n}} \quad (4)$$

where n is a power constant and the isotherm parameters, b_{io} , b_1 , $a_{i,1}$ and $a_{i,2}$ are calculated by isotherm experiments by using CO₂ and N₂ gases and zeolite 13X (Table 3).

The Langmuir isotherm models the adsorption of gas molecules on the surface of a solid sorbent at constant temperature on a fixed absorption bed. It simulates the surface

coverage of a monolayer without intermediate forces between the gas molecules already adsorbed on the surface of sorbent.

TABLE 3. Langmuir Isotherm Parameters for CO₂ and N₂[55]

Gas	$a_{i,1}$ (mol/g)	$a_{i,2}$ (K)	$b_{i,0}$ (1/mmHg)	$b_{i,1}$ (K)
CO ₂	-1.95	2.03	87.84	2200
N ₂	-1.03	0.61	2.81	2520

Purity and Recovery of zeolite. Another important property of zeolites is resultant gas purity and gas recovery calculated from data obtained in cyclic processing with the same sample. Of these two characteristics, purity is the ratio of the molar amount of a certain gas species produced over the total amount produced during the cyclic operation at steady state [45]:

$$\text{Purity(\%)} = \frac{\int_0^{T_{\text{cycle}}} v \cdot y_{\text{product}} dt}{\int_0^{T_{\text{cycle}}} v dt} \quad (5)$$

where T_{cycle} is adsorption/desorption cycle time, t is reaction time, v is feed rate, and y is the mole fraction of the component of interest.

Recovery is defined as the ratio of the molar amount of a given gas species in the product over the amount of the same species in the feed [45]:

$$\text{Recovery(\%)} = \frac{\int_0^{T_{\text{cycle}}} v_{\text{product}} \cdot y_{\text{product}} dt}{v_{\text{feed}} \cdot y_{\text{feed}} \cdot T_{\text{ad}}} \quad (6)$$

where T_{cycle} is adsorption/desorption cycle time, t is reaction time, v is fluid velocity, y is the mole fraction of the component of interest, t is reaction time, and T_{ad} is adsorption time.

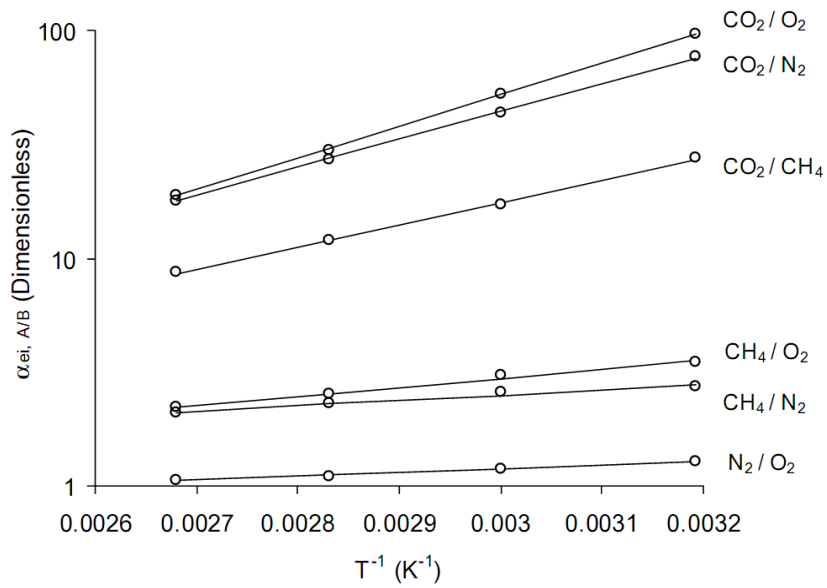
In typical PSA processes, the CO₂ purity increases with an increase in cycle times and the operating time of adsorption/desorption due to the accumulation of the molar amount of

CO₂. Thus, in order to operate the system efficiently, with enhanced CO₂ purity and recovery, one needs to optimize various parameters such as operating cycle times, flow rates, adsorption times, product purge step times, and inert mole fractions (the fraction of inert gas species to total feed species) [8, 45, 56]. For example, the purity improved approximately linearly with cycle time based on the effect of cycle time on the purity and recovery of N₂ (Figure 12b). An optimum cycle time was observed at ~300 seconds for zeolite 13X since the separation of CO₂ and N₂ on zeolites is equilibrium rather than kinetically controlled, resulting from the favorable operation under relatively long adsorption/desorption times [45].

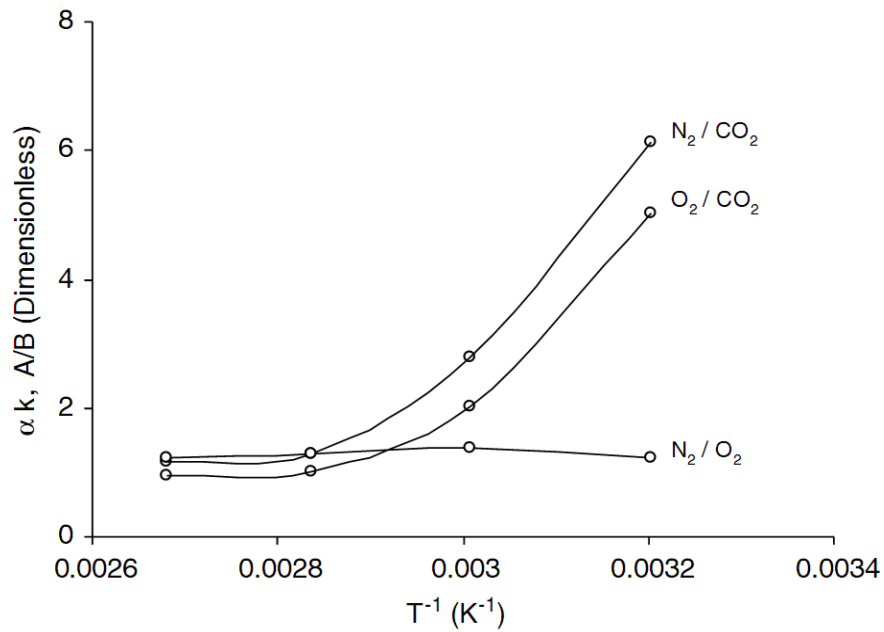
Equilibrium and kinetic adsorption. Li, *et al.* [73] carried out the studies of adsorption equilibrium and kinetic separation for multi-gas stream (CO₂, N₂, O₂ and CH₄) on zeolite β in a TSA system (Figure 13). Between adsorption equilibrium and kinetic separation, equilibrium selectivity is most commonly used for TSA processes. The adsorption equilibrium separation factor is defined as [73]:

$$\alpha_{e,A/B} = \frac{x_A / x_B}{y_A / y_B} \quad (7)$$

where x_A , x_B , y_A and y_B are the mole fractions of components A and B in the adsorbed (x) and fluid phases (y) at equilibrium, respectively.



(a) Adsorption equilibrium separation factor as a function of temperature.



(b) Adsorption kinetic separation factor as a function of temperature.

Figure 13. The adsorption equilibrium and kinetic separation factor for a TSA process with zeolite β [73].

For typical Langmuir isotherms, this factor is constant and is found as the ratio of the Henry's Law constants [73]:

$$\alpha_{ei,A/B} = \frac{K_{pA}}{K_{pB}} \quad (8)$$

where K_{pA} and K_{pB} are the Henry's Law coefficient of adsorption equilibrium for components A and B, respectively.

The adsorption equilibrium separation factor is described as a function of inverse temperature. When the temperature increases, the equilibrium separation factor decreases, resulting from the relative magnitudes of the heats of adsorptions of the two gas species (Figure 13b) [73]. This phenomena is captured by the Van't Hoff equation where the value of $\frac{-(\Delta H_A - \Delta H_B)}{RT}$ reduces as temperature, T increases [73]. The selectivity of CO₂ over other gases dominates at higher temperatures due to the higher Henry's Law constant of CO₂ among several gas components. A kinetic separation factor can be useful to examine the separation mechanism of any binary gas system. Similar to PSA systems, the kinetic separation factor is related to the diffusion process, which is the major mass transfer mechanism in TSA. The kinetic separation factor is defined as [73]:

$$\alpha_{k,A/B} = \frac{D_{c,A}}{D_{c,B}} \quad (9)$$

where $D_{c,A}$ is the diffusivity within a crystal of component A (m²/s), $D_{c,B}$ is the diffusivity within a crystal of component B (m²/s), D_c (diffusivity within a crystal) is given by the

Arrhenius equation: $D_c = D_0 \exp\left(-\frac{E_a}{RT}\right)$ with D_0 being a pre-exponential factor (m²/s), E_a

the diffusional activation energy (kJ/mol), R the gas constant (0.08206 atm.L.mol⁻¹K⁻¹), and

T the temperature in Kelvin. Kinetic separation factors for N_2 over CO_2 and O_2 over CO_2 decreases as temperature increases whereas the separation factor of N_2 over O_2 increases slightly, depending on the relative magnitudes of the diffusion activation energies [73]. These results indicate that at low temperature, kinetic separation prefers N_2 over CO_2 and O_2 over CO_2 for zeolite β .

Effect of water vapor.

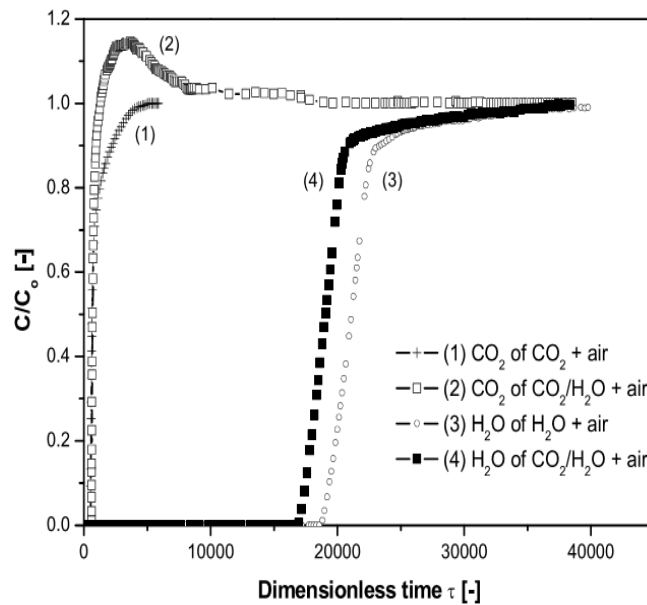


Figure 14. Vacuum Swing Adsorption for CO_2 +air, H_2O + air and CO_2/ H_2O + air in zeolite 13X at $30^\circ C$ [7].

CO_2 adsorption in the presence of water vapor is an important consideration for the application of CO_2 separation technologies to power plants due to the presence of water vapor in a flue gas mixture. Li *et al.* studied CO_2 adsorption on zeolite 13X in a VSA system at $30^\circ C$ to evaluate the effect of water vapor [7]. CO_2 capture capacity in the presence of water vapor becomes lower than that in the absence of water vapor due to the higher affinity

of H₂O molecules to zeolite surfaces than that of CO₂ molecules [69]. The breakthrough curve of CO₂ with water vapor showed a considerable effect of water vapor on the CO₂ capture capacity (Figure 14), although H₂O adsorption capacity was minimally impacted by the presence of CO₂ [7, 113]. These results show a drawback in the use of zeolites without a water vapor removal in a flue gas mixture. The temperature should be kept above 100°C to avoid water condensation and saturation over the adsorbent, leading to its evaporation. However, this could damage the sorbent and cause pressure increases.

The cost of CO₂ separation using PSA and VSA on zeolite. Capture cost is one of the most important factors to consider before using a process in realistic industrial applications. Since the goal of CO₂ capture and storage (CCS) is to reduce CO₂ emissions to the atmosphere, the amount of CO₂ emission avoided is more important than that of CO₂ captured per unit of production (e.g. per kWh electricity) [114]. CCS requires additional energy input per unit of output. The amount of CO₂ produced per unit of production may increase because the power plant with CO₂ capture produces the same output, but generates more CO₂ [114]. As a result, the amount of carbon dioxide avoided is less than the amount of carbon dioxide captured.

The capture cost of CO₂ for a given adsorbent, is given by [47]:

$$\text{Cost of CO}_2\text{avoided} = \frac{\sum_{i=1}^n \frac{K_i + O_i}{(1+d)^i}}{\sum_{i=1}^n \frac{(\text{CO}_2 \text{ avoided})_i}{(1+d)^i}} \quad (10)$$

where K_i and O_i are the capital and operating costs (US\$ million) in the *ith* year, *d* is the discount rate (% pa), and “CO₂ avoided” is the annual amount of avoided CO₂ emissions in millions of tons. Avoided CO₂ is defined as the difference between CO₂ emitted and CO₂

captured. The lower amount of CO₂ avoided than that of CO₂ captured suggests that the costs per ton of CO₂ avoided will be higher than the costs per ton of CO₂ captured. The capital and operating costs involve CO₂ recovery and purity, and CO₂ compression [47]. The total capital cost is estimated as the cost of all processing equipment in a given facility used for CO₂ capture, and the operating costs include fixed general maintenance costs comprising labor, payable non-income government taxes, and insurance costs as well as energy costs [47].

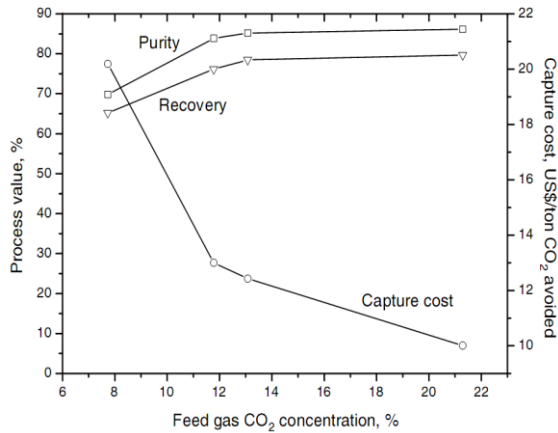
TABLE 4. Capacity cost and capital cost of CO₂ capture with zeolite 13X

	PSA ¹ [47]	VSA ² [47]	PSA (IEA GHG) ³ [115]
Cost year	2006	2006	1992
CO ₂ recovery rate (%)	85	85	95
CO ₂ purity (%)	48	48	
Energy penalty (%)	30	35	40
Total Capital Cost (US\$/kW)	1.3	1.45	1.5
Capture Cost (US\$/ton of CO ₂ avoided)	51	57	64

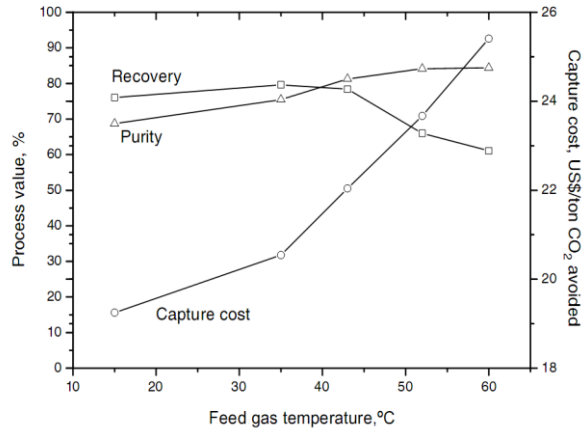
¹ PSA denotes pressure swing adsorption; ²VSA vacuum swing adsorption; ³IEA GHG International Energy Agency for Green House Gas.

Ho *et al.* [47] and Rueiner *et al.* [115] represent estimated CO₂ capture costs for pressure swing adsorption (PSA) and vacuum swing adsorption (VSA) with commercial zeolite 13X in the range from \$51 to \$57/ton of CO₂ avoided (Table 4). Capital costs ranged from \$1.3×10⁶ to \$1.5×10⁶. The International Energy Agency for Green House Gas (IEA

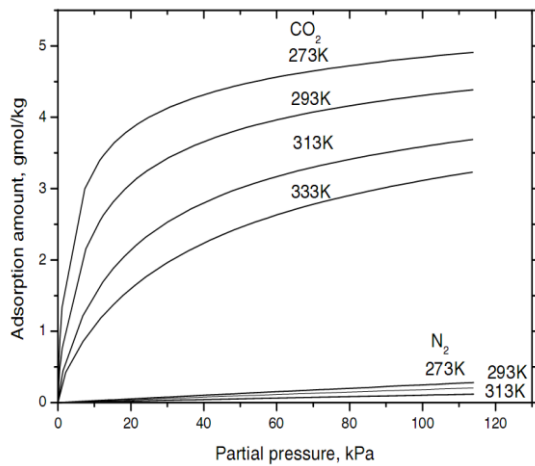
GHG) studied CO₂ adsorption costs with the PSA process applied to the flue gas of power plants [115]. It estimates that capture cost and capital cost are US \$64/ton of CO₂ avoided and 1.5 US\$/MW, respectively.



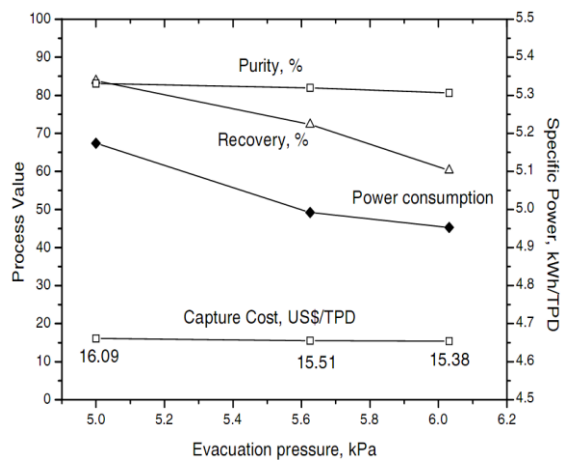
(a) Effect of initial concentration at 20°C and evacuation pressure of 3kPa



(b) Effect of temperature at 12.1% CO₂ concentration and evacuation pressure of 3kPa



(c) Isotherms for CO₂ and N₂ adsorption



(d) Effect of evacuation pressure at 15°C and 12.1% CO₂ concentration

Figure 15. CO₂ Vacuum Swing Adsorption (VSA) on zeolite 13X [7].

Zhang *et al.* [7] studied purity, recovery, and capital cost for the VSA process with zeolite 13X as a function of initial CO₂ concentration, temperature and evacuation pressure (Figure 15). The purity and recovery of VSA increased as the inlet CO₂ concentration increased (Figure 15a). When the concentration of CO₂ was 12%, over 80% purity and 80% recovery were shown and the estimated process cost reduced from ~ \$21/ton CO₂ avoided to ~\$10/ton CO₂ avoided. Overall, for 12.1% CO₂ concentration at 20°C, process cost is ~ \$19.5/ton CO₂ avoided. This suggests that the VSA process can be suitable for CO₂ flue gas concentrations larger than 40% in water gas shift reactors in integrated gasification combined cycle (IGCC) systems. However, it might not be suitable for low CO₂ streams (~3%) of gas turbine processes because the capture cost of VSA dramatically increases as CO₂ concentration decreases [7].

It is desirable to optimize the design parameters of VSA by adding some steps in VSA such as an improvement of vacuum pressure intensity, an increase in reaction temperature, and the development of appropriate adsorbents to use VSA in IGCC systems. Capture costs increased with temperature due to an additional energy input (Figure 15b). Purity improved as the temperature increases predicted by the adsorption isotherms, but the trend of recovery was different from that of purity (Figure 15b). Recovery increased slightly up to 35°C, and then gradually decreased due to the decrease in capture capacity of the zeolite 13X [62].

In VSA, optimizing vacuum pressure is a key to cost-effective operation. The higher the evacuation pressure, the higher the power consumption and the lower the recovery (Figure 15d). Adsorption isotherms for CO₂ also explained the relationship among purity, recovery, and vacuum pressure (Figure 15c). At low pressure (0 to 6 kPa) through the

temperature range, the increment levels in the isotherms have steep slopes, indicating that selection of the right pressure at desired temperatures is important to achieve optimal purity and recovery in the VSA process.

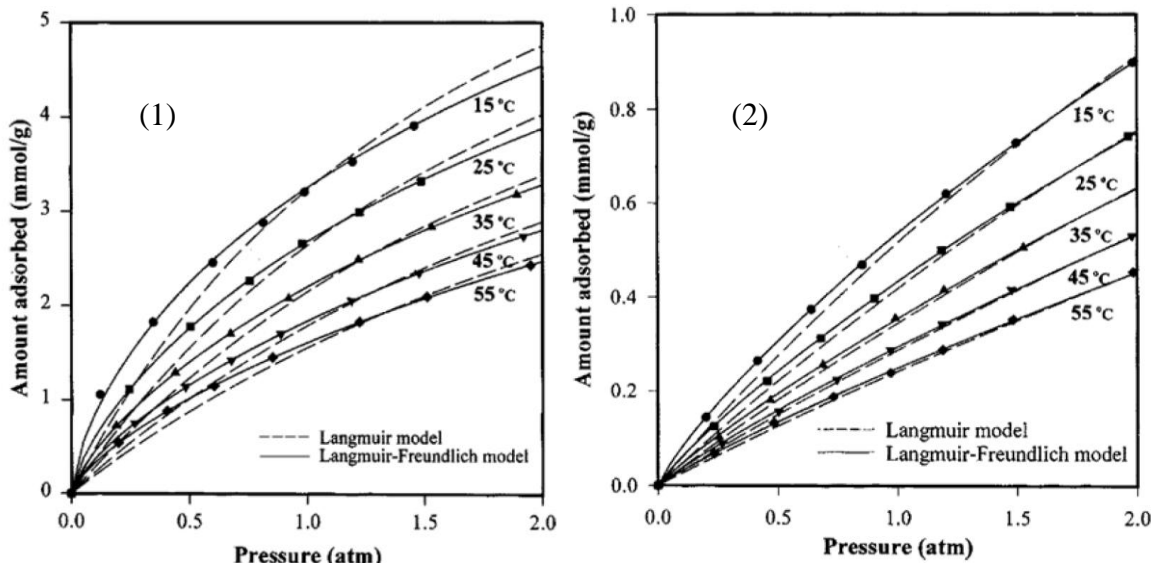
There are a few issues with the use of zeolites. First, in the presence of water vapor in concentrations typical of flue gas from power plants, CO₂ capture capacity is reduced due to the higher affinity to zeolite surfaces for water molecules compared to CO₂ molecules [69]. Secondly, the CO₂ sorption capacity of these sorbents decreases as temperature increases [67, 72, 87, 90] while many other sorbents show the opposite behavior [3, 14, 16, 78, 92, 98, 116]. Thus, in applications to commercial systems, it is important to find the optimal temperature range.

2) Activated carbon

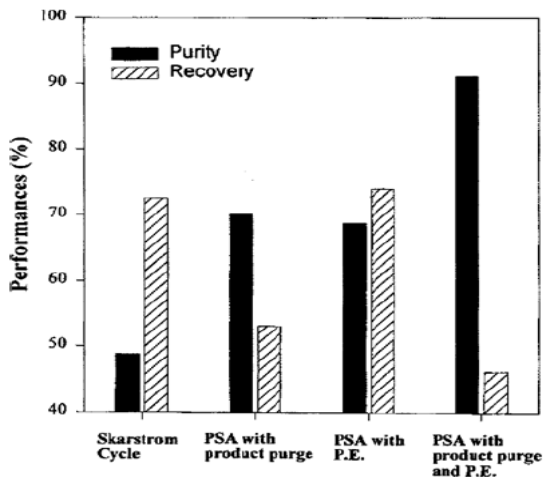
The meso- or microporous carbonaceous structures of activated carbons (AC) are widely considered as some of the strongest molecular sieves due to their highly adsorptive properties, which results from their potentially high surface area (over 1000m²/g) and large pore volume (over 0.6 mL/g). In addition, ACs have lower cost and higher hydrophobicity than zeolites.

The adsorption isotherms of CO₂ and N₂ on activated carbon have been carried out in the pressure range of 0 atm to 2.0 atm and the temperature range of 15°C to 55°C to evaluate the adsorption properties (Figure 16a) [8]. CO₂ was adsorbed on activated carbon in amounts that were over four times larger than N₂ over the temperature range, showing that activated carbon has a high selectivity for CO₂ over N₂. The Langmuir-Freundlich model (Eq. 3) simulated the isotherms better than the ordinary Langmuir model (Eq. 2) for both gases. This

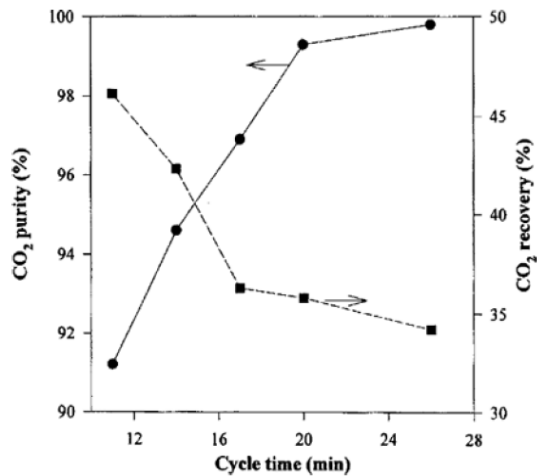
higher accuracy in describing the adsorption process is due to the larger number of parameters (three) in the Langmuir-Freundlich model compared to those in the ordinary Langmuir model [117].



(a) Adsorption Isotherm of CO₂ (1) and N₂ (2)



(b) Purity and recovery of CO₂ with various processes in PSA system.

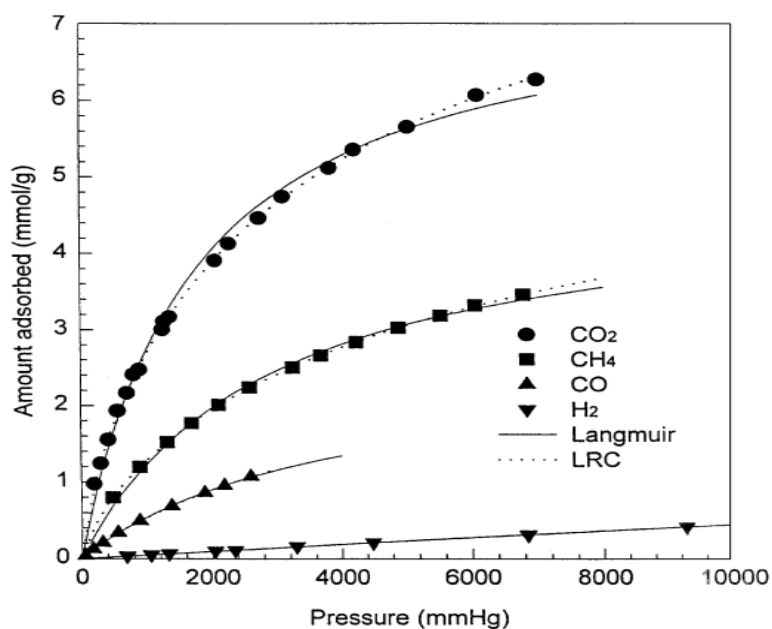


(c) Effect of cycle time on the purity and recovery of CO₂

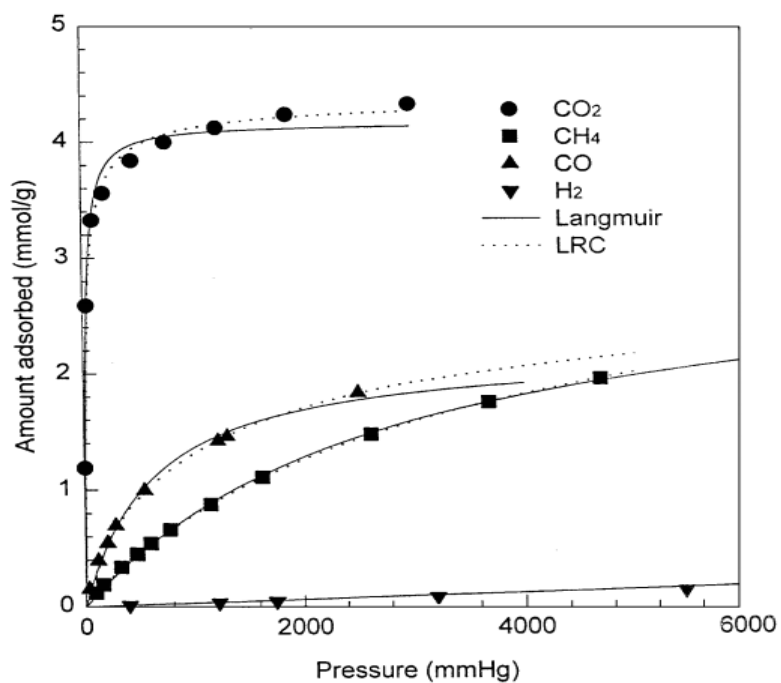
Figure 16. Evaluation of activated carbon on the basis of isotherm, purity and recovery [8].

Na *et al.* [8] employed product purge and pressure equalization, and discussed the purity and recovery of CO₂ in the PSA system to evaluate the addition of operating processes for the improvement of the adsorption capacities (Figure 16b). The purity and recovery of CO₂ were ~50% and ~72%, respectively for the typical PSA operating cycle, including pressurization, adsorption, depressurization and regeneration. The amount of N₂ gas adsorbed during desorption in the depressurization step resulted in the differences in purity and recovery [8]. The PSA system with additional processes (i.e., product purge and pressure equalization) produced similar performances for purity. When both product purge and pressure equalization are included, the purity of CO₂ increased significantly to ~ 91%. However, the recovery decreased to ~46%, leading to poor overall performance because the purge step does not enhance the N₂ desorption rate. Thus, the most cost-effective process with the highest recovery of gas species for PSA uses only pressure equalization. As for the effect of adsorption/desorption cycle times on the purity and recovery of CO₂ and N₂, the purity increases with an increase in the cycle time, whereas the recovery decreases (Figure 16c) [45]. An optimum cycling times is observed at ~15 minutes.

Park *et al.* [48] investigated the PSA process using a double-layered sorbent bed with two adsorbents, activated carbon and zeolite 5A for multi-component (H₂, CO₂, CH₄, and CO) adsorption for another configuration of process improvement to enhance adsorption capacity. For activated carbon (a) and zeolite 5A (b), the selectivity of CO₂ is significantly higher compared to the selectivity of other gases on both adsorbents (Figure 17). However, strong CO₂ adsorption at low pressures (high affinity) on zeolite 5A is an issue because low pressure swings are not effective for selectivity.



(a)Equilibrium isotherms on activated carbon at 299K



(b)Equilibrium isotherms on zeolite 5A at 298K

Figure 17. Equilibrium isotherms of a double layer PSA system for multi-gas components [48]. LRC denotes the loading ratio correlation (LRC) isotherms.

Park *et al.* [48] evaluated an optimal design of a layered column to determine the maximum capacity of adsorbents, adjusting feed quantities of each adsorbent since two adsorbents have a different affinity of inlet gas species in the double layered column. A short layer height of the activated carbon resulted in an unused region in the zeolite layer when CO₂ begins to break through the activated carbon whereas a long layer height of the activated carbon can cause an unused region in the activated carbon layer when CO or CH₄ initiate to be adsorb through the entire column length [48]. Therefore, the layer height of activated carbon should be optimized to reduce the unused column portion, and the feed amount for adsorption in the double layered column should also be maximized at this optimal column height. When the activated carbon bed length was ~74 cm out of the total bed length of 120cm, the rate of feed quantities on the double layered sorbent reached their maximum (Figure 18). Thus, the optimal ratio of layered bed length for activated carbon over zeolite 5A was found to be 0.62.

According to the bidisperse pore models involving the micropore or macropore structures of the activated carbons, the CO₂ adsorption of activated carbons is dominated by diffusional mass transport. Because of their equilibrium capacity over the short kinetic time, the CO₂ adsorption kinetics on activated carbons is comparable to those on zeolites. However, since activated carbons have a high affinity for water vapor, resulting in their low CO₂ adsorption capacity, an additional modification of the surface functionalities of activated carbon is required for feasible application because the flue gas of coal-fired power plants contains 8% to 12% water vapor.

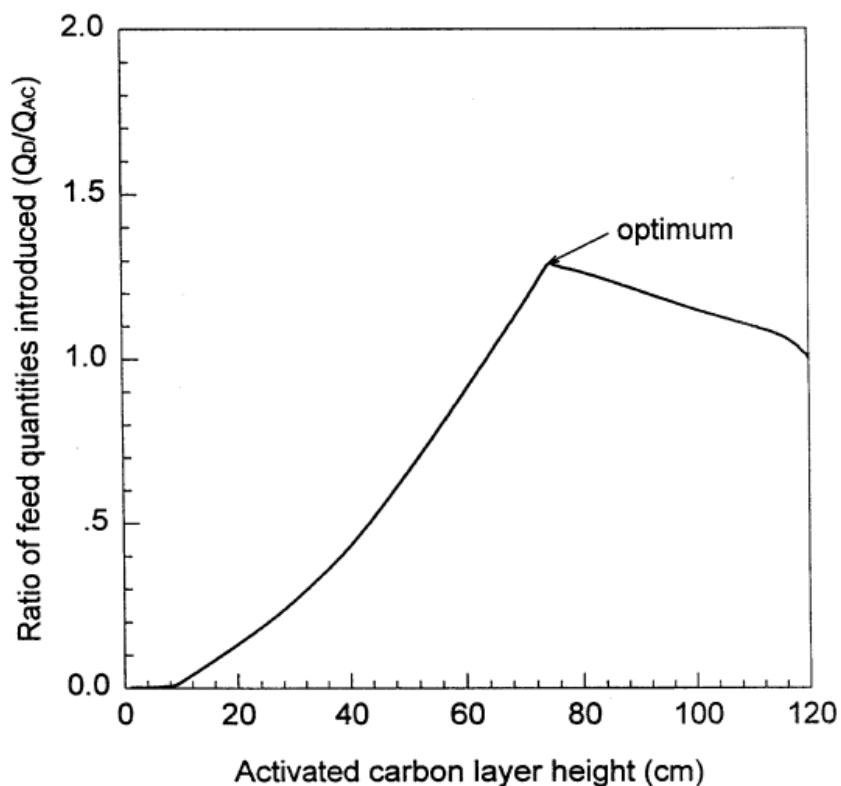


Figure 18. The effect of layer length on a double layer PSA system for multi-gas components [48]. Total bed length: 120cm; Q_D : total inlet into a layered bed; Q_{AC} : total inlet into a pure carbon bed, 14.8% vol CO_2 at 17.0 atm

3) Amines

Monoethanolamine (MEA) has been utilized to make detergents, emulsifiers, polishes, pharmaceuticals, corrosion inhibitors, and chemical intermediates [118]. Moreover, the reaction of MEA with ammonia produces the chelating agent, ethylenediamine (EDA) [118]. Both EDA and MEA have been utilized for CO_2 separation in the gas and oil industries for several decades. Based on the thermodynamics of amine-modified supports, CO_2 adsorption capacity decreases as the temperature increases due to the negative values of the heat of adsorption and the entropy of adsorption. For the evaluation of adsorption kinetics, heat-transfer limitations are a concern for the adsorption reactivity of the different types of amines

or inorganic compound-supported amines due to the high heat of CO₂ adsorption on amines and the inhibited thermal exchange of many supports, which leads to an increase in heat effects during adsorption kinetics.

Gray *et al.* [75] proposed a CO₂ adsorption mechanism on amines or amine-modified adsorbents for primary, secondary, and tertiary alkanolamines, which react with dissolved CO₂ to produce amine carbamates and carbonates. Solid amine CO₂ sorbents provide similar reaction patterns to those produced with CO₂, water vapor, and the amine functional group. DRIFTS and in-situ infrared (IR) analysis support these proposed sorption pathways on aminated adsorbents. IR peaks correspond to carbamate, carbonate, and bicarbonate species produced via CO₂ adsorption with amine functional groups. The mechanisms of the interaction between CO₂ and amines depend on the amine structure. The reaction mechanism for CO₂ adsorption on primary, secondary, or tertiary amines that contain an amine functional group surrounded by a crowded steric environment is as follows [119-121]:

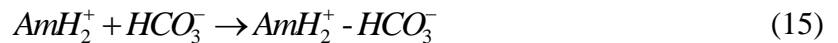


where AmH is alkanolamine that contains hydroxyl (-OH) and amino (-NH₂, -NHR, and -NR₂, R=C₂H₅) functional groups on an alkane backbone and B is a base. Primary and secondary amines can react with CO₂ to form carbamate compounds through the production of zwitterionic intermediates. For the zwitterionic mechanism and the formation of carbamate suggested by Caplow *et al.* [119], the lone pair of the amine functional group is attached to the carbon from CO₂ to produce the zwitterions, and then a free base deprotonates the

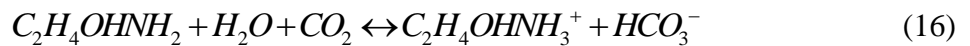
zwitterions to form the carbamate. In the aqueous phase, this base can be another amine, H₂O, or OH⁻.

For secondary amines, the amino group is bound to a secondary or a tertiary carbon atom [122]. Under dry conditions without H₂O and OH⁻, the maximum amine efficiency (i.e., the quantity of absorbed CO₂ over amine loading) of an amine adsorbent is 0.5 mol CO₂ per mol N, whereas under moist conditions with H₂O acting as a base, the maximum amine efficiency is 1.0 mol CO₂ per mol, indicating that an amine reacting with H₂O or OH⁻ provides more capacity for CO₂ capture.

In the case of tertiary amines, the reaction mechanism for CO₂ adsorption is different from those using primary and secondary amines. Rather than reacting directly with CO₂, tertiary amines catalyze the production of bicarbonate. Donaldson *et al.* [123] discusses the mechanism of the base-catalyzed hydration of CO₂ for the reaction of CO₂ with tertiary amines. The reaction mechanism for CO₂ adsorption on tertiary amines is as follows [120, 121, 123]:



First, the tertiary amine dissociates H₂O to produce a quaternary cationic species, and OH⁻ reacts with CO₂ to produce the bicarbonate anion. Then, the ion of the protonated amine and bicarbonate are coupled. For example, the MEA equilibrium for CO₂ capture in aqueous medium is:



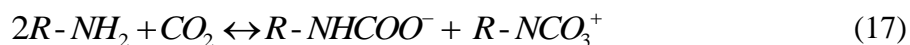
Following this reaction pathway, 1 mole of CO₂ reacts with 1 mole of MEA to form stable bicarbonate compounds. Forward rate constants for the reactions of CO₂ with various amines, such as, MEA, diethanolamine (DEA), triethanolamine (TEA), and methyldiethanolamine (MDEA) are in the range from 9 to 7600 mol/L·s (Table 5).

TABLE 5. Typical values of forward rate constant for CO₂-amine reactions [76]

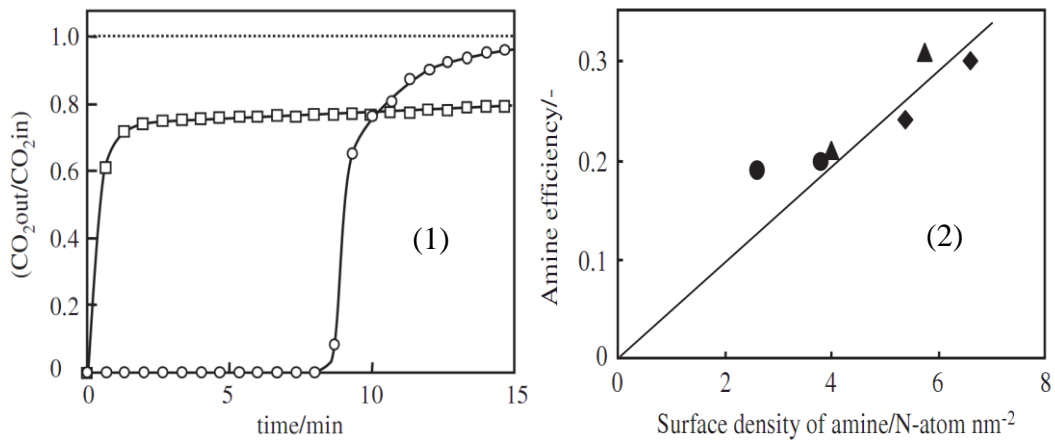
Amine type	K ₁ (mol/L s)
MEA	7600
DEA	1500
TEA	16.8
MDEA	9.2

MEA is regarded as a high potential sorbent for CO₂ separation among the various amines because the high rate of reaction results in the high rate of mass transfer [76]. However, CO₂ sorption with MEA solutions has several drawbacks: (1) low CO₂ capture capacity; (2) high energy and water consumption due to the constant temperature adjusting (up to 70% of the total operating costs in CO₂ separation plants); (3) high energy requirements for CO₂ desorption due to its high reaction heat; (4) high equipment corrosion rate; and (5) amine degradation by SO₂, NO₂, HCl, HF, and O₂ [26, 83, 124-126]. Therefore, attempts have been made with various types of solid amines, or solid amines modified by metal oxides in order to offset the weaknesses of the MEA based solution process [3, 14, 26, 38, 59, 75, 79, 83, 100, 124, 125, 127-134].

Hiyoshi *et al.* [69] investigated CO₂ adsorption on amine modified SBA-15 in the presence of water vapor (Figure 19). 3-aminopropyltriethoxysilane (denoted as APS), N-(2-aminoethyl)-3-aminopropyltriethoxysilane (AEAPS) and (3-trimethoxysilylpropyl)-diethylenetriamine (TA) were utilized as grafting agents. The impregnated samples were denoted as APS/SBA (obtained by APS impregnation into SBA-15), AEAPS/SBA and TA/SBA, respectively. The adsorption capacity of amine modified SBA-15 was much higher than that of APS/SBA (Figure 19a) [69]. Figure 19b describes the relationship between amine efficiency and amine surface density. Note that the surface density of amine is the number of nitrogen atoms over 1 nm² of the SBA-15 surface. In this study, amine efficiency is defined as the quantity of absorbed CO₂ (mmol/g) over amine content (mmol/g) at 60°C with CO₂ (15%), H₂O (12%) and balanced with N₂ (74%). The adsorption process on amine grafted SBA-15 forms ammonium carbonate is as follows [135]:



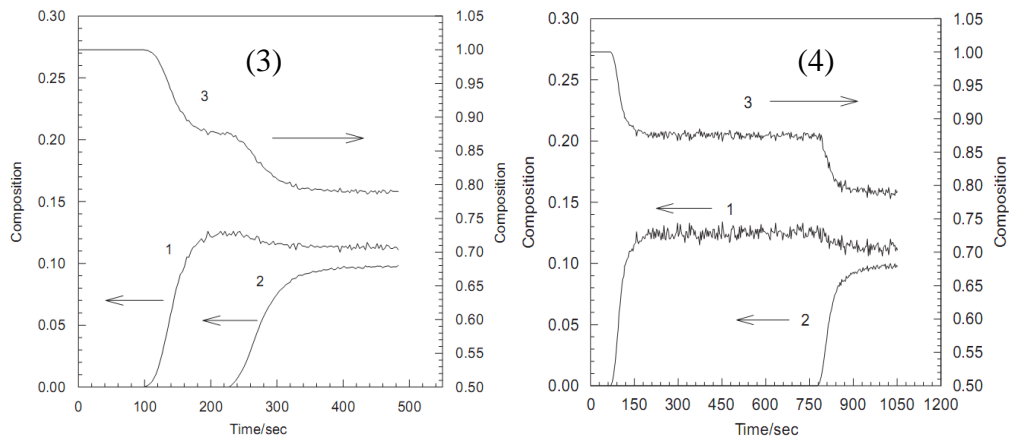
As shown, two moles of amino groups react with one mole of CO₂ to produce one mole of ammonium carbamate; isolated amine on the SBA-15 surface does not attract CO₂ for adsorption, but densely tethered aminosilane affects available adsorption sites [69].



(1) CO₂ Breakthrough profile at 60°C over TA/SBA (○) and APS/SBA(□): The mixture of 15% CO₂, 12% H₂O with N₂ balance; total flow rate: 30 cm³/min.

(2) Relationship between amine efficiency and surface density of amine over 3-aminopropyltriethoxysilane (APS (●)), N-(2-aminoethyl)-3-aminopropyltriethoxysilane (AEAPS (▲)),(3-trimethoxysilylpropyl)-diethylenetriamine (TA (◆))

(a) Adsorption of carbon dioxide on amine modified SBA-15 with water vapor



(3) CO₂ Breakthrough profile on SBA-15 without TEA-modification: The mixture of 9.74% CO₂, 11.22% CH₄ with He balance; total flow rate: 100 cm³/min; pressure: 0.5Mpa. 1:CH₄; 2: CO₂; 3:He

(4) CO₂ Breakthrough profile on SBA-15 with TEA-modification: The mixture of 9.74% CO₂, 11.22% CH₄ with He balance; total flow rate: 100 cm³/min; pressure: 0.5Mpa. 1:CH₄; 2: CO₂; 3:He

(b) Separation of carbon dioxide and methane on TEA grafted SBA-15

Figure 19. Breakthrough profiles of carbon dioxide on amine modified SBA-15 [59, 69].

Amine efficiency, defined again by the quantity of sorbed CO₂ (mmol/g) over amine content (mmol/g) at 60°C with CO₂ (15% vol), H₂O (12% vol) and balanced with N₂, shows nearly linear dependence with N-atom surface density (the number of nitrogen atoms on the surface area) for different supports, indicating that the length among tethered amines on the surface is an important parameter for CO₂ adsorption (Figure 19b). The increase in the surface density leads to an increase in the N-H bond and C=O stretching intensities from ammonium carbonate.

TEA grafted SBA-15 was selected for the evaluation of the selectivity of modified amines, the study yielded the breakthrough curves of CO₂ and CH₄ without TEA and with TEA (Figures 19c and 19d). The breakthrough profile of Helium (He), the balance gas for the gas mixture, is much more different than CO₂ and CH₄. Without TEA modification, the breakthrough profile of CO₂ and CH₄ is not suitable for separation due to the high affinities of carbon to the SBA-15 frame work. On the other hand, with TEA impregnation, the breakthrough time of CH₄ becomes shorter, from ~100 seconds to ~40 seconds, and for carbon dioxide the breakthrough time becomes much longer, from ~230 seconds to ~775 seconds, indicating that TEA grafted SBA-15 enhances the separation capability of CO₂ from a gas mixture.

4) Organic/Inorganic Hybrid Materials

Recently, new organic/inorganic hybrid materials have shown great potential for carbon dioxide capture, resulting from an increase in the accessible number of sorption sites per mass of sorbent. Sorbents in this category include covalently amine-impregnated silica supports such as amine-modified silane and polymerized reactive amine on silica. The

common synthesis methods for covalently amine-impregnated adsorbents are saline chemistry and polymerization. The schematic structures of various amines found on amine-impregnated mesoporous silica (SBA-15) created by surface reaction and surface polymerization, as shown in Figure 20 [77]. The grafting process of the hybrid aminosilica is achieved by accumulating alkoxy groups from using silane chemistry on the surface silanols to create covalent bonds to the silica surface through the breaking of Si-O-Si bonds, including organic functionalities through substitution on the silane [136]. These silane-modified samples can be reformed to make large amine-loaded dendritic structures that are tethered mainly in the pore space [136].

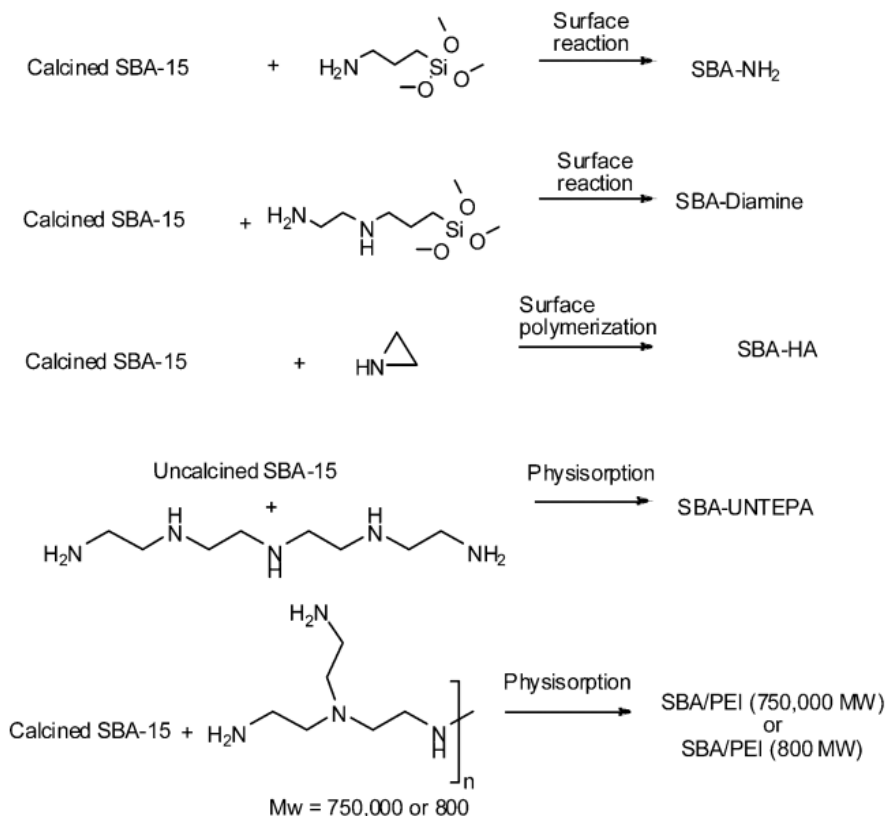


Figure 20. Schematic structure of various amines modified SBA-15 [77].

Due to the distinct chemical nature of individual species, meaning their different structures, morphologies, and spatial arrangements, the complex structural layer of organic materials formed during amine impregnation can be easily changed with a simple modification of synthesis conditions. In addition, inorganic supports can themselves become suitable supplementary materials for a complex structural layer of organic and inorganic materials.

Organic polymers and inorganic materials have also been combined by mutual dispersion at the molecular level [137-140]. Since sorbents with a three-dimensional structure of inorganic components such as silica dispersed at molecular dimension in organic components provide more stability for dynamic intermediate species, these hybrid materials can be readily regenerated for adsorption [140]. Unlike many different kinds of amine-modified silica, organic/inorganic hybrid aminosilica with high amine-loading has good stability and recovery capacity for multiple cycles. However, the regeneration ability of the amine-tethered supports synthesized by physisorption methods is inhibited. Although physically tethering low molecular weight amines onto the supports leads to a high loading of amine, the materials suffer from degradation due to leaching of the organic polymers from the supports because of weak linkages between amines and supports. If an approach can be found to make the organic polymers remain linked, the regeneration stability will improve [77].

Hick *et al.* [77] synthesized covalently silica-grafted hyperbranched aminosilica (HAS) with a high loading of amine adsorption sites. Such organic/inorganic hybrid aminosilicas are easy to synthesize, have strong covalent organic/inorganic linkages, and are potentially low cost [77]. HAS created by polymerization of aziridine is prepared by mixing

the silica substrate with a precursor of the amine polymer in solution [77]. The HAS synthesis produces Si-O-C bonds through ring-opening polymerization with surface OH groups on the silica surface. Aziridine can be polymerized off of silane-functionalized surfaces that contain nucleophilic reactive amines [136]. In the final product, the amine polymer is bound on the silica surface. Since HAS has a low surface area, mesoporous silica (SBA-15) supports are substituted to produce hybrid aminosilicas with high-loading amine adsorption sites over a high surface area. The synthesis leads to highly cycleable CO₂ capture capacities because SBA-15 supports have strong covalent bonds between amines and supports, leading to fully regenerable capacity during multiple cycles of ad/desorption [77].

Other organic/inorganic hybrid materials which have recently received significant attention are the metal-organic frameworks (MOFs) developed by Yaghi and coworkers [109]. MOFs are attractive because of their high thermal stability, modifiable chemical functionality, and crystalline, highly well-ordered, porous structures [109]. MOFs typically have three-dimensional organic–inorganic hybrid networks bound by different combinations of the metal–ligand bonds, creating hubs, linked by struts consisting of organic compounds. The special nature of MOFs provides a number of combined networks of topologies, many types of arrangements for strut linkages, and strong metal-ligand bonds in the structure, resulting in the production of various types of MOFs. MOF-5 ($Zn_4O(BDC)_3(DMF)_8(C_6H_5Cl)$, where BDC=1,4-benzenedicarboxylate and DMF=N,N'-dimethylformamide) consisted of tetranuclear supertetrahedral clusters connected by bidentate BDC ligands into an octahedral arrangement [141]. The DMF molecules were substituted for dichloromethane molecules by solvent exchange, and the void sites were created by application of a vacuum removing clusters of dichloromethane.

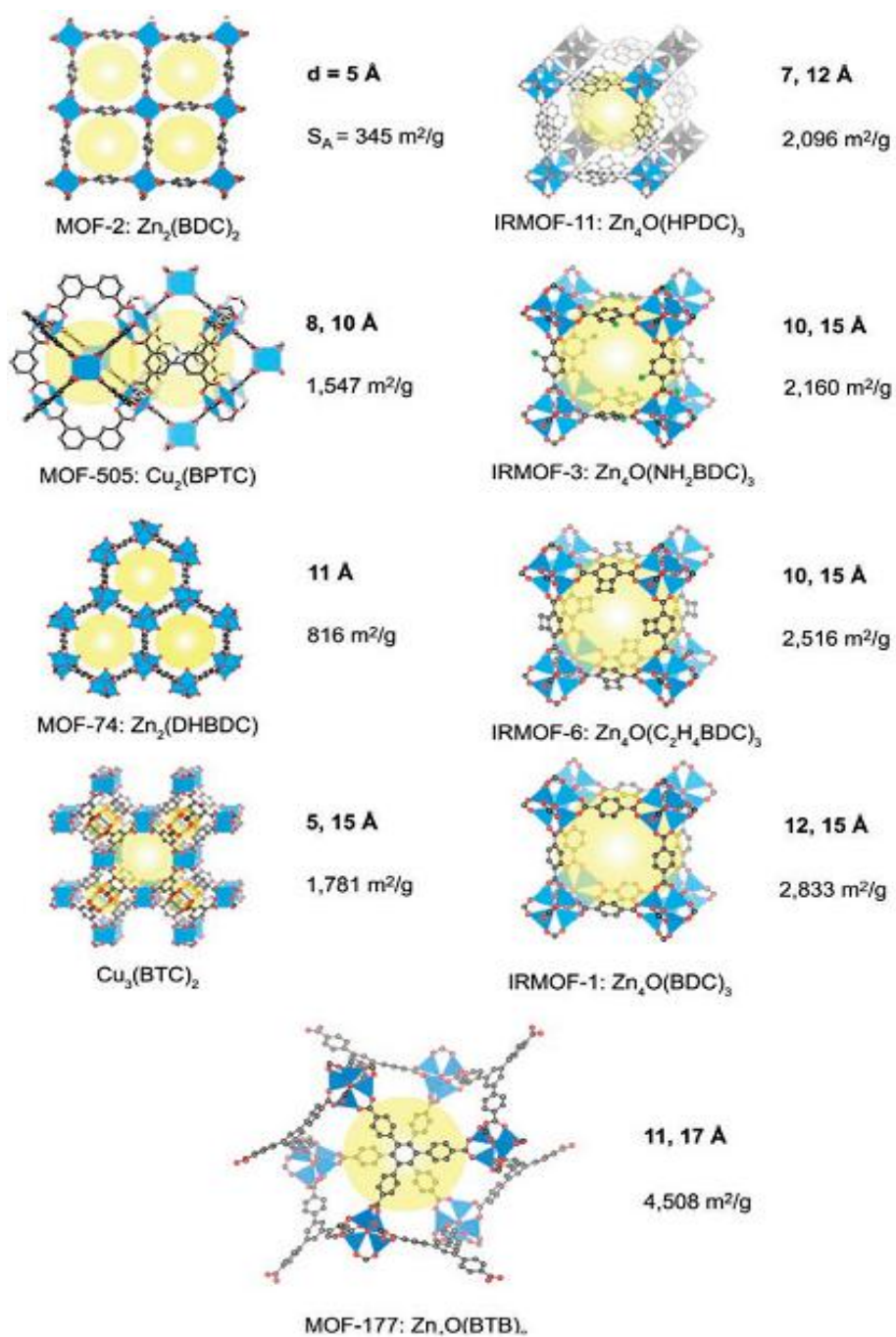


Figure 21. Different crystal structures of MOFs at room temperature. For each MOF, the framework formula, pore size, surface area are shown [109].

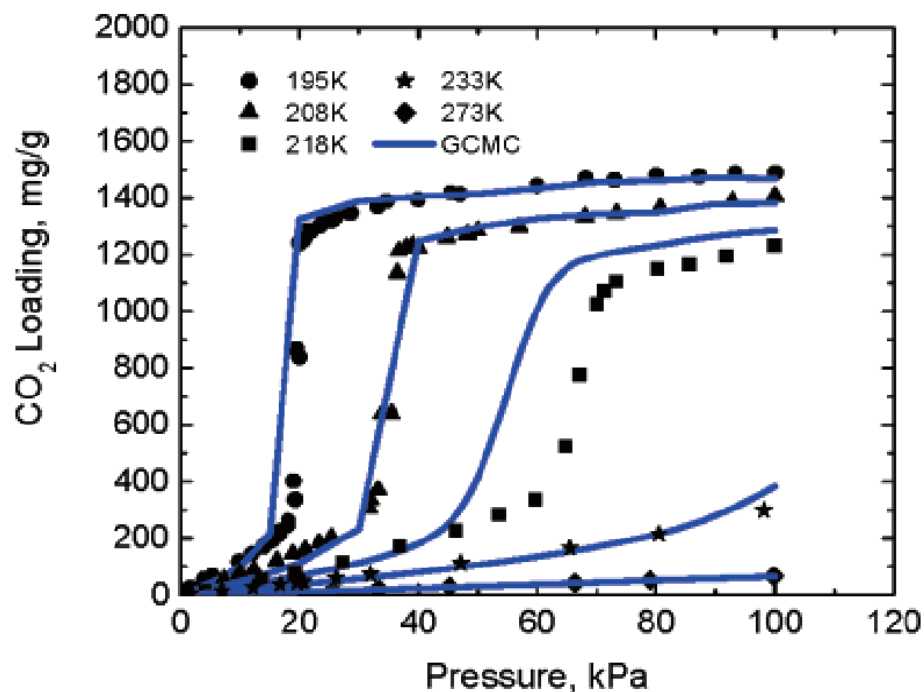


Figure 22. Comparison of GCMC simulations and experimental adsorption isotherms for CO₂ in IRMOF-1 [110].

MOFs provide many types of cross-section framework schemes, such as square channels (MOF-2), pores decorated with open metal sites (MOF-505 and Cu₃(BTC)₂), and hexagonally-packed cylindrical channels (MOF-74). Other types of MOF are interpenetrated structures (IRMOF-11), MOFs with amino- and alkyl-functionalized pores (IRMOFs-3 and -6, respectively), and the extra-high porosity frameworks, IRMOF-1 and MOF-177 (Figure 21) [109].

Millward and Yaghi presented the results of adsorption equilibrium at room temperature to evaluate the adsorption capacity for CO₂ on different MOFs [109]. They found MOF-177 has a higher adsorption capacity than conventional adsorbents such as zeolite 13X and activated carbon. For the evaluation of adsorption properties, Figure 22 shows experimental adsorption isotherms developed using a molecular model in IRMOF-1

(MOF-5). The molecular model can provide the reaction patterns and steps that account for the mechanism of CO₂ adsorption over a wide temperature range. Grand canonical Monte Carlo (GCMC) simulation provides the modeling results. Adsorption isotherm models show S-shaped isotherms that result from the very large pore sizes [110].

Many kinds of MOFs have a potential to adsorb CO₂ in the range of 0.15 to 1.5g CO₂ per g MOF [109]. IRMOF-1 also has a high adsorption capacity, about 1.5 g CO₂/g MOF. The molecular model shows good agreement with the experimental results. Below the state of a rapid increase in capture capacity in the isotherm graph (Figure 22), CO₂ molecules mainly fill the pores of the networks of the MOF cavities with an increase in pressure. This profile trend, known as a type V isotherm, can lead to hysteresis, but the experimental and model results have not find this to be the case in this material [142]. The shape of the isotherm plots results from favorable electrostatic interactions between CO₂ molecules [142].

5) Lithium zirconate

Alkali metal materials (e.g., Li₂O, Na₂O, K₂O, Rb₂O, and Cs₂O) generally provide lower adsorption capacity and require more energy for carbonation and calcination compared to alkaline-earth minerals such as CaO and MgO. Another type of lithium-based oxide, however, Lithium zirconate (Li₂ZrO₃) has attracted attention as a promising sorbent for CO₂ adsorption at high temperatures (in the range of 400°C to 800°C) due to its highly stable adsorption reactivity and thermal stability. Carbonation and calcination are expressed by the reversible equilibrium reaction as follows:



Lithium zirconate has a high capture capacity (~4.5 mmol/g) and good stability over many regeneration cycles [81, 86, 103]. Moreover, it has high selectivity for CO₂ and low affinity for N₂ [81]. At atmospheric pressure, the forward reaction (carbonation) is thermodynamically favorable up to 800°C. Calcination dominates at temperatures above 800°C. The XRD pattern for structure modification during sorption and desorption indicates that CO₂ carbonation using Li₂ZrO₃ is reversible [86].

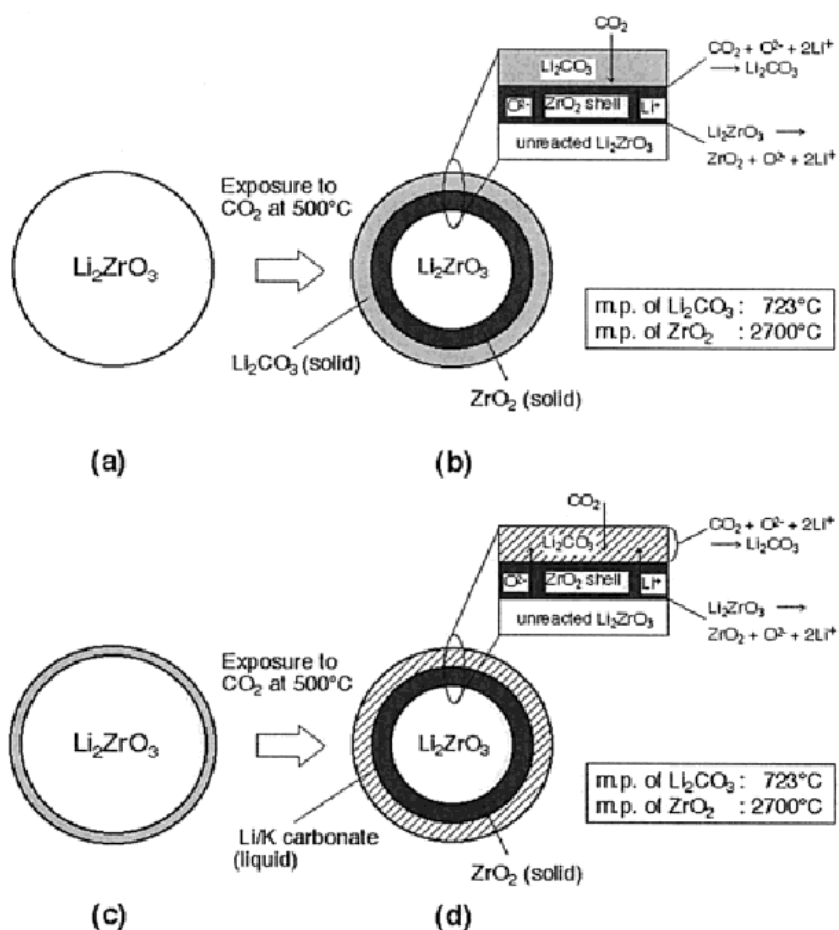


Figure 23. Schematic diagram of the proposed mechanism for CO₂ adsorption on Li₂ZrO₃ [86].

Fauth *et al.* [80] examined Li_2ZrO_3 carbonation modified with alkali (Li, K, and Na) and with alkali/alkaline (K, Mg) carbonate. The CO_2 adsorption rate increases as the CO_2 diffusion rate increases in the range of 400°C to 800°C [86, 103]. In addition, binary $\text{K}_2\text{CO}_3/\text{MgCO}_3$ and KF with pure Li_2ZrO_3 have a faster CO_2 sorption rate at 500°C than only pure Li_2ZrO_3 since the additional carbonation reaction using potassium occurs and then forms carbonates. Li_2ZrO_3 , modified by NaF/ K_2CO_3 with Na_2CO_3 , had the highest capture capacity and the fastest CO_2 sorption rate at 600°C and 700°C .

Ida *et al.* [86] described a proposed double-shell mechanism for CO_2 adsorption and desorption on Li_2ZrO_3 (Figures 23 and 24, respectively). For adsorption, the relatively fast CO_2 sorption may initiate before the formation of a dense Li_2CO_3 shell on the surface and before the formation of a dense solid ZrO_2 shell in the core surrounded by the non-reacted solid Li_2ZrO_3 [86]. After the formation of the Li_2CO_3 and ZrO_2 shells, the carbonates thicken, inhibiting CO_2 sorption into the non-reacted pore regions of materials. Thus, the process rate decreases even though adsorbates continue to react with the exposed surface and pore of the sorbents. After dominant kinetics, additional reactions on the non-reacted Li_2ZrO_3 surface produces Li^+ and O^{2-} ions, and CO_2 may diffuse interstitially through the Li_2CO_3 shell and react with Li^+ and O^{2-} on the surface of the ZrO_2 shell [86]. O^{2-} can fill up open sites and Li^+ can diffuse through the ZrO_2 shell since ZrO_2 provides a large number of oxygen vacancies in its crystals [86, 143]. Because the ion sizes of Li^+ and O^{2-} are considerably smaller than those of CO_2 , the diffusion rate of CO_2 into the Li_2CO_3 layer is slower than that of both ions; thus, CO_2 diffusion is the rate-limiting step.

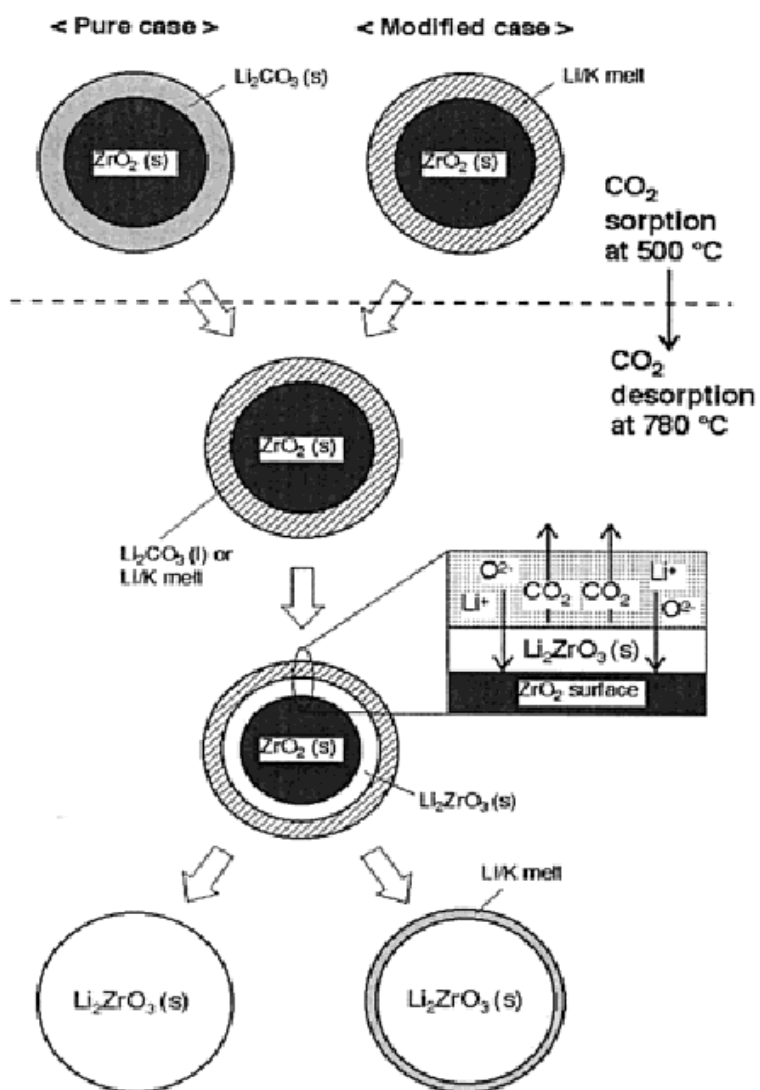


Figure 24. Schematic diagram of the proposed mechanism for CO₂ desorption on Li₂ZrO₃ [86].

The Li₂CO₃/K₂CO₃ layer encompasses Li₂ZrO₃ at high temperatures, and changes into molten carbonates due to its lower melting point. CO₂ diffuses through this layer and reacts with Li₂ZrO₃ since CO₂ diffusion in the molten carbonate is much faster than in the solid carbonate Li₂ZrO₃ (Figure 23c and 23d) [86, 144]. At the same time, Li₂CO₃, which is immediately produced, combine with the molten carbonate. This step results in an increase in

the volume of the molten carbonate layer, which can lead to a higher CO₂ sorption rate on the modified Li₂ZrO₃. Therefore, the carbonation reaction is limited by Li₂CO₃ formation as well as the ion transport in the ZrO₂ shell.

For a CO₂ desorption process, the experimental temperature is increased to 780°C, which is higher than the melting point of Li₂CO₃. Thus, both Li₂CO₃ in the Li₂ZrO₃ and the lithium/potassium carbonate mixture in the modified Li₂ZrO₃ are formed in the molten phase (Figure 24) [86]. First, Li₂CO₃ reacts with ZrO₂ to form Li₂ZrO₃ and CO₂ reversibly. Second, CO₂ diffuses through a liquid Li₂CO₃ or Li₂CO₃/K₂CO₃ mixture to the outside, and during the formation of the dense Li₂ZrO₃ shell, Li⁺ and O²⁻ keep diffusing through the Li₂ZrO₃ shell for CO₂ desorption [86]. Ida *et al.* [86] and Fauth *et al.* [80] found that the CO₂ sorption rate depends on CO₂ diffusion and Li⁺ and O²⁻ ions transport within the outer layer of the solid Li₂O₃ shell.

6) Sodium based sorbent

Alkali metal carbonates such as K₂CO₃ and Na₂CO₃ have received some attention since they easily react with carbon dioxide and water vapor to form alkali metal bicarbonate. In the presence of water vapor, chemical reactions can be reversed at relatively low temperatures for the regeneration of the sorbents. Seo *et al.* [16] carried out CO₂ carbonation and calcination with water vapor on a sodium-based solid sorbent.

The reaction sequence is:



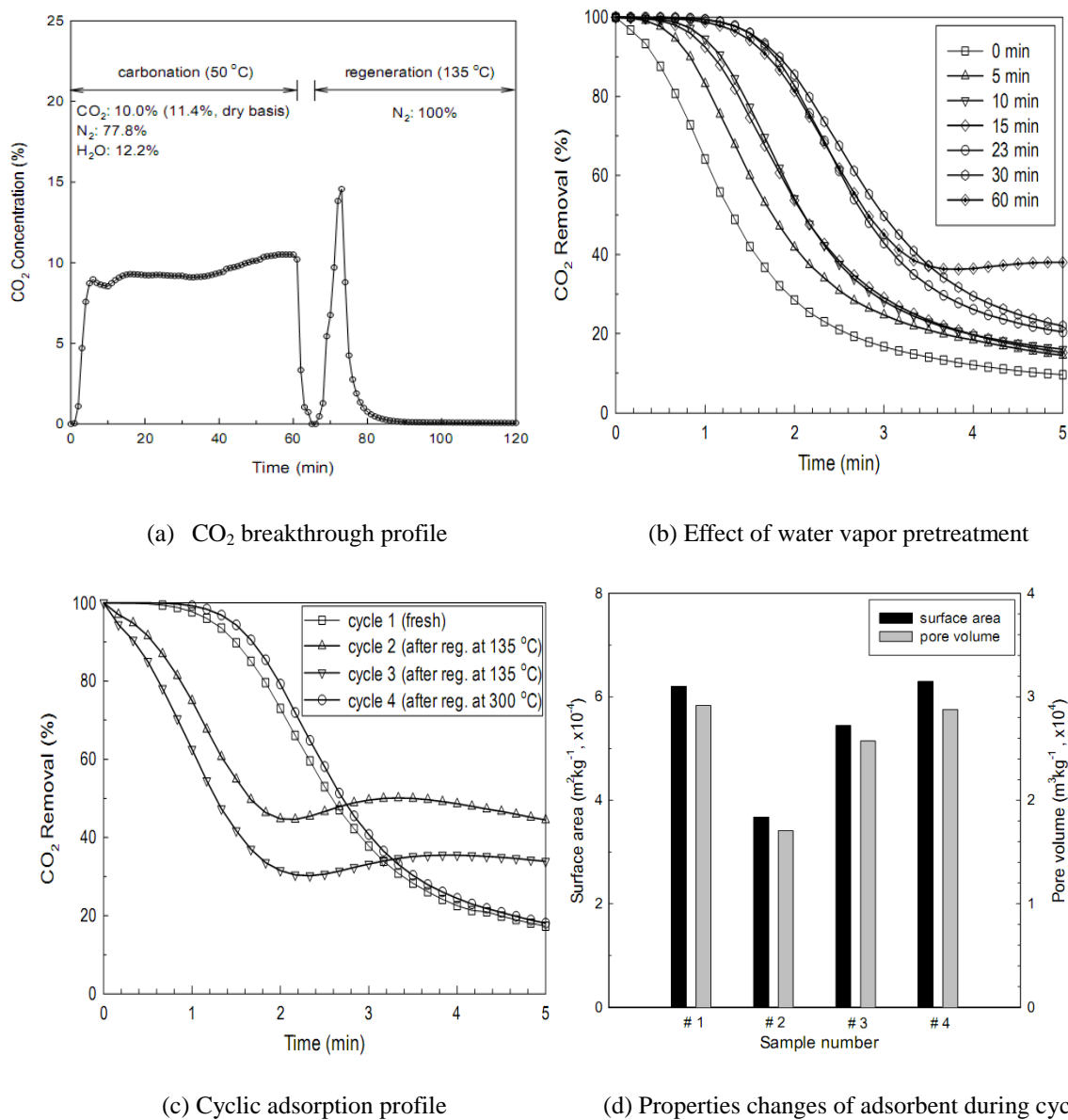


Figure 25. The Temperature Swing Adsorption (TSA) System on sodium-based solid sorbent [16]. Note for (d): sample #1: Dried fresh sample at 300°C; #2: 50°C carbonation for 1hr after 30min pretreatment; #3: 135°C regeneration for 1hr under N₂ after sample #2; #4: 300°C regenerated for 1hr under N₂ after sample #2.

Seo *et al.* [16] used a fluidized-bed reactor for the high rate of mass and heat transfer since heat release can reverse the carbonation process during the highly exothermic chemical adsorption. They created Sorb NX35 (35% Na₂CO₃, and 65% support and binder) and used it with water vapor pretreatment in a bubbling fluidized-bed reactor using the TSA system (Figure 25a). They conducted the adsorption experiments at 50°C using a simulated flue gas mixture (10% CO₂, 77.8% N₂ and 12.2% H₂O) and the regeneration experiments at 135°C using pure N₂.

Experiments using a Sorb NX35 adsorbent with water pre-treatment show a high capture capacity of 8.1g CO₂/g adsorbent and 90% regeneration capacity because a pre-treatment step enhances the capture capacity (Figure 25b). Without water vapor pretreatment, CO₂ capture capacity decreases exponentially whereas with water vapor pretreatment, it increases with the length of duration of the pretreatment. This result suggests that water vapor pretreatment, instead of being just a reactant in the reaction (Na₂CO₃ +CO₂ +H₂O ↔ 2NaHCO₃), can play an important role in the reaction of CO₂ with Sorb NX35. However, overexposure to water pretreatment above the appropriate duration causes a loss of CO₂ capture capacity and of regeneration level due to the damp agglomeration of the adsorbent and a higher affinity of the H₂O molecules to the sorbent's surface compared to that of CO₂ molecules.

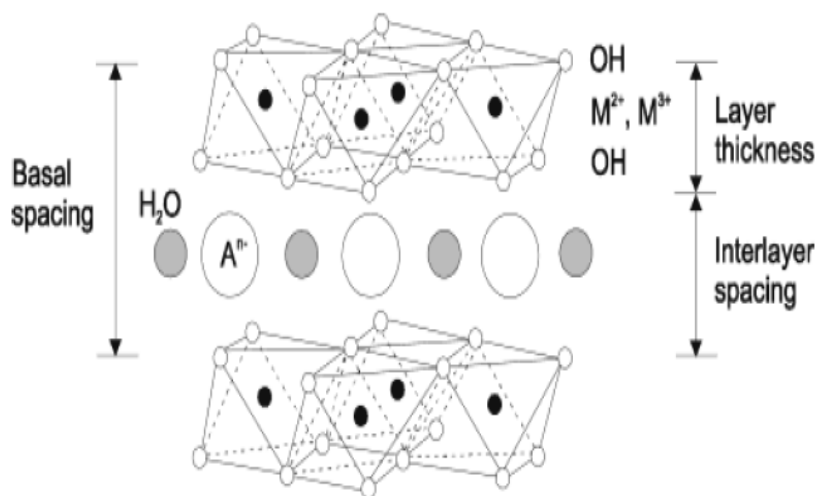
During cyclic adsorption after desorption at 135°C, CO₂ capture capacity decreases sharply (Figure 25c). This could be due to water vapor accumulation inside the sorbent pores, resulting in poor contact between the CO₂ molecules and the sorbents. When regeneration is carried out at 300°C instead of 135°C, CO₂ capture capacity closely returns to the initial capacity due to effective water removal from the sorbents and more favorable temperatures

for regeneration. They evaluated the BET surface area and pore volume of Sorb NX35 sorbents to determine the adsorption properties before and after reaction since the properties of Sorb NX35 change during multiple carbonation-regeneration cycles (Figure 25d). After adsorption, surface area and pore volume decreases significantly. These properties partly recovered after regeneration with a pure N₂ stream at 135°C. After regeneration at 300°C, they fully recovered, supporting the high regeneration capacity of the sorbents.

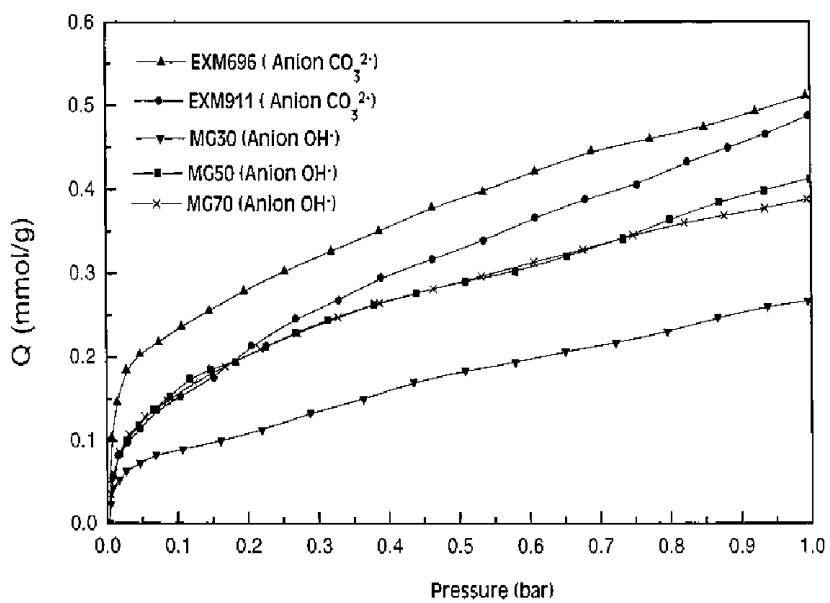
7) Hydrotalcite-like compounds (HTlcs)

Hydrotalcite-like compounds (HTlcs) are anionic and basic clays, known as layered double hydroxides (LDHs). They have been utilized as catalysts, adsorbents, catalyst supports, ion exchangers, filters, decolorizing agents, and stabilizers [71]. HTlcs consist of positively charged bidimensional layers of metal oxides (e.g., MgO) or hydroxides (e.g., Mg(OH)₂) with trivalent and divalent cations at the center of the octahedral sites in the hydroxide layer, negatively charged interlayers compensating anions, and water molecules, all of which finally result in a charge balanced framework (Figure 26a) [98, 145].

The general formula of HTlcs is described as follows: $[M_{1-x}^{2+}M_x^{3+}(OH)_2]^{x+} \cdot [A_{x/n}^{n-} \cdot mH_2O]^{x-}$, where M²⁺ and M³⁺ are divalent cations (e.g., Mg²⁺, Zn²⁺, Ni²⁺, or Cu²⁺) and trivalent cations (e.g., Al³⁺, Fe³⁺, or Cr³⁺), respectively; Aⁿ⁻ are interlayer anions (e.g., CO₃²⁻, SO₄²⁻, NO₃⁻, Cl⁻ or OH⁻), and the x value is typically (but not necessarily) in the range of 0.17 to 0.33. Excess positive charges obtained by the replacement of trivalent cations are compensated by anions and water molecules in the interlayer zone, forming a charge-balanced structure [71].



(a) Schematic structure of Hydrotalcite-like compounds



(b) CO_2 adsorption dependent on the anion type at $300^\circ C$

Figure 26. Carbon dioxide adsorption on Hydrotalcite-like compounds (HTLcs) [71, 98].

In recent years, Yong *et al.* [71] have dealt with an application of the materials for CO₂ adsorption because of their stable anion exchange, highly stable adsorption behavior, high mobility of both anions and water molecules, which result from large surface areas and the high stability of the frame structure. The adsorption activity can be enhanced when the chemical structures of hydrotalcites are modified by interchanging the metal composition of the framework or combining dopants, alkali metals, which prevents sintering of the particle. CO₂ adsorption capacities on HTlcs significantly depend on the type and amount of divalent cations, trivalent cations, and anions. Based on CO₂ adsorption for different samples with two types of anions (CO₃²⁻ and OH⁻) (Figure 26b), HTlcs with CO₃²⁻ show higher capture capacities than those with OH⁻ because HTlcs with the carbonate ions have more void space and larger interlayer spacing than the ones with OH⁻ (0.765 μm vs. 0.755 μm), so they can adsorb more CO₂ molecules [71, 146].

Reddy *et al.* [116] proposed that the optimized composition ratio of divalent (Mg²⁺) and trivalent (Al³⁺) cations is a 1:1 ratio. This ratio provides a maximum capacity of CO₂ adsorption. An increase in the amount of aluminum results in the reduction of the interlayer spaces since incorporated aluminum enhances layer charges in HTlcs, leading to a decrease in adsorption sites [116]. When anion is altered from OH⁻ to CO₃²⁻, adsorption capacities increase from 0.25 to 0.5mmol/g at 300°C and 1 bar due to larger interlayer spacing and higher layer charges in the HTlcs with CO₃²⁻ anions [116]. These results show that HTlcs with CO₃²⁻ are the optimized composition.

TABLE 6. CO₂ adsorption capacities on Mg-Al-CO₃ Layered double oxide (LDO) dependent on temperatures at 100kPa [116]

Temperature (°C)	Combined (mmol/g)	Reversible (mmol/g)	Irreversible (mmol/g)	Reversible (%)
100	0.231	0.192	0.039	87.0
200	0.486	0.429	0.057	88.3
300	0.249	0.208	0.041	83.5
400	0.169	0.132	0.037	78.1

Unlike other sorbents which provide either physisorption or chemisorption, HTIcs have a combined-sorption mechanism. Reddy *et al.* showed the properties of combined CO₂ adsorption (both physisorption and chemisorption) and of combined desorption, reversible (physical) and irreversible desorption (chemical), on Mg-Al-CO₃-layered double oxide (LDO) (Table 6) [116]. Adsorption capacities typically decrease with increasing temperatures. However, the highest capture capacity is observed at 200°C instead of 100°C because physical adsorption dominates at 100°C. This indicates that CO₂ adsorption on Mg-Al-CO₃-layered double oxide (LDO) results from both physical and chemical adsorption on different sites [98]. Over the temperature range, reversible (physical) adsorption composes over 78% of the overall adsorption. At higher temperatures (higher kinetic energies), desorption from the sorbent surface becomes favorable.

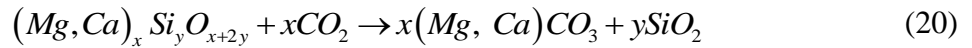
2.4 CO₂ Sequestration by Mineral Carbonation

2.4.1 Overview of mineral carbonation

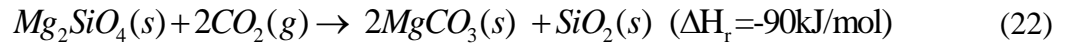
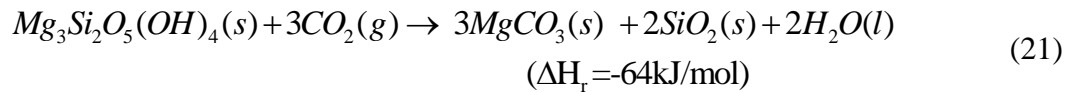
Magnesium and calcium-based minerals are considered feasible sorbents for CO₂ separation from gas mixture streams because mineral carbonation provides enormous storage capacity and the sorbent reaction is naturally exothermal [20, 34, 36]. Moreover, solid

byproducts can beneficially supply mine reclamation or be used for soil amendments because magnesite ($MgCO_3$) and silica (SiO_2) exist naturally as serpentinized rocks [18]. These potentially useful byproducts can contribute significantly to improve the cost-effectiveness of CO_2 capture [18, 36].

Large amounts of magnesium-based silicate minerals, such as olivine ($(Mg, Fe)_2SiO_4$) and serpentine ($Mg_3Si_2O_5(OH)_4$), are widely existed around the world, particularly in coastal areas [34]. Over geological time scales, olivine is eventually transformed into serpentine and magnesite ($MgCO_3$). CO_2 capture by mineral-based solids occurs when magnesium or calcium-rich minerals react with CO_2 to produce stable carbonates which are almost insoluble in water, leading to the permanent formation. The general reaction of minerals with CO_2 is as follows [18]:



For magnesium-based minerals, magnesium silicate reacts with CO_2 to form magnesium carbonate. This reaction is naturally exothermic as follows:



The heat released can be employed for CO_2 adsorption since the mineral carbonation reactions of both olivine and serpentine are exothermic [20, 34]. They are thermodynamically favorable and exothermic, but the mineral carbonation reactions are slow near ambient temperatures ($25^\circ C$) [18-20]. Therefore, a significant speeding of the carbonation reaction rate is needed for the development of an efficient system that will allow the feasible application of these sorbents. In order to improve the efficiency of CO_2 capture on these

minerals, several pretreatment processes such as magnetic separation, heat treatment, and acid treatment have been developed. This section discusses the mineral preparation, the pretreatment processes and the process of direct and indirect carbonation.

2.4.2 Mineral carbonation: A DFT quantum study

Alkaline-earth oxides are composed of silicate minerals such as wollastonite (CaSiO_3) and olivine (Mg_2SiO_4) since calcium and magnesium are not naturally available as binary oxides such as magnesium oxide (MgO) and calcium oxide (CaO), respectively. For the coordination of CO_2 to an oxygen ion, CO_2 reacts with metal oxide to form a relatively weakly bound carbonate at the MgO surface compared to a strongly bound carbonate at the CaO surface because of their different basicity (i.e., the ability degree of the surface to donate charge to the adsorbed molecule and the reactivity (i.e., decomposition of the interaction energy into electrostatic polarizations and charge transfer contributions). In terms of the electrostatic stabilization of the surface anion, the stabilization of an O^{2-} ion at the surface is defined by the Madelung potential of the ionic crystal. The smaller Madelung energy leads to the higher growth of the lattice constants, resulting in the high reactivity [40]. Since the Madelung energy of CaO is smaller than that of MgO , the reactivity of CaO is a higher that of MgO [40, 147].

A density functional theory (DFT) quantum study of CO_2 adsorption on the MgO surface is used to understand the chemical activity of the oxygen site on MgO adsorbents and to establish the molecular structures and the molecular reaction mechanism because a DFT calculation yields high accuracy for adsorption energy and geometry [148, 149].

The adsorption energy and geometry information are shown in Table 7, including the experimental results and quantum calculations using the electron Hartree-Fock calculation by the Pacchioni group (Table 7) [150, 151]. In the interaction between the MgO surface and the CO₂ molecule, a charge rearrangement results in linking between the CO₂ molecule and the O site. The charged site on the surface provides the strong bond (bond length = 1.41Å) of O_{surface}-CO₂ because the adsorbed CO₂ at the charged O site forms charged molecules. The results of the DFT calculation indicate that CO₂ molecule is adsorbed on MgO, which forms a stable surface carbonate.

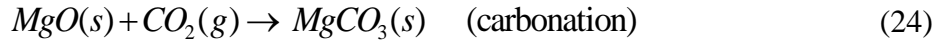
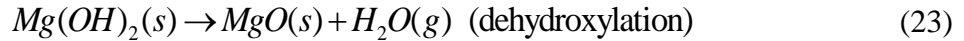
TABLE 7. Adsorption properties of single molecular CO₂ on the (2×2) MgO (100) surface

	Bond length (O _{surface} -CO ₂) (Å)	Bond length (O-C, CO ₂) (Å)	Bond angle (°)	Adsorption energy (eV)
Experiment [151]	-	-	-	-0.46
[152]	-	-	-	-0.48
Theory[147]	1.41	1.22	137	-0.49

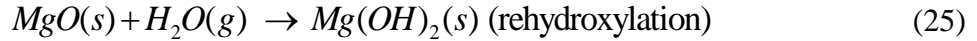
2.4.3 Kinetics of surface Mg₂SiO₄ carbonation

Surface carbonation, which occurs in the direct solid-gas phase reaction, is relatively uncomplicated. Solid calcium and magnesium minerals, including oxides or hydroxides, produce surface-adsorbed carbonates without any liquid phase. During the carbonation reaction, filling and pluggage of the pores of minerals are observed and the carbonate layer thickens, prohibiting CO₂ sorption into the unreacted pore sites of materials. Thus, the process rate is decreased although the sample continues to react with CO₂ at the pores of the sorbents. After the fast carbonation period, the structure modification of sorbent could occur during the formation of carbonates, indicating the mineral carbonation to capture CO₂.

The carbonation of CaO and Ca(OH)₂ proceeds relatively fast in a forward reaction, occurring within several minutes at a high temperature (< 680K) and pressure (at 1 bar) compared to MgO and Mg(OH)₂ [153]. Despite the rapid reaction, the feasible application of calcium based sorbents as feedstock is limited due to their relatively low quantity as naturally occurring ores. Therefore, Mg(OH)₂ dehydroxylation to MgO has been broadly used for the industrial MgO production, due to its simple chemical property and structure. In particular, this process leads to the MgO carbonation to capture CO₂. The reaction mechanism of the carbonation of Mg(OH)₂ is:



The first step (eq.24) is reversible:



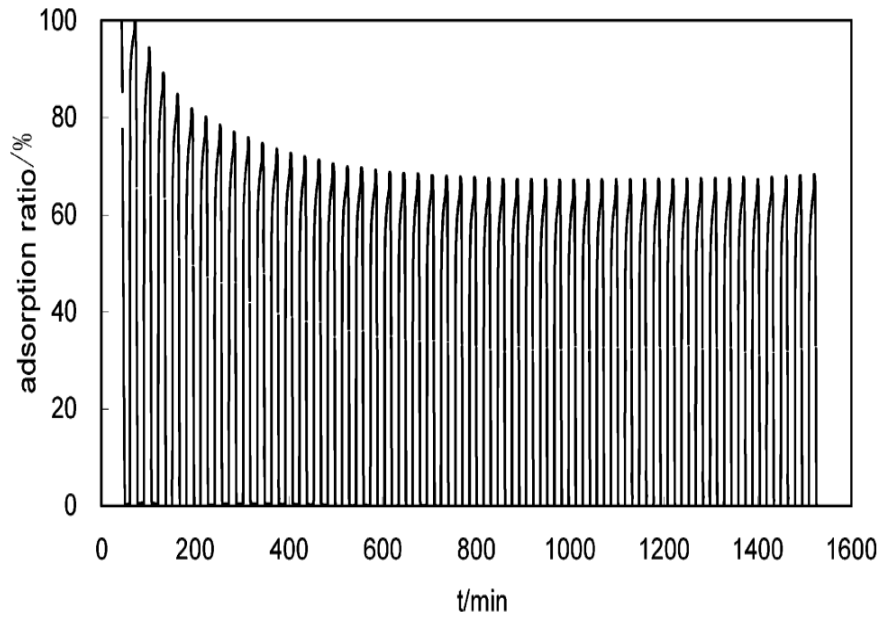
Final carbonation proceeds through the intermediate formation of magnesium oxide layers. During the surface carbonation process, a thin layer of the carbonates forms as a diffusion barrier to both the outward diffusion of H₂O and the inward diffusion of CO₂, decreasing the process rate.

Kinetic Improvements. Given the nature of the slow reaction kinetics, additional process and sorbent developments are required for commercial application. Slow kinetics can be enhanced by increasing surface area, reaction temperature, and pressure, or by using intermediate steps for the final reaction. This section will briefly discuss mechanical and chemical approaches to accelerate the rate of mineral carbonation.

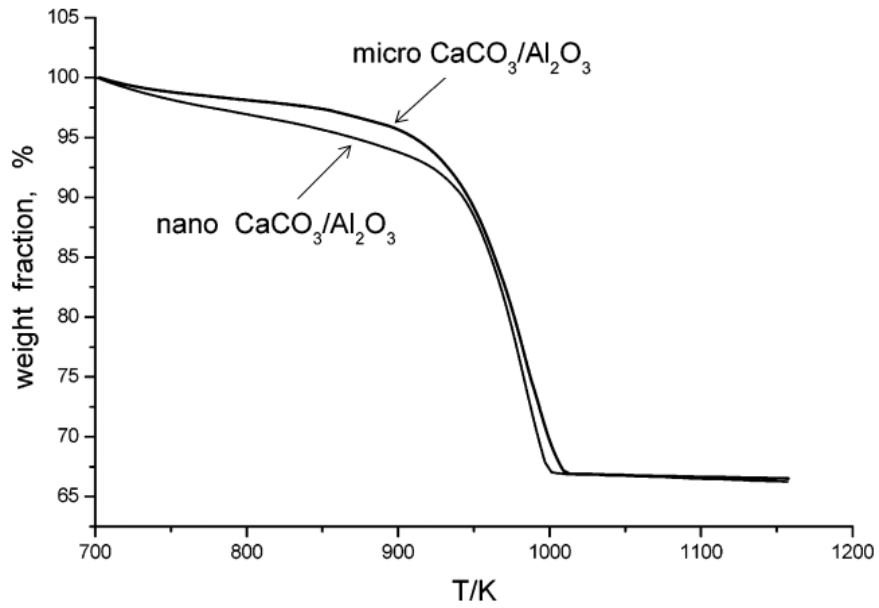
Using a mechanical activation by the formation of defects, increasing surface area, and delocalization, Balaz *et al.* [97] was able to enhance the carbonation rate. The study carried out an mechanical activation of olivine samples in three high energy mills: (1) a laboratory attritor mill is run at rotation (1500 revs/min) for milling times of 5–120 min and is operated at ambient temperatures and free access to air; (2) a laboratory planetary mill is run at the planet carrier rotation speed (450 revs/min) for milling times of 2–30 min and is also operated at ambient temperature and free access to air; and (3) a industrial nutating mill is run at 900 revs/min, and operated in a dry mode at ambient temperature and free access to air. In several tests, they examined the milling with the presence of water (50 mL, 100 mL, 200 mL and 500 mL) [97]. During high-energy milling processes, particles are crushed and rounded, becoming smaller and leading to overall larger surface area as represented in Table 8. Attritor milling shows the largest improvement in olivine surface area (from 0.25m²/g to 35.2m²/g).

TABLE 8. The milling parameters and physicochemical properties of olivine samples [97]

Type of mill	Revolutions (revs/min)	Milling time (min)	H ₂ O Addition (ml)	Specific Surface area (m ² /g)	Milling Energy E (kWh/kg)
Raw	-	-	-	0.25	-
Attritor	1500	120	100	35.2	2.31
Planetary mill	450	30	-	5.2	6.03
Nutating mill	900	10	500	9.4	0.51



(a) Adsorption ratio of Carbonation and calcination for 50 cycles



(b) The comparison of desorption profile dependent on temperature on nano- and micro- $\text{CaCO}_3/\text{Al}_2\text{O}_3$ sorbents

Figure 27. Adsorption and desorption on nano $\text{CaO}/\text{Al}_2\text{CO}_3$ sorbent [92].

For chemical treatment of sorbents, nanomaterials have been used for carbon dioxide capture. Wu *et al.* [92] performed CO₂ adsorption at 600°C and desorption at 800°C on nano-CaO/Al₂O₃ adsorbent (Figure 27). The adsorption ratio, defined as the percentage of adsorbed CO₂ within 10 min, begins at 100%, then stabilizes at about 75% after 15 cycles [92]. During cycling, the average pore size increases ~75.9%, whereas pore volume and surface area significantly decrease (~56.7% and ~73.5%, respectively) due to the sintering of nanoparticles and the formation of new products with larger particle size (Table 9).

The desorption rate of CO₂ from nano-CaCO₃/Al₂O₃ is higher than that of micro-CaCO₃/Al₂O₃ because the surface energy of adsorbents improves with the decrease in the size of adsorbent particles. High surface energy at reaction sites causes high hydration heat. This result supports that nano-CaCO₃/Al₂O₃ can be a suitable CO₂ adsorbent.

TABLE 9. BET analyses of CaO/Al₂CO₃ sorbent before carbonation and after 20 cyclic carbonations [92]

	Pore size (nm)	Total pore Volume (mL/g)	Surface Area (m ² /g)
Before	8.631	0.2578	115.5
After	15.18	0.1116	30.57

2.4.4 Mineral selection

Both alkali and alkaline earth metals can be carbonated, but alkali carbonate cannot provide a stable formation due to its high solubility and would need to be stored in salt caverns. Of the non-alkali and non-alkaline earth metals, a few metals can form carbonates (e.g. Mn, Fe, Co, Ni, Cu and Zn), but most of these elements are too rare or too valuable.

Alkaline earth metals (calcium and magnesium) are regarded as suitable adsorbents for mineral CO₂ sequestration because they are common in nature. Calcium carbonation is a higher reactive than magnesium carbonation, but magnesium-containing minerals are favorable for the implementation of the reaction process because large deposits with relatively high purity are available worldwide although

Since igneous rocks are particularly appropriate for CO₂ capture due to the essential nature of free carbonates, feasible adsorbents of magnesium-rich minerals for CO₂ carbonation are dunites, peridotites and serpentinites due to their large abundance in nature and the high molar ratio of the alkaline earth oxides in olivine, (Mg₂SiO₄), and serpentine (Mg₃Si₂O₅(OH)₄) matrix (Figure 28).

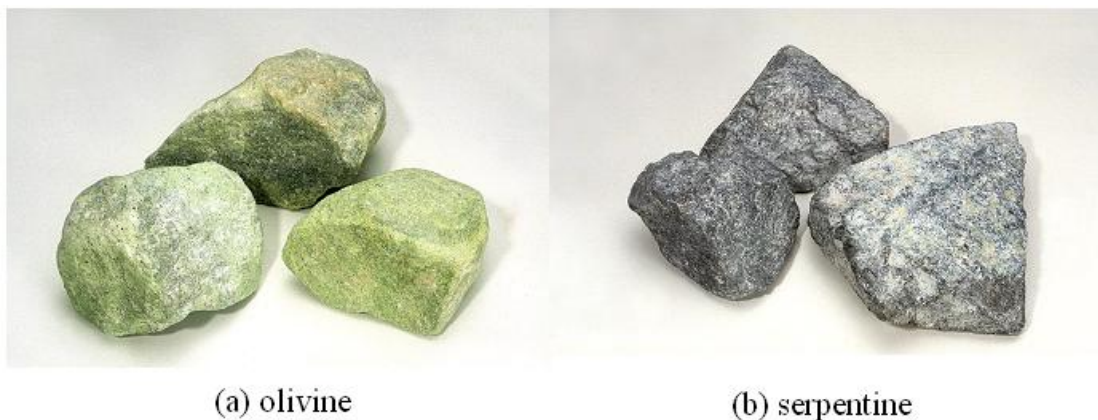


Figure 28. Bulk size of olivine and serpentine mineral [154].

Among other alkaline earth minerals, talc ((Mg₃Si₄O₁₀(OH)₂) and wollastonite (CaSiO₃) can also be considered as candidate minerals for mineral sequestration. Basalt, which is rich in calcium is ubiquitous, but it is difficult to extract the reactive components from the mineral [155]. The identification of alternative feedstock sources for CO₂

sequestration has been in progress and research has started to find them on the field of industrial by-products, which is favorable for carbonation.

2.4.5 Mineral availability in the United States

For the mineral CO₂ sequestration, the large deposits of mineral sorbent at the quarry mouth determine the location of the CO₂ capture plant instead of the CO₂ point sources such as power plant. In North America, large abundance of olivine and serpentine is found along both the east and west coasts. The seven major regions in the U. S. all contain significant mineral deposits that could be employed for mineral carbonation (Figure 29) [42, 156]. Figure 30 shows the picture of a quarry for mineral carbonation.

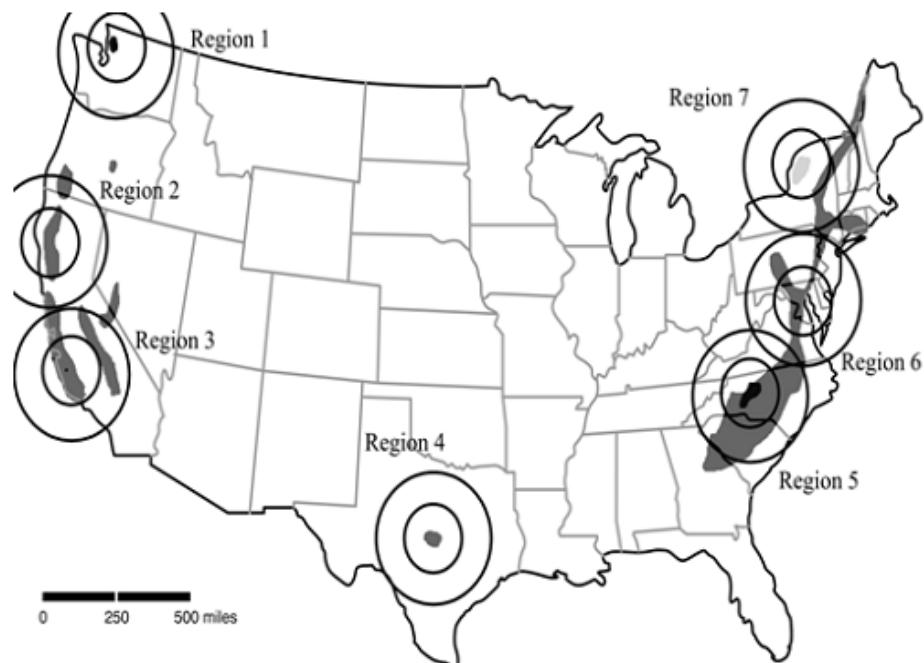


Figure 29. Ultramafic mineral carbonation regions [42]. Circles denote radius coverage of mineral carbonation in local regions. (Small circle: 100 mile; Large circle: 200 mile)



Figure 30. Mineral quarry in Pittsburgh, PA [154].

TABLE 10. Annual CO₂ emissions and minimum mineral requirement with region [157]

Region	Mining location	Mineral	Size of deposit	R _{CO2}	Radius coverage	Coal (Mt)	CO ₂ (Mt)	Mineral (Mt)
1	Twin sister, WA	Olivine	1.8Gt	1.8	0-100	5	13	23
					100-200	2	5	9
2	Trinity-SiskyouMtn, CA-OR	Serpentine	Large	2.5	0-100	4	10	26
					100-200	0	0	0
3	Coast range Southern, CA	Serpentine	Large	2.5	0-100	4	10	26
					100-200	0	0	0
4	Liano Uplift, TX	Serpentine	>1Gt	2.5	0-100	13	30	75
					100-200	18	42	104
5	Asheville, NC	Olivine	200Mt	1.8	0-100	20	54	98
					100-200	49	133	239
6	State Line, MD-PA	Serpentine	Large	2.1	0-100	39	106	222
					100-200	46	125	262
7	Willsboro, NY	Wollastonite	14 Mt	2.8	0-100	4	11	30
					100-200	24	65	182

Table 10 represents the annual CO₂ emissions from coal-fired power plants within a 100- and 200-mile radius of the deposits and the annual amount of minerals from the deposit requirement, assuming 100% carbonation of the mineral and 100% sequestration of the CO₂.

R_{CO_2} shows the ratio of the mass of mineral required to carbonate one unit mass of CO_2 , with the assumption that 100% conversion of Mg or Ca is available in the mineral matrix. The lower R_{CO_2} (1.8) for olivine indicates that considerably less olivine would be required to be mined for the sequestration of the same CO_2 quantity compared to serpentine (2.1 to 2.5) wollastonite ($R_{CO_2} = 2.8$). The total demands of the regional ore are very large, but the mineral resources significantly exceed these demands except these in regions 5 and 7. Additionally, the amount of mineral is 4.6 (olivine) to 7.5 (wollastonite) times more abundant than the amount of coal required. Therefore, this study selected olivine for the mineral carbonation.

2.4.6 The Process of mineral carbonation

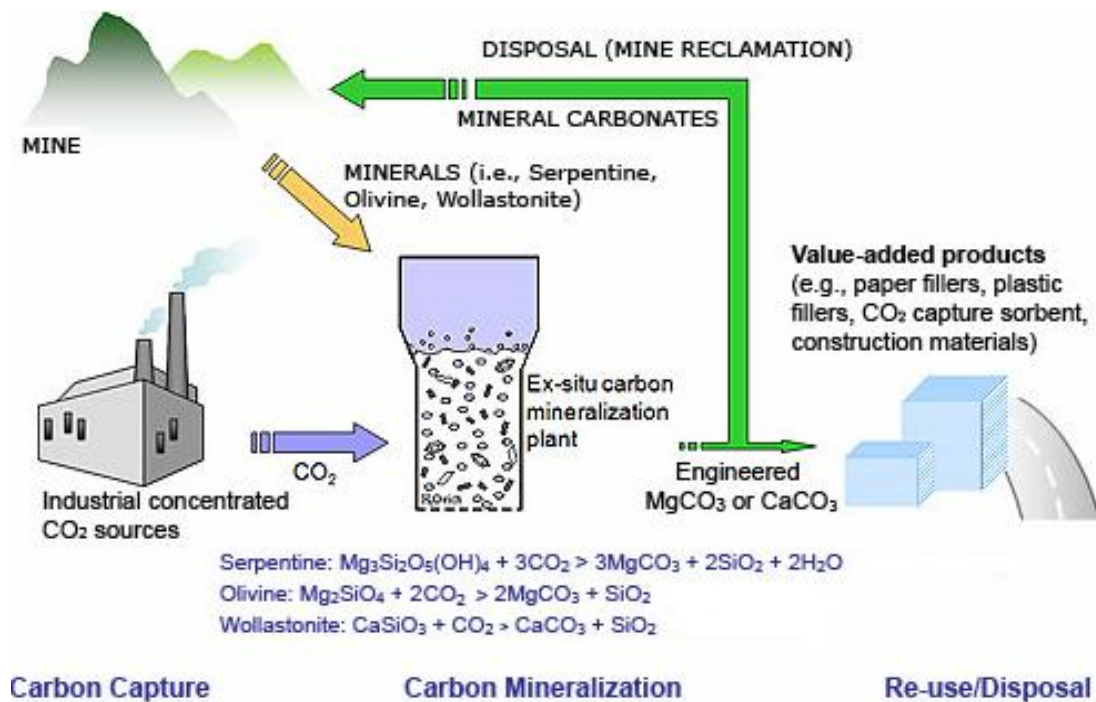


Figure 31. Schematic diagram of carbonation for CO₂ sequestration [158].

Mineral carbonation for CO₂ sequestration is achieved in the following sequence: (1) pre-treatment, (2) mineral transport to a mineralization plant to capture CO₂ from a plant, (3) direct/indirect mineralization, and (4) re-use/disposal (Figure 31) [32].

1) Pre-treatments

To increase the active surface area for effective carbonation reaction of the minerals, the following pre-treatment options can be used: (1) the mechanical treatment and (2) the thermal treatment.

- Mechanical treatment- To increase the reaction activity of minerals, they must be grinded for the size reduction. Instead of normal grinding, high-energy attrition grinding, where small balls mixed with the minerals are stirred in a chamber, is employed to uniformly reduce the particle size.
- Thermal treatment- By heating the minerals to 600°C to 650°C, the wet sample is refined and their structures are opened to the reactive surface. In addition, the porosity of the mineral can be increased by steam or supercritical water treatment [159].

The pre-treatment step is required to achieve the rate of highly active carbonation in direct gas-solid phase reaction, but it causes additional costs and energy consumption for extra processes. For example, the pre-treatment process of olivine and hydrated magnesium silicate (serpentine) causes an energy penalty of 70kW·h/ton to 150kW·h/ton and 300kW·h/ton of mineral, respectively. This significantly decreases the CO₂ avoided for mineral carbonation from 72% to 38%. Therefore, the necessity and desirable effect of the pre-treatment process should be balanced with the practical design and control criteria of the system through the improvement of treatment efficiency.

2) Carbonation processes

The carbonation process can be conducted using two methods: (1) direct carbonation and (2) indirect carbonation.

- Direct carbonation- The simplest process is the direct gas-solid phase carbonation.

Figure 32 shows a typical flow diagram of the direct carbonation process. A commercial process generally provides mining, crushing, milling of the mineral-bearing ores, and a plant for mineralization.

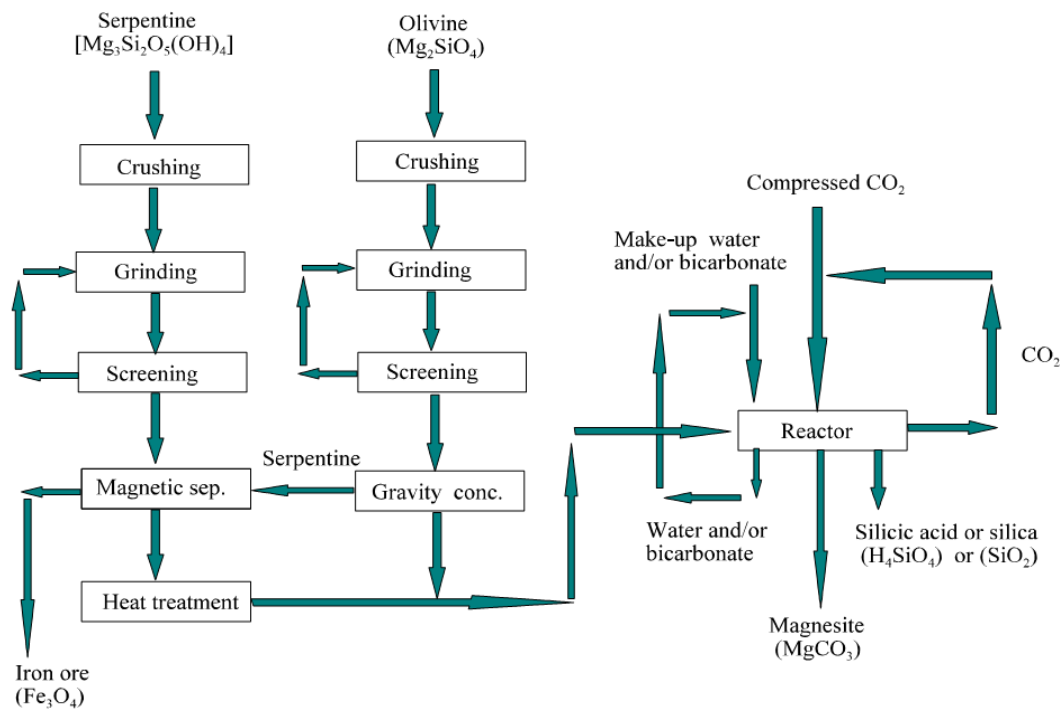
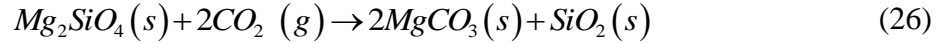
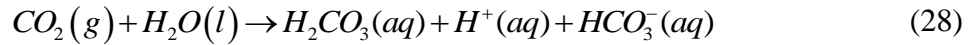


Figure 32. Process flow diagram of the direct carbonation using magnesium-based minerals [160].

The direct gas-solid reaction of olivine (Eq. 26) and the hydrated magnesium silicate, serpentine (Eq. 27) is as follows:



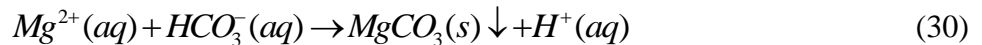
Since water improves the reaction rate for natural rock weathering, a process developed on the basis of this principle is the carbonic acid route, in which CO₂ reacts at high pressure in an aqueous suspension of olivine or serpentine [159, 161]. First, CO₂ dissolves in the water and dissociates to bicarbonate and H⁺, which results in a pH of about 5.0 to 5.5 at high CO₂ pressure:



Then Mg²⁺ is generated from the mineral matrix after Mg₂SiO₄ reacts with H⁺.



Finally, Mg²⁺ reacts with bicarbonate and precipitates as magnesium carbonate (magnesite):



- Indirect carbonation-, an additional process can be employed in order to improve the reaction rate. The reactive compound is extracted from the material matrix, leading to the easy formation of carbonates. The indirect processes involve the extraction of magnesium or calcium with hydrochloric acid and acetic acid, but the application of HCl limits the selection of minerals due to the corrosiveness problem [153].

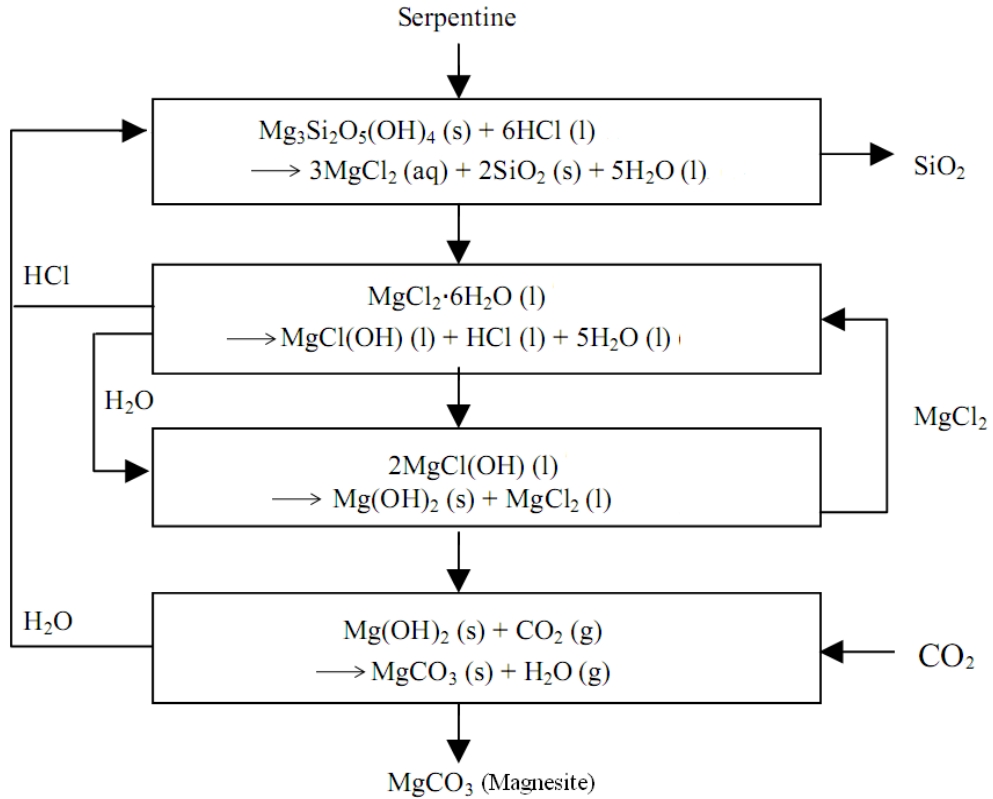
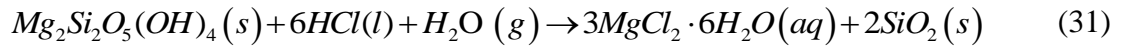
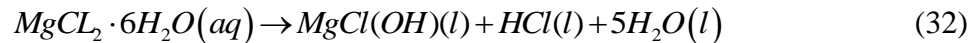


Figure 33. Process diagram of the indirect carbonation using serpentine [162].

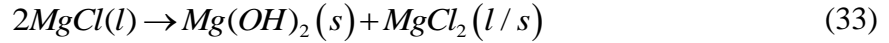
To extract magnesium from serpentine, hydrochloric acid (HCl) can be used (Figure 33) [153, 163]. In the first step, the magnesium is extracted from the serpentine matrix with the addition of HCl which leads to an acid solution in which the magnesium dissolves as $\text{MgCl}_2 \cdot 6\text{H}_2\text{O}$.



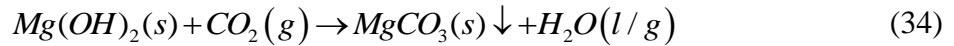
In the second step, HCl is recovered through heating the solution from 100°C to 250°C. $\text{MgCl}_2 \cdot 6\text{H}_2\text{O}$ firstly dissociates water, producing $\text{MgCl}_2 \cdot \text{H}_2\text{O}$. Finally, it reforms to $\text{MgCl}(\text{OH})$ with the release of HCl and water into the solution. Overall, this step is described as:



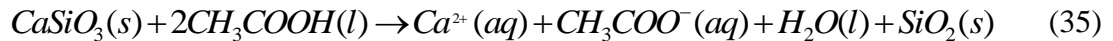
In addition, MgCl(OH) converts to magnesium hydroxide (Mg(OH)₂) during the water cycle.



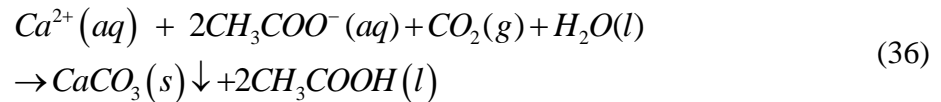
Lastly, the reaction between Mg(OH)₂ and CO₂ produces carbonate:



Compared to the HCl extraction processes, the acetic acid extraction methods provide lower energy consumption and use a less severe extraction medium. To extract calcium ions from wollastonite (CaSiO₃), acetic acid can be employed [164]. The process consists of two steps. First, CaSiO₃ is treated with acetic acid as follows:



Then limestone (CaCO₃) is produced, and the acetic acid is recovered in a combined step:



This process can accelerate the carbonation process by extracting reactive compounds from the adsorbent matrix without using hydrochloric acid. This alleviates the acid recovery issue, caused by the undesirable side-reaction during the carbonation step.

3) Final products

Carbonated products can be disposed for reclamation in mine regions or re-used for construction purposes and paper filtered in spite of such small amounts of re-use (Figure 34).



Figure 34. Olivine deposit for mine reclamation in Twin Sisters, WA [154].

Olivine and wollastonite are the best candidates for the implication of the mineral carbonation in an industrial process, but current mineral resource estimates indicate that only olivine could meet regional demands. The broadest occurrence and abundance of serpentine can make it the most widely available potential materials. However, current processes cannot activate serpentine as a reactive matrix without a heat-treatment step. Thus, many research activities have been initiated to discover reaction process pathways that can enhance the reaction rates.

2.5 The Cost of CO₂ Capture and Storage

2.5.1 General cost of CCS

Total cost of CCS mainly includes the spending on three different components: CO₂ capture with compression at a power plant, transport and storage of captured CO₂ as shown in Table 11. CCS costs of different power plants vary significantly due to the difference in their operation conditions. In general, the range of the total cost of capturing 1 ton CO₂ in a

power plant is \$21.5 to \$115.0. The CO₂ capture process with compression accounts for 80% to 90% of the total cost while transport and storage steps account for 10% to 20%.

TABLE 11. Estimated costs of CO₂ capture, transport, and geological storage (2007 US\$/t CO₂). IPCC(2005) data adjusted to 2007 cost basis [165]

CCS System component	Cost range (\$)
Capture: Fossil fuel power plant	\$20-95/t CO ₂ net captured
Capture: Hydrogen and ammonia production or gas-processing plant	\$5-7-/t CO ₂ net captured
Capture: other industrial sources	\$30-145/t CO ₂ net captured
Transport: pipeline	\$1-10/t CO ₂ net transported
Storage: Deep geological formation	\$0.5-10/t CO ₂ net injected

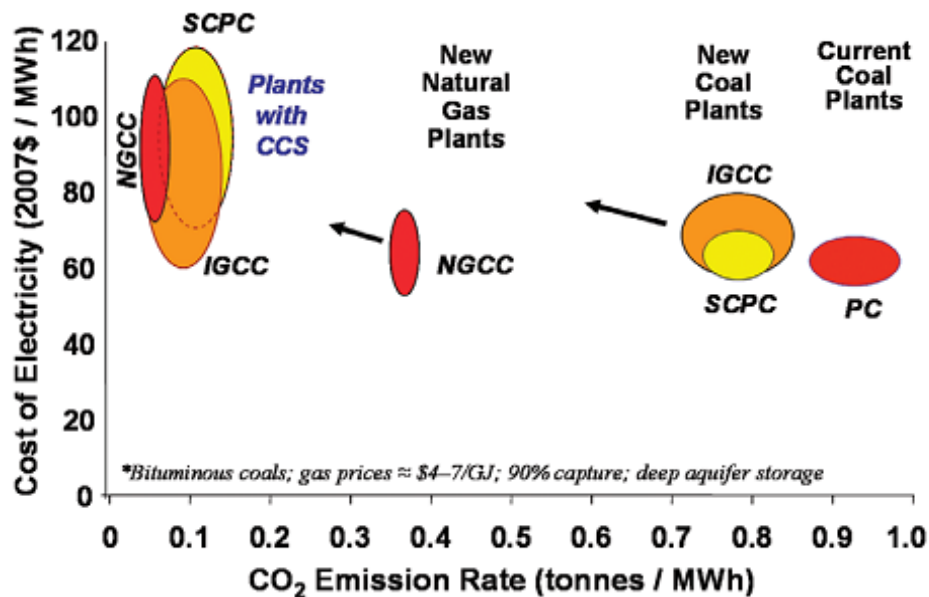


Figure 35. Cost of electricity generation (2007 US\$/Mwh) as a function of the CO₂ emission rate (t CO₂/Mwh) for new power plants burning bituminous coal or natural gas (PC = subcritical pulverized coal units; SCPC = supercritical pulverized coal; IGCC = integrated gasification combined cycle; NGCC = natural gas combined cycle). Ranges display differences in technical and economic parameters affecting the cost of plant[166].

The cost of generating electricity with and without a CCS system depends on the type of power plant (Figure 35). The total electricity cost (\$/MWh) is represented as a function of the CO₂ emission rate (t CO₂/MWh) for power generation using bituminous coal or natural gas in a wide range of cost values. The expected cost of operating plants with or without CCS is highly uncertain, but CCS increases the cost of generating electricity by approximately 60% to 80% at new coal combustion plants and by about 30% to 50% at new coal gasification plants. Consequently, the cost of generating electricity increases to approximately \$40 to \$70/MWh for PC plants and \$30 to \$50/MWh for IGCC plants using bituminous coal. These high costs result from 1) additional energy requirements for the capture and compression of CO₂, 2) additional capital costs resulting from the addition of fuel requirements of a plant with CCS by about 25% for a coal-fired plant and about 15% for a gas-fired plant, and 3) storage and other supplementary system costs of 30% to 60%, depending on the different environments [167].

As mentioned at the beginning of this thesis, captured carbon can be stored by being forced underground at great pressure. One advantage of storing carbon underground in this way is that it can be used to help energy companies in the extraction of oil from oil fields using the enhanced oil recovery system (EOR). EOR is used for petroleum industry to extract extra oil from oil fields and those storages could generate additional net benefits of \$10 to \$16 per ton of injected CO₂ (based on 2003 oil prices), which could compensate for the expensive cost of the capture process in conventional power plants [167]. If cost-effective CCS technologies are developed and applied to currently available power plants, the implementation cost of CCS systems could decrease to below \$50/tCO₂, including all components.

2.5.2 Mineral carbonation: energy penalties and costs

Enough mineral feedstock deposits are available in some regions of the country within a 100- or 200-mile radius of point CO₂ sources such as coal-fired power plants to install an ex-situ plant. For an in-site plant, flue gas mixture is transported to plant through pipe [31]. However, energy costs are high because the reaction rate of carbonation is slow, leading to the requirement of additional pretreatment processes such as mining, crushing and milling, and thermal treatment for mineral activation to accelerate the carbonation rate. The energy requirements for pretreatment might be 30% to 50% of the capture components. The processes of capturing carbon, in turn, increase energy consumption and operating costs for the energy generators. Generally, the cost of mineral sequestration, including capture and storage, is \$50 to \$70 per ton of CO₂ sequestered when laboratory processes are scaled up [19].

TABLE 12. Energy losses for mineral carbonation process [157]

Mineral	Pretreatment	Energy (kW h/ton)	Reaction efficiency (%)	Mineral (kton/day)	% Total plant energy
Olivine (100%)	200mesh	18	16	286	15
	400mesh	83	61	75	26
	Ultra fine	233	81	56	55
Serpentine (100%)	200mesh	13	9	706	37
	Heat treat- 200mesh	339	40	158	222
Wollastonite (50%)	400mesh	97	165	165	67
	Ultra fine	167	87	87	61

Table 12 shows the total energy consumption of mineral pre-treatment steps, the extent of reaction in one hour achieved with feed preparation, the amount of mineral required for 100% CO₂ sequestration from a 1.3GW coal-fired power plant, and the parasitic energy

loss [157]. The daily mineral requirement decreases and carbonation reactivity improves with an increase in additional pretreatments, but the energy demand dramatically increases, resulting in net energy losses. For instance, 15% of the total plant energy is required for the formation of < 200-mesh olivine and results in 16% extent of carbonation in one hour whereas ultra-fine grinding improves reaction efficiency to 81%, but increases the parasitic energy loss to 55%, indicating that the energy loss negates the savings that result from the improved reaction efficiency. For serpentine minerals, energy loss surpassing 100% means that more CO₂ is emitted by the pretreatment operation than is sequestered because of the thermal-activation operations. The high energy consumption of serpentine carbonation leads to a negative effect on the cost management of CCS. A CCS system with mineral carbonation requires 60% to 180% more energy input/kW-hr than that with other separation methods [168].

TABLE 13. The required quantities of minerals for CO₂ sequestration

Potential Mineral for carbonation	Ton required to sequester 1ton of CO ₂ *
Wollastonite (CaSiO ₃)	2.6
Olivine (Mg ₂ SiO ₄)	1.6
Serpentine (Mg ₃ Si ₂ O ₅ (OH) ₄)	2.1
Anorthite (CaAl ₂ Si ₂ O ₈)	6.3

*Mineral mass that should be processed to carbonate 1 unit mass of CO₂, assuming 100% mineral carbonation

For suitable mineral carbonation, the wet carbonation of natural olivine is suggested since only a small amount of olivine is required per ton of CO₂ stored and its reaction rate

becomes faster than the dry carbonation (Table 13). The mineralization process, however, practically requires 5.8 tons to 23 tons of olivine per ton of CO₂ to be mined and forms 6.8 tons to 24 tons of carbonates to be disposed of per ton of CO₂ sequestered due to partial carbonation [35]. The anticipated cost of this process is roughly \$50/t CO₂ to \$100/t CO₂ net sequestered, but the cost can fall to \$30 per ton of CO₂ sequestered when the pre-treatment process and the dewatering problem are avoided and the carbonation rate increases to capture more CO₂ within a limited time [19].

2.6 Summary of CO₂ Adsorption and Capture Development Strategies

High attention has been paid to the reduction of anthropogenic CO₂ emissions from large point sources in the world. Among various separation technologies for the flue gases of coal-fired power plants, which include absorption, adsorption, membrane separation, cryogenic distillation, and chemical-looping, adsorption using solid sorbents is one of the most promising processes. This literature review discussed the various adsorption technologies for carbon dioxide capture using PSA, VSA, and TSA on several solid sorbents. Due to the interaction between the sorbents and the CO₂ gas species, CO₂ molecules are bound on the surface of the sorbents. In general, CO₂ adsorption processes with various adsorbents show highly stable and cyclic capture capacities and low energy consumption for regeneration in comparison with aqueous systems. Adsorption kinetics depend on temperature, pressure, interaction energy between the sorbent and the CO₂, and the pore size or the surface area of the adsorbents, supporting the fact that multi-parameters affects capture capacity, operation cost, and process efficiency.

The major issues with the adsorption processes include limited CO₂ selectivity in

separating CO₂ from actual flue gases and low adsorption rates. In order to overcome these issues, current research efforts are focused on developing solid sorbents with fast sorption kinetics, high selectivity, high capture capacity, high recycle stability, and targeting realistic applications. Further adsorbent research is needed to: (1) understand the mechanism of CO₂ adsorption on the various solid adsorbents, (2) improve the kinetics of adsorption and desorption of CO₂ over different sorbents, and (3) modify sorbents to optimize their performance [68]. In addition, adsorption technologies can be improved by process modifications such as: (1) combined temperature and pressure swing adsorption (TPSA), pressure swing adsorption using temperature swing system to improve recovery, (2) fractionated vacuum-pressure swing adsorption (FVPSA), a dual-bed process which simultaneously produces a 98% nitrogen-enriched gas and an 80% to 90% oxygen-enriched gas from ambient air to improve the CO₂ purity as well as the N₂ purity [15], (3) combined temperature and vacuum swing adsorption (TVSA), (4) insertion of more steps in the PSA and VSA processes, and (5) addition of multi-columns for adsorption and desorption process. Finally, the cost effective scalability to megaton CO₂ capture fluxes is critical to enable CCS and transition it from bench top to a power plant scale (e.g., German power plant pilot study).

In summary, the progresses in the adsorption technology, which were reviewed, suggest it can be a competitive approach for CO₂ separation from gas streams based on both economic aspects and technical performance.

CHAPTER 3

REACTION KINETICS OF Mg_2SiO_4 BASED CO_2 SORPTION

SOONCHUL KWON,[†] MAOHONG FAN,^{*,†,‡} HERBERT F. M. DACOSTA,[§] AND
ARMISTEAD G. RUSSELL,[†]

School of Civil and Environmental Engineering, Georgia Institute of Technology, Atlanta, GA 30332, Department of Chemical and Petroleum Engineering, University of Wyoming, Laramie, WY 82071, Caterpillar's Product Development Center of Excellence, TC-E / 854, P.O. Box 1875, Peoria, Illinois 61656

Chapter 3 presents the results of pure Mg_2SiO_4 carbonation to determine the reaction properties and to evaluate a reaction kinetics model. Based on changes in the CO_2 concentration with sorption time, kinetic parameters of the reaction of pure Mg_2SiO_4 are obtained.

Mg-rich minerals are promising materials to carbonate CO_2 due to the advantages of the corresponding CO_2 capture technologies, including the low-prices and wide availabilities of the minerals and stabilities of CO_2 carbonation products, carbonates. The kinetic models of the reactions between the Mg-rich minerals and CO_2 within simulated environment are important to the scale-up designs and thus the commercialization of the technologies. Unfortunately, these models have not been available so far. This research was initiated to fill the gap. Magnesium silicate Mg_2SiO_4 , a representative compound in Mg-rich minerals, was used for study of the CO_2 carbonation reaction kinetics under given simulated flue gas

*Corresponding author phone: (307)766-5633; fax: (307)766-6777; e-mail: mfan@uwyo.edu.

[†] Georgia Institute of Technology

[‡] University of Wyoming

[§] Caterpillar's Product Development Center of Excellence

conditions. It was found that the CO₂ interaction with water on the surface of the sorbent is the rate controlling step of the CO₂ capture process. The calculated reaction order with respect to CO₂ in the reaction between CO₂ and Mg₂SiO₄ is 1.1±0.2. The apparent activation energy of the reaction in the temperature range of 100°C to 200°C is 76.2 ±4.8 kJ/mol.

3.1 Introduction

Emissions of carbon dioxide (CO₂) have been increasing about 3.3% per year since 2000, and the CO₂ concentration in the Earth's atmosphere since 2000 has grown 35% faster than in the 1990s [3]. About 40% of the total CO₂ emissions in the U.S. are from power plants that use fossil fuels, especially coal, as the major energy sources. Thus, much effort has been made in developing advanced technologies for CO₂ capture and sequestration from the flue gas stream of power plants.

Among various technologies to separate CO₂, adsorption appears to be the most promising one because it can lead to lower energy demands for its regeneration with low costs and high capture efficiencies if the sorbent has a high CO₂ selectivity and high CO₂ adsorption capacity [3]. Consequently, the development of economical and effective sorbents is desirable. Solid sorbents are a better choice than liquid ones because they are easy to handle, have low deployment costs, and cause negligible corrosion problems. Further, if they are reusable, they may have low environmental impacts [11, 12].

Flue gases from power plants typically contain 8–12% (vol) of CO₂ and 8–10% steam (H₂O). Due to the tendency of H₂O molecules to be combined preferentially to CO₂ molecules, many sorbents lose their CO₂ adsorption capacity in the presence of steam [69]. As a result, few studies have been performed to investigate CO₂ separation in the existence of

typical flue gas stream concentrations. In fact, sorbents with high adsorption capacity for CO₂ in the presence of steam are highly desirable for practical applications of CO₂ capture.

Magnesium-rich minerals have become promising candidates for CO₂ sequestration because of their low cost as well as their high tendency to react with CO₂ [18, 19, 153]. Compared to other CO₂ removal processes, this option minimizes the risk of leakage because the carbonates formed are stable, thereby providing permanent CO₂ sequestration. Moreover, solid products from the carbonation process can be used for mine reclamation or soil amendments [18]. However, the natural mineral carbonation process is inherently slow as it takes more than thousands of years for meaningful conversion, even though the reaction is thermodynamically favorable [18-20]. Identification of potentially attractive reaction approaches and evaluation of the reaction rates of the minerals for the development of highly energy efficient processes are required to expand the commercial application of these sorbents. To evaluate such mineral carbonation here, pure magnesium silicate (Mg₂SiO₄) mineralization is selected because it is the major component of various abundant minerals, such as olivine and serpentine, which have been considered for large scale applications of CO₂ mineralization. The overall reaction of Mg₂SiO₄ with CO₂ to form MgCO₃ in the presence of steam is expressed as:



For typical temperature swing adsorption (TSA) processes, an adsorption process occurs at a lower temperature than its corresponding desorption does. In order to reduce the energy requirement, isothermal desorption, i.e., desorption happening at the same temperature as the adsorption process, can be adopted.

In this study, the adsorption capability of Mg_2SiO_4 with CO_2 in the presence of steam was investigated by varying the temperature. A similar composition of flue gas from fossil-fuel power plants was used for adsorption process. After adsorption, Mg_2SiO_4 was regenerated by purging 100 % nitrogen purge via isotherm desorption. Based on the experimental data, kinetic parameters, including the reaction order and the activation energy for Mg_2SiO_4 carbonation, were derived.

3.2 Experimental methods

3.2.1 Materials

The sample of Mg_2SiO_4 was supplied by Alfa Aesar and employed without further treatment. Mg_2SiO_4 is in the form of white powder with 99% purity, a median particle size of 3.5 μm , and a bulk density of 3.21 g/cm^3 . The X-ray diffraction (XRD) patterns were analyzed for measuring the carbonated sorbent sample with the Philips X'PERT powder model using Cu $\text{K}\alpha$ radiation, performing scans in the 2θ range from 5° to 95° with $0.02^\circ/\text{s}$.

3.2.2 Experimental apparatus

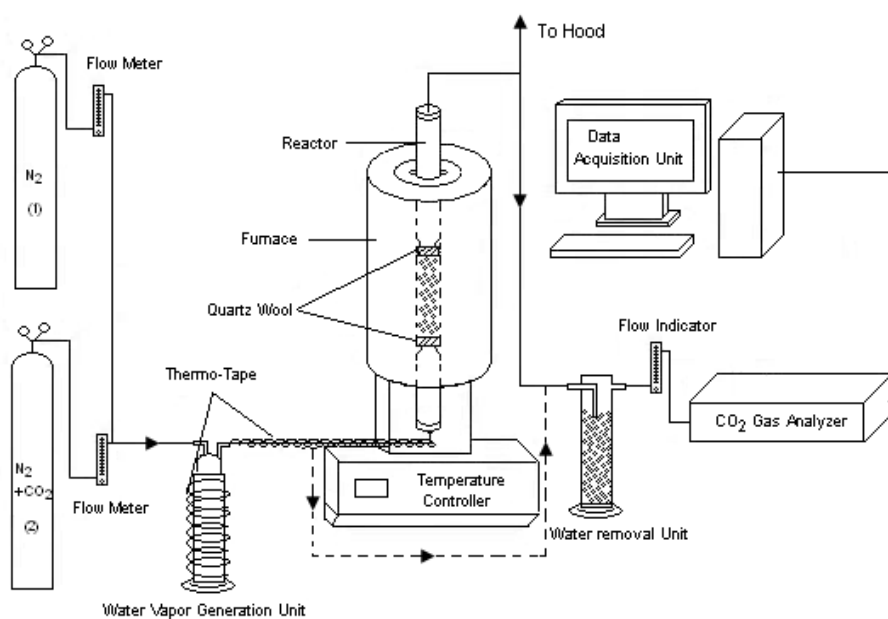


Figure 36. Schematic diagram of experimental apparatus for CO₂ adsorption.



Figure 37. Picture of experimental set-up.

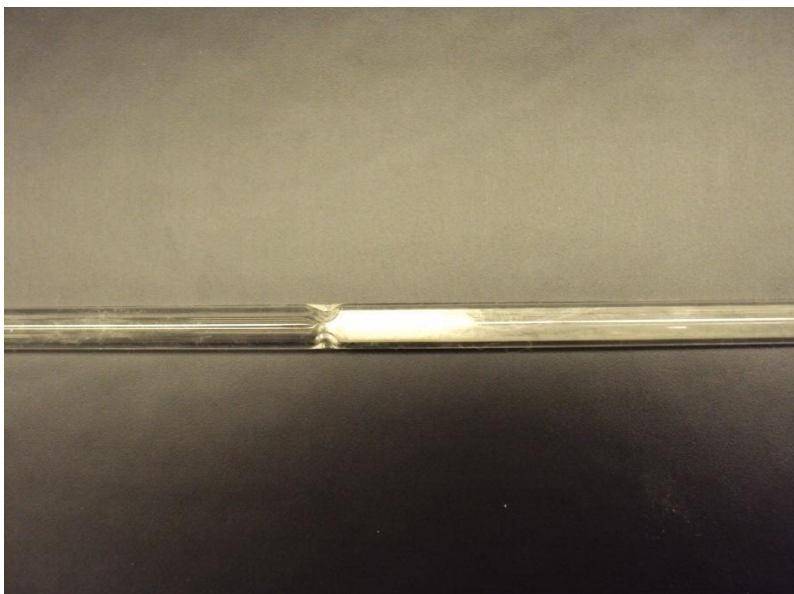


Figure 38. Picture of olivine adsorbent inside quartz wool tube.

Figure 36 and Figure 37 show the schematic diagram and the actual apparatus of the experimental set-up, respectively. The experimental setup for CO₂ capture consists of three parts: a gas simulation unit, a CO₂ sorption unit, and a CO₂ analysis unit. Gas cylinders containing pure N₂ and a mixture of 4.1 mmol/dm³ CO₂ with N₂ were used. Flow rates of the feed gases were manually controlled with Matheson Tri-gas FM-1050 flow meters. An additional flow meter was used to check the inlet gas flow into the gas analyzer.

Adsorption of CO₂ with Mg₂SiO₄ was carried out in a quartz tubular reactor with a length of 610 mm and an inside diameter of 9 mm (Figure 38). The fixed bed is formed by placing the sorbent particles between small amounts of quartz wool serving as the bed holder. The quartz reactor was placed inside a TF55030A-1 tube furnace (manufactured by Thermo Corporation, Asheville, NC) with a UT150 temperature controller (Yokogawa M&C Corporation, Newnan, GA) to control the CO₂ sorption temperature. The CO₂ sorption unit was connected with a steam generation unit to introduce steam into the dry inlet gas stream.

Thermo-tape was used to avoid steam condensation in the gas-carrying line, and temperature controllers were employed to control the temperature of gas stream flowing through the copper gas lines. Outlet gas from the reactor passed through a steam removal unit before entering the CO₂ analyzer where the CO₂ concentration was measured. CO₂ concentrations in the simulated flue gas stream were monitored before and after sorption using the ZRE analyzer (California Analytical Instruments, Inc.). The gas analyzer was directly connected to a data acquisition system recording the continuous changes in CO₂ concentration every one second.

3.2.3 Operating procedures

The CO₂ adsorption capacity of Mg₂SiO₄ was determined by measuring the concentration of CO₂ before and after adsorption. Each test run was conducted with fresh Mg₂SiO₄. First, the tubular reactor loaded with 0.50 g of Mg₂SiO₄ was preheated for 10 min to ensure constant operation conditions at the desired reaction temperature. The tubular reactor was connected to the gas supply unit and to the gas analyzer. At the same time, the data acquisition unit was turned on. The composition of the effluent gas from the steam removal unit was measured immediately by the gas analyzer. When the CO₂ concentration in the effluent gas stream was within 1% of the initial inlet stream indicated by the gas analyzer, indicating that the sorbent was nearly saturated with CO₂, the flow of CO₂ gas stream into the reactor was stopped. For the regeneration process, the inlet CO₂ gas stream was stopped, and pure N₂ was passed through the system. The aforementioned procedure was repeated five

times with fresh samples at one set temperature, and an average value of the data was used to estimate the carbonation breakthrough profile.

3.3 Results and discussion

3.3.1 Determination of the temperature range for kinetic study

Our thermodynamic calculations have shown that the Gibbs free energy changes of eq. 37 are -32.95 kJ/mol, -20.88 kJ/mol, and -3.88 kJ/mol at the temperatures of 25°C, 100°C, and 200°C, respectively, indicating that the Mg_2SiO_4 based CO_2 mineralization should occur in the given temperature range, which is supported by the results (Figure 39). CO_2 adsorption occurred on the surface of Mg_2SiO_4 at 200°C as demonstrated by the peaks of carbonation products (MgCO_3 and SiO_2) of Eq. 37 (Figure 39), which is consistent with the observation of other researchers [153, 168, 169].

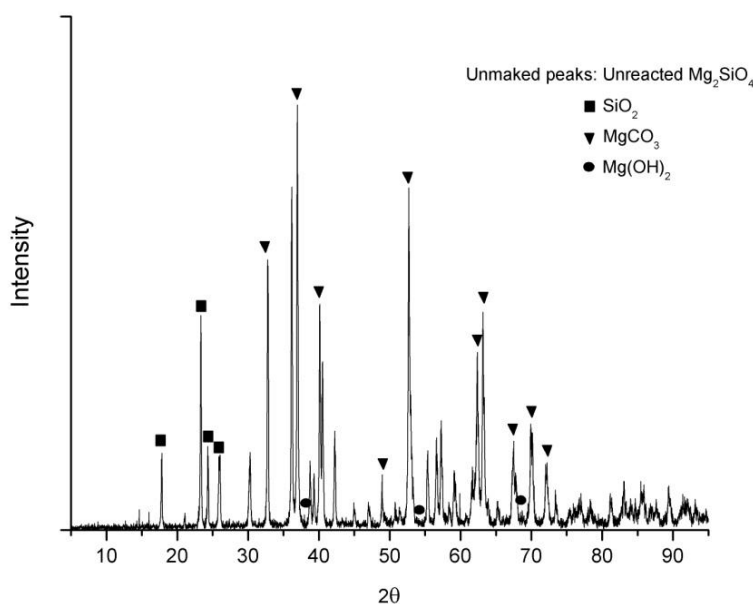


Figure 39. XRD patterns of the Mg_2SiO_4 carbonation products.

The increase in the Gibbs free energy changes of Eq. 37 with temperature signifies that higher temperatures could have considerable negative effect on the adsorption of CO₂ on Mg₂SiO₄. Therefore, an appropriate temperature range should be chosen for study of the reaction kinetics of Eq. 37. In the chosen temperature range, Mg₂SiO₄ should have both good CO₂ sorption capacities and acceptably fast CO₂ sorption rates. Our preliminary tests showed that the reaction rates of Eq. 37 were very slow in the temperature range of 0°C to 100°C even though the sorbent could achieve reasonably large CO₂ sorption capacities during very long sorption periods. In other words, the sorbent can reach high CO₂ sorption capacity under certain conditions given that a long sorption time is allowed. However, the reality in coal-fired power plants is that the volume of the emitted CO₂-containing flue gas is so large that slow sorption leads to the need for construction of very bulky adsorber units to considerably extend the contact between Mg₂SiO₄ and CO₂ to achieve high CO₂ capture efficiencies. Such a construction is very expensive, which should be avoided. Furthermore, it should be mentioned that a good sorbent should not only have a high total sorption capacity but also a high breakthrough capacity. The high break-through capacity of a given sorbent is determined by its inherent characteristics such as molecular structure, pore structure, surface defect or active site and BET (Brunauer, Emmett and Teller) surface area, and sorption operation conditions.

Temperature is expected to be one of the more important operational factors affecting the break-through capacity of Mg₂SiO₄ since it is directly related to the reaction kinetics of eq. 37. The total and breakthrough CO₂ sorption capacities of Mg₂SiO₄ at 150°C, 175°C, and 200°C (Figure 40) show that Mg₂SiO₄ has good CO₂ sorption performance at the three temperatures as compared to other solid sorbents [8, 14, 15, 57, 77, 83, 93, 102].

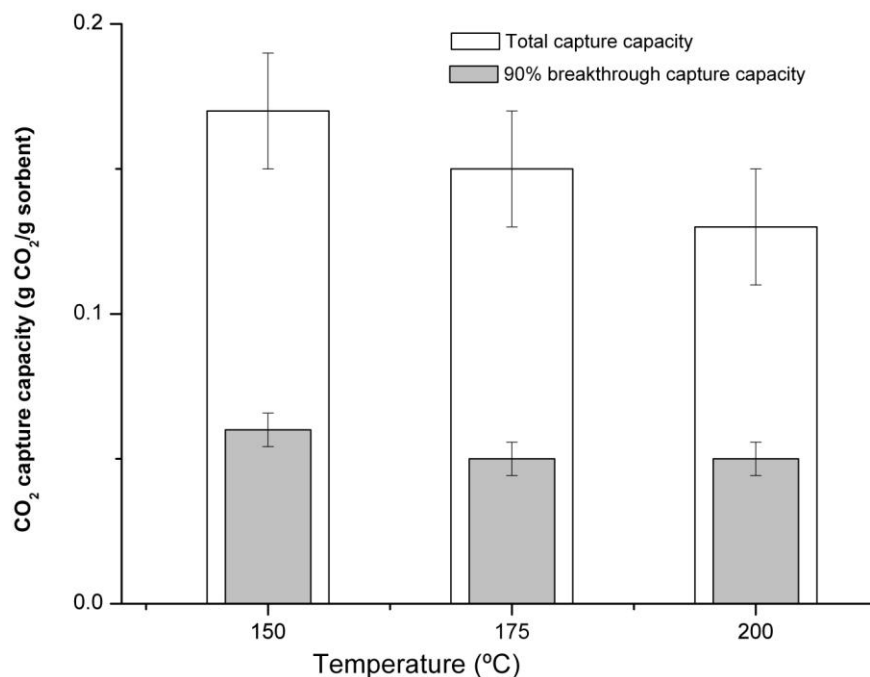


Figure 40. Total and 90 % breakthrough CO₂ capture capacities as a function of temperature. Total capacity is denoted the CO₂ capture capacity until the CO₂ concentration reaches the initial inlet CO₂ concentration. 90% breakthrough capture capacity is denoted the CO₂ capture capacity when the CO₂ concentration reaches 90% removal. Uncertainty results from 5 time multiple tests.

Total sorption capacity of Mg₂SiO₄ decreases with an increase in temperature. However, the breakthrough capacity does not change considerably with temperature. Our tests found that the breakthrough sorption capacity achieved at 150°C when the CO₂ separation efficiencies were close to 100% is lower than that at 200°C. The ratio of breakthrough sorption capacity to total sorption capacity increased with the increase of the sorption temperature under the given experimental conditions (Figure 40), higher than those of most of the reported sorbents [8, 14, 15, 46, 51, 57, 70, 71, 77, 83, 93, 111]. The performance of Mg₂SiO₄ in the temperature range of 150°C to 200°C, suggests that the sorbent could react with CO₂ reasonably fast and should have considerable CO₂ sorption capacities. Therefore,

the temperature range of 100°C to 200°C was chosen to study the kinetics of the reaction between Mg_2SiO_4 and CO_2 .

3.3.2 Multiple carbonation– regeneration cycles

Figure 41 depicts results of another set of tests to evaluate the regeneration capacities of Mg_2SiO_4 adsorbent after 10 carbonation and regeneration cycles using the same sorbent.

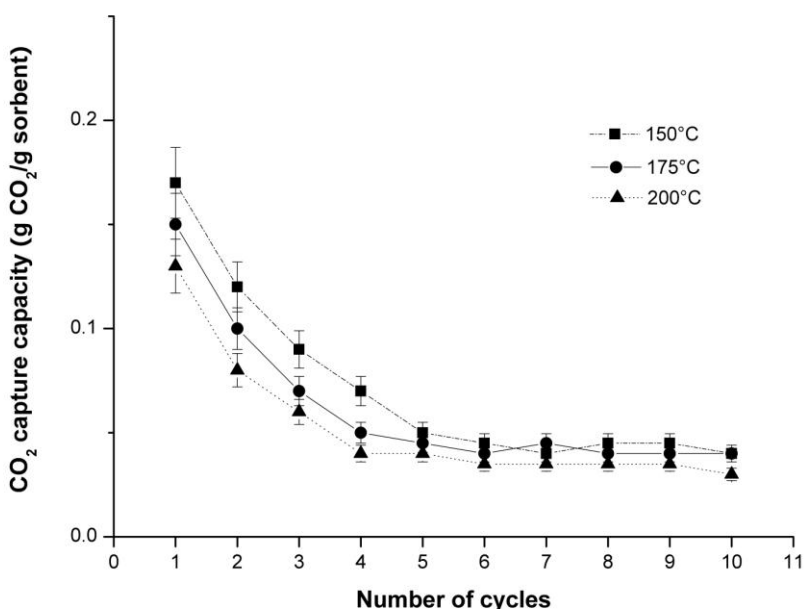


Figure 41. Cyclic CO_2 adsorption processes at different temperatures. (CO_2 concentration, 4.1mmol/dm^3 ; H_2O concentration, 4.1mmol/dm^3). Error bars result from 5 times multiple tests.

The focus is on evaluating the multi-cycle behavior of CO_2 adsorption on magnesium silicate, in particular the partial CO_2 regeneration at constant temperature. Initially, the capture capacities decrease abruptly with the increase in the number of cycles and tend to flatten out after five cycles at 1/3 of the total capacity. Also, the higher the temperature increases, the lower the capture capacities. This multi-cycle behavior could be due to an

increase in the formation of (possibly bidentate) stable surface carbonates which decreases the formation of (monodentate) molecularly adsorbed CO₂. As the number of cycle increases, the products during carbonation overlap moderately through filling and pluggage of the micropores. The slight change of reduction in CO₂ capture capacities suggests that the carbonation process has been mostly completed and physical CO₂ adsorption at the surface may be dominant after 5 cycles.

3.3.3 Sorption kinetics

1) Rate equation determination

The CO₂ adsorbed in the small time interval Δt , ΔF_{CO_2} , can be calculated as follows

$$\Delta F_{CO_2} = v(C_{CO_2,t} - C_{CO_2,t+\Delta t}) = -v\Delta C_{CO_2} \quad (38)$$

where $C_{CO_2,t}$ and $C_{CO_2,t+\Delta t}$ represent the mole concentrations of the reactant CO₂ in the simulated flue gas at the times t and $t + \Delta t$ during a sorption process at a given temperature, and v is the volumetric flow rate (L/s) of the simulated flue gas. The consumption rate of CO₂, $-r_{CO_2}$ [mole/(g-Mg₂SiO₄·s)], can be defined as

$$-r_{CO_2} = \Delta F_{CO_2} / w_{Mg_2SiO_4} = -v(\Delta C_{CO_2}) / w_{Mg_2SiO_4} \quad (39)$$

where $w_{Mg_2SiO_4}$ is the mass of Mg₂SiO₄ loaded into the tubular reactor during each sorption operation. The reaction rate of CO₂, $-r_{CO_2}$, can also be expressed as

$$-r_{CO_2} = kC_{CO_2}^{n_{CO_2}} \quad (40)$$

where k is the apparent reaction rate constant of Eq. 37 at a given temperature and n_{CO_2} is the apparent reaction order with respect to CO₂. It should be mentioned that n_{CO_2} may not be an

integer since Eq. 37 may not be an elementary reaction. Combining Eq. 39 with Eq. 40 leads to

$$-r_{CO_2} = -\nu(\Delta C_{CO_2}) / w_{Mg_2SiO_4} = kC_{CO_2}^{n_{CO_2}} \quad (41)$$

or

$$\ln(-r_{CO_2}) = \ln[-\nu(\Delta C_{CO_2}) / w_{Mg_2SiO_4}] = \ln k + n_{CO_2} \ln C_{CO_2} \quad (42)$$

Eq. 42 shows that $\ln(-r_{CO_2})$ or $\ln[-\nu(\Delta C_{CO_2}) / w_{Mg_2SiO_4}]$ should be linearly related to $\ln C_{CO_2}$.

The apparent reaction order, n_{CO_2} , and the apparent rate constant, k , at a given temperature can be obtained by plotting $\ln(-r_{CO_2}) \sim \ln C_{CO_2}$ since n_{CO_2} and $\ln k$ are the slope and intercept of the plot according to Eq. 42.

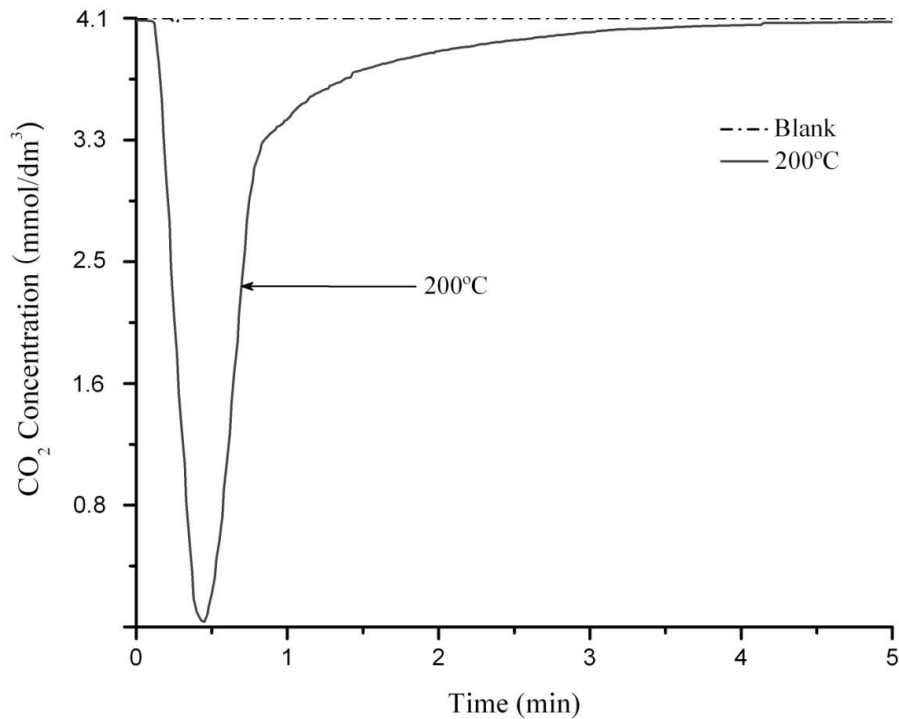


Figure 42. CO₂ carbonation and regeneration profiles in the presence of (4.1 mmol/dm³) steam as a function of temperature (CO₂ concentration=4.1 mmol/dm³; flow rate, 0.5 L/min; weight of magnesium silicate, 0.5g). Blank testing is performed without sorbent at 200°C.

If the reaction mechanism of Eq. 37 does not change within 100-200°C, n_{CO_2} should not vary either so the reaction order can be obtained with the sorption data collected at any temperature within the range. We chose to use the sorption profile obtained at 200°C as shown in Figure 42 to derive n_{CO_2} . The corresponding $\ln(-r_{CO_2}) \sim \ln C_{CO_2}$ plot (Figure 43) finds a linear relationship with a slope of 1.1 ± 0.2 , indicating that the apparent reaction order with respect to CO_2 , n_{CO_2} , is 1.1 and is within experimental uncertainty of one. Thus, the reaction mechanism associated with Mg_2SiO_4 based carbonation process appears first order, as further supported as discussed below.

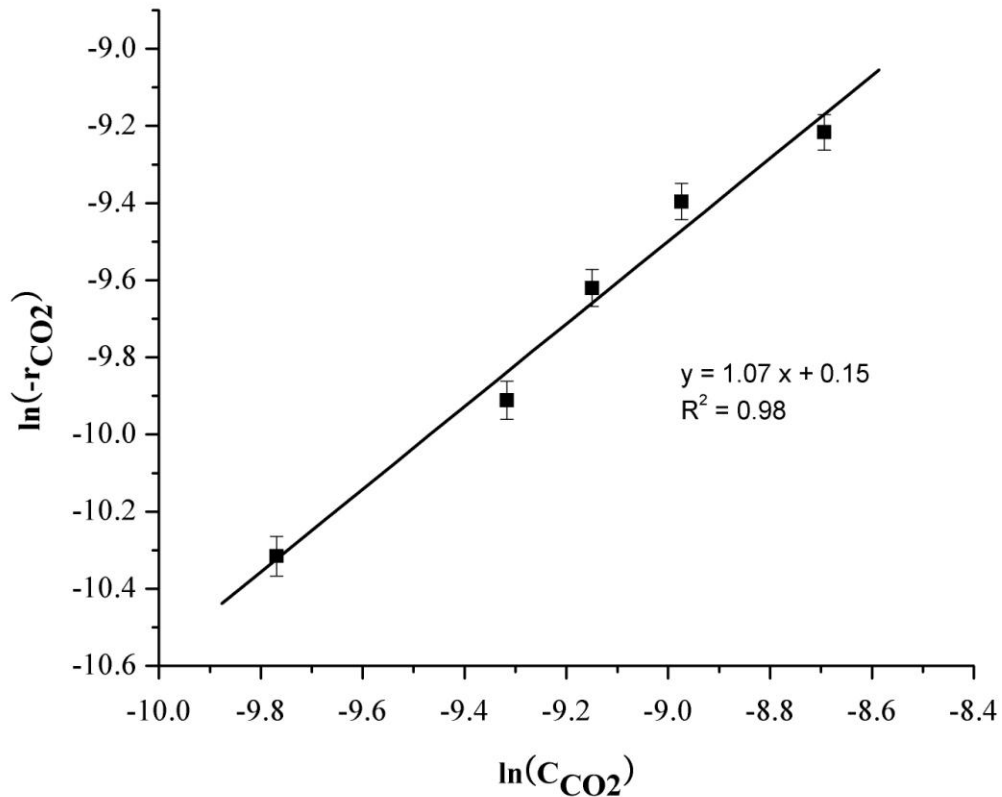
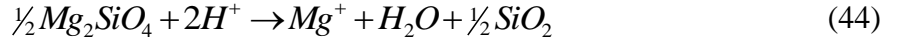


Figure 43. Determination of the reaction order at 200°C for Mg_2SiO_4 carbonation with CO_2 in the presence of steam. Uncertainty results from 5 time multiple tests.

Assuming Eq. 37 proceeds through the following elementary steps in the presence of water during the CO₂ sorption process,



according to rate law the consumption rate of CO₂ can be expressed as

$$-r_{CO_2} = k_{R2,forward} C_{CO_2} C_{H_2O} - k_{R2,reverse} C_{H^+}^2 C_{CO_3^{2-}} \quad (46)$$

where $k_{R2,forward}$ and $k_{R2,reverse}$ represent the forward and reverse reaction rate constants of Eq. 37, respectively, C_{CO_2} , C_{H_2O} , C_{H^+} and $C_{CO_3^{2-}}$ correspond to the concentrations of the CO₂, H₂O, H⁺ and CO₃²⁻ on the surface of Mg₂SiO₄. C_{H_2O} can be treated as a constant since H₂O is actually neither consumed nor generated when both Eq. 43 and Eq. 44 are considered. H₂O is just a H⁺ carrier. Then Eq. 46 becomes

$$-r_{CO_2} = k'_{R2,forward} C_{CO_2} - k_{R2,reverse} C_{H^+}^2 C_{CO_3^{2-}} \quad (47)$$

where $k'_{R2,forward} = k_{R2,forward} C_{H_2O}$. Furthermore, both C_{H^+} and $C_{CO_3^{2-}}$ should be very low for two reasons. The first one is that the forward reaction rate of Eq. 43 is very slow since CO₂ has low solubility in water in the tested temperature range, resulting from the exothermal characteristics of the reaction, particularly at 200°C, a relatively high temperature for sorption. Secondly, Eq. 44 and Eq. 45 are much quicker than the forward reaction of Eq.43. Thus C_{H^+} and $C_{CO_3^{2-}}$ can be considered to be very small, and their product as negligible so Eq. 47 can be further simplified as

$$-r_{CO_2} = k'_{R2,forward} C_{CO_2} \quad (48)$$

which is very similar to Eq. 48. In other words, the reaction orders with respect to CO_2 , n_{CO_2} , derived with postulated reaction mechanism and obtained with experimental results, are consistent. Two conclusions can be inferred from the consistence. The first one is that the proposed CO_2 carbonation mechanism described in Eq.43-45 reflects the reaction reality of Eq. 37. Secondly, Eq. 43 is the rate controlling reaction in the overall Mg_2SiO_4 based CO_2 sorption process.

2) Arrhenius form

It is well known that the relationship between the reaction rate constant (k) and reaction temperature (T) can be correlated using the Arrhenius form

$$k = Ae^{-E_a/RT} \quad (49)$$

where A is the preexponential factor which is treated as a constant in the studied temperature range as many people do during their kinetic studies even though it is actually affected by temperature, E_a is the apparent activation energy of the Mg_2SiO_4 based carbonation process as shown in Eq. 37, and R is the ideal gas constant. The pre-exponential factor would also be impacted by reactor conditions (e.g., geometry, loading), and these were kept constant between experiments. k values at 100°C, 125°C, 150°C, 175°C and 200°C were obtained using the corresponding CO_2 sorption profiles and plotted (Figure 44). Regression found a slope of 76.2 ± 4.8 kJ/mol and an A value of $1.35 \pm 0.18 \times 10^9$ (mmol/dm³)^{-0.1} .s⁻¹.(g-sorbent)⁻¹, respectively. Thus, the Arrhenius form of CO_2 carbonation with Mg_2SiO_4 within H_2O environment for the geometry of our experiments is

$$k = 1.35 \times 10^9 \pm 0.18 e^{-\frac{9160}{T}} (\text{mol}^{-0.1} \text{dm}^{0.3} \text{s}^{-1} (\text{g} \cdot \text{sorbent})^{-1}) \quad (50)$$

Reaction order and activation energy of Eq. 37 should not be affected by the flow rate of the simulated flue gas mixture under the given sorption operation conditions, and this was verified by conducting CO₂ sorption tests with the same initial CO₂ concentration but gas flow rates of 0.25 and 1.0 L/min. The derived values of the reaction order and activation energy values of Eq. 37 for the three flow rates (0.25 L/min, 0.5 L/min, and 1.0 L/min) were consistent (Table 14).

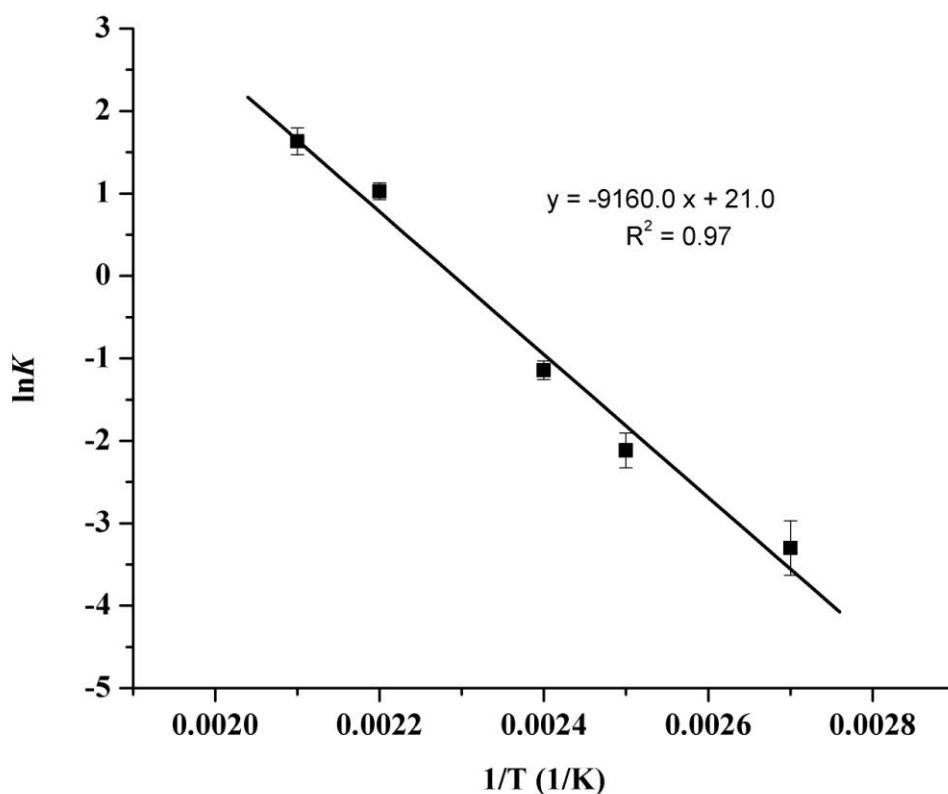


Figure 44. Determination of the apparent activation energy, E_a for Mg₂SiO₄ carbonation with CO₂ in the presence of steam (CO₂ concentration, 4.1 mmol/dm³; H₂O concentration, 4.1 mmol/dm³; Experimental temperature of 100-200°C with 25°C interval). Uncertainty results from 5 time multiple tests.

TABLE 14. Reaction order and activation energy of the carbonation in the presence of steam as a function of different flow rates. Uncertainty results from 5 time multiple tests.

Flow rate (L/min)	Reaction order (n_{CO_2})	Activation Energy, E_a (kJ/mol)
0.25	1.1 ± 0.3	76.5 ± 3.7
0.5	1.1 ± 0.2	76.2 ± 4.8
1	1.2 ± 0.1	77.2 ± 5.4

The Mg_2SiO_4 carbonation reaction was carried out as a laboratory scale demonstration for the CO_2 sequestration directly out of exhaust streams, without need for previous CO_2 separation and/or pressurization. For exhaust streams or flue gases containing steam, magnesium silicate can also be used temperatures up to 200°C. Steam was found to enhance that amount of CO_2 removed from the gas stream significantly. The empirical kinetic model developed in this work provides relevant information for the feasible application of CO_2 sequestration by stable carbonates on the olivine surface.

CHAPTER 4

MINERAL CARBONATION USING NATURAL OLIVINE SORBENT IN THE PRESENCE OF WATER VAPOR

Soonchul Kwon¹, Maohong Fan^{1,2,*}, Herbert F. M. DaCosta³, and Armistead G. Russell¹

¹School of Civil and Environmental Engineering, Georgia Institute of Technology, Atlanta, GA 30332, U.S.A, ²Department of Chemical and petroleum Engineering, University of Wyoming, Laramie, WY 82071, U.S.A., Chem-Innovations LLC, P.O. Box 3665, Peoria, Illinois 61612, U.S.A

To evaluate the feasible application of natural olivine for CO₂ sequestration, chapter 4 describes natural olivine mineralization in the presence/absence of water vapor under variable conditions of temperature, concentration, and residence time. This chapter also evaluates thermodynamic parameters of olivine carbonation and the role of water vapor.

The adsorptive surface carbonation of olivine, which is the most abundant mineral occurring naturally in the upper mantle, in the presence of water vapor was investigated to determine their potential for CO₂ sequestration. Based on the thermodynamics for a basis of the reaction mechanism, the olivine carbonation reaction is thermodynamically favorable. Water vapor functions in an important role to improve the carbonation rate and capture capacities. Experimental results reveal that carbon dioxide can bind to the surface of olivine minerals, consisting of various compounds to form stable surface carbonates. High stable capture capacities of CO₂ were determined by observing CO₂ adsorption activity in the

* To whom correspondence should be addressed. E-mail: mfan@uwyo.edu. Tel: 307-766-5633. Fax: 307-766-6777.

presence/absence of water vapor at different temperatures in a flow reactor packed with olivine adsorbent. Moreover, carbonation reactions at different reactant concentrations and residence times were carried out to establish the reaction activity of the sorbent.

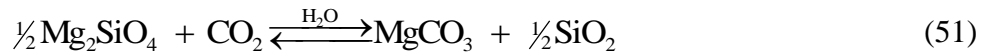
4.1 Introduction

The rapid growth in the demands of industrial energy has led to the accumulation of carbon dioxide, the primary factor responsible for global climate change. The International Panel on Climate Change (IPCC) report (2005) also stated that CO₂ concentration in the Earth's atmosphere has increased from 280 ppmv before industry development to 380 ppmv in 2005, and it is expected to rise to 590 ppmv by 2100. Since about 40% of the total CO₂ emissions in the U.S. are released from power stations employing fossil fuel energy sources, many studies have focused on the promotion of highly efficient CO₂ capture or storage technologies from the flue gas stream of coal-fired power plants [32].

Among the various CO₂ separation processes, the adsorption process is considered the most promising, requiring low management costs with low energy consumption because of its deployment and high capture efficiency particularly when the sorbent involves high CO₂ selectivity and high CO₂ adsorption capacity compared to conventional chemical sorption with high energy demands and limited CO₂ loadings [3, 10, 37, 38]. Instead of liquid sorbents, solid adsorbents are relatively easy to handle and mitigate corrosion problems [11, 12]. In addition, due to their reusable property, they are environmentally benign. Therefore, the development and application of cost-effective solid sorbents is desirable.

As a potential CO₂ sequestration process, mineralization (the process of chemical weathering by alkaine-earth minerals to form stable carbonates that exist in great quantities

in the Earth's crust) can be adopted. Olivine [(Mg, Fe)₂SiO₄] is a feasible candidate for mineral feedstock carbonation due to its high reactivity to CO₂, its simple structure, its low supplying cost (\$4~\$5/ton) from mined and milled feedstock, and its environmentally-friendly chemical reaction [18, 19, 153]. In addition, solid byproducts contribute environmentally-friendly benefits of mine reclamation or soil amendments [18]. The reaction of olivine with CO₂ in the existence of water vapor is shown in Eq. 47:



Due to its inherently slow reaction in nature despite its exothermic and thermodynamically favorable properties, mineral carbonation may not be a practical system [18-20]. Therefore, to accelerate the carbonation rate, many pretreatment processes such as magnetic separation, heat treatment, various acid treatments, and HCl extraction have been developed. However, these methods are all energy intensive, resulting in increased energy penalty to the electricity output of a power plant of about 20% [18, 19]. Thus, the development of an efficient process that would allow the commercial application of these sorbents requires a significant increase in the reaction rate and the low energy demand of the natural mineral carbonation process.

To improve the reaction rate, water vapor was added to the gas mixture. Flue gas streams from power generation facilities generally contain 8–12% vol of CO₂ and 8–10% vol of water vapor and minor impurities such as SO_x and NO_x. The gas mixtures are pre-treated with a wash tower, but up to 5% vol of saturated water vapor still remains at ambient conditions [7, 8]. The high tendency of H₂O instead of CO₂ molecules to be adsorbed results in many sorbents, and the CO₂ capture capacity of the sorbents in the presence of water vapor

is less than that in the absence of water vapor; few studies in which CO₂ is separated with realistic concentrations of water vapor in flue gas have been conducted [69]. However, this carbonation process was in fact aided by water, which plays a significant role in increasing the reaction rate of carbonation.

For assessing its applicability for use in an the economically competitive regeneration carbonation process, isothermal desorption, performed at the same temperature as the adsorption process, was carried out. Using the same temperature for adsorption and desorption reduces the energy requirement unlike general temperature swing adsorption (TSA), adsorption at a lower temperature and desorption at a high temperature, requiring high energy.

In this study, the mineralization of olivine for CO₂ sequestration in the presence of water vapor was performed by varying temperatures, initial concentrations, and residence times under real compositions of flue gas from power plants. The thermodynamics for CO₂ adsorption on the olivine sorbent were also evaluated.

4.2 Experimental section

4.2.1 Materials

The olivine sample, supplied by Unimin Corporation (New Canaan, CT) and used without additional treatment, was composed of 92% forsterite (Mg₂SiO₄) and 8% fayalite (Fe₂SiO₄). The sorbent samples were characterized by structural, morphological, and analytical methods such as a BET surface area, a scanning electron microscope (SEM) with energy-dispersive X-ray spectroscopy (EDS), and X-ray diffraction (XRD). The BET surface

areas, pore volumes, and olivine sample sizes were measured before and after mineral carbonation with a Micromeritics ASAP 2020 analyzer. The particle size and morphology of the olivine samples were analyzed in a Hitachi SEM before and after a reaction. XRD patterns, which were performed with a D8 X-ray diffractometer (Bruker-AXS), provided scans in the 2θ range from 0° to 90° with $0.005^\circ/\text{s}$ before and after contact with carbon dioxide.

4.2.2 Experimental apparatus

The experimental setup of the mineral carbonation for CO_2 sequestration was made up of three parts: a gas simulation unit, a CO_2 sorption system, and equipment for CO_2 analysis in the gas stream (Figure 36). The N_2 in gas cylinder 1 was used for system cleaning and isotherm desorption. A gas mixture consisting of CO_2 balanced with N_2 was drawn from cylinder 2. Both gas streams were mixed to make the desired concentration of the gas stream. Flow rates of the inlet gases were controlled by Matheson Tri-gas FM-1050 flow meters. An additional flow meter indicated the flow condition of the inlet gas into the gas analyzer.

Olivine carbonation was performed in a quartz tubular reactor with a length of 610 mm and an inside diameter of 9 mm. The fixed bed was prepared by loading the adsorbent between small amounts of quartz wool that functions as the bed holder. The loaded reactor was placed inside a TF55030A-1 tube furnace (manufactured by Thermo Corporation, Asheville, NC) with a UT150 temperature controller (Yokogawa M&C Corporation, Newnan, GA) to manage the experiment temperature. A water vapor generation unit was designed to supply water vapor to the inlet mixed gas stream. Thermo-tapes were installed to prevent the condensation of water vapor inside the gas tubing with temperature controllers.

An effluent gas stream from the reactor entered the CO₂ analyzer, which acquired the CO₂ concentration profile, after passing a water vapor removal unit. CO₂ concentrations in the gas stream were measured before and after carbonation using the same ZRE analyzer (California Analytical Instruments, Inc.). The data acquisition system directly recorded the continuous outlet CO₂ concentration from the gas analyzer every second.

4.2.3 Operation procedure

The olivine carbonation activity was estimated by measurements of the CO₂ conversion before and after the carbonation. Each test run was carried out with new samples. Initially, the tube furnace was preheated to the desired reaction temperature; meanwhile, several equal-sized tubular glass reactors were loaded with 0.50 g of olivine. When the set temperature was reached and maintained in the tube furnace, a sorbent-loaded quartz reactor was introduced into the furnace. To maintain constant operation conditions, we heated the sorbent for 10 minutes and connected the reactor to the gas supply unit and to the gas analyzer with the data acquisition unit. When the outlet CO₂ concentration was the same as the initial inlet CO₂ concentration, indicating that the sorbent was saturated with CO₂ molecules, the loading of CO₂ gas stream into the reactor stopped. For the regeneration step, the CO₂ gas flow was stopped, and pure N₂ was introduced without water vapor. The procedure was repeated five times with new samples at a desired experimental temperature, and an average value of the results was used to determine the olivine carbonation reaction profile.

4.3 Results and discussion

4.3.1 Characterization of olivine materials

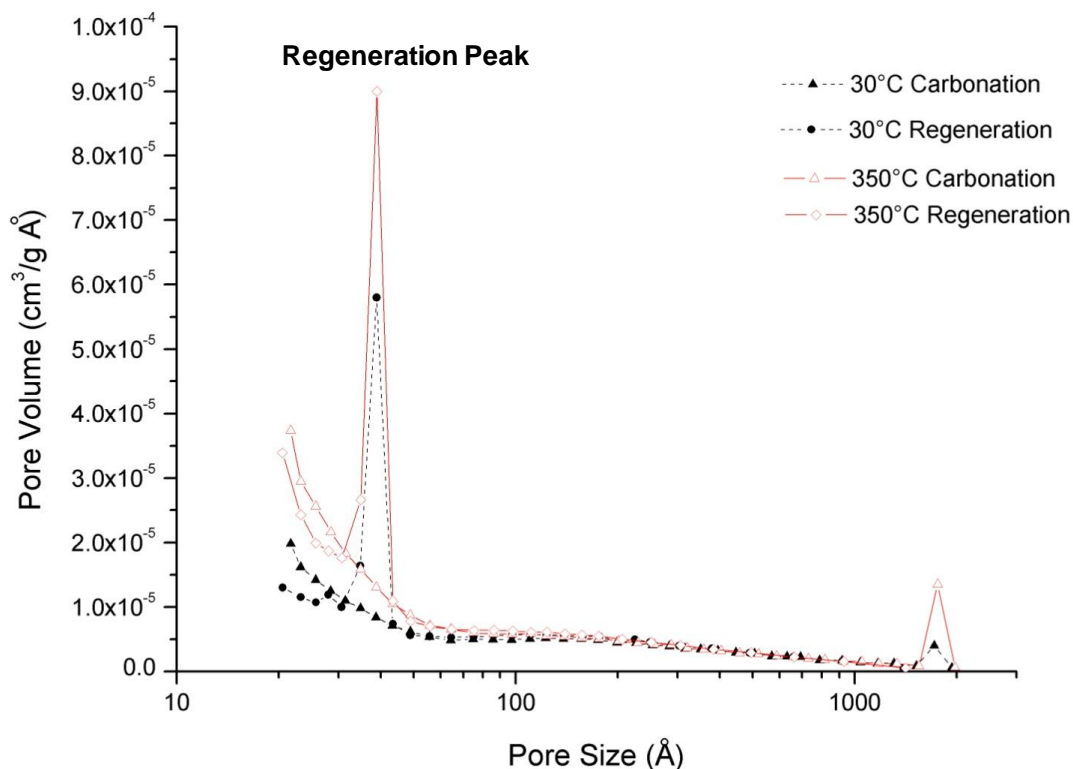


Figure 45. Pore size distribution for olivine after carbonation/regeneration.

Figure 45 shows the pore size distribution for olivine carbonation and regeneration. After carbonation reaction at 350°C ($1.63 \text{ m}^2/\text{g}$), the BET surface area is reduced 36% compared to that before carbonation ($2.63 \text{ m}^2/\text{g}$), because carbonates fill up the available void regions of the surface after reaction. Pore volume and size distribution for olivine samples were characterized after carbonation and regeneration at two different temperatures, 30°C

and 350°C for 4 hours. The pore volume of the adsorbent after regeneration was greater than that after carbonation since desorption resulted in the extraction of CO₂ from the filled region of the pores at high temperature (350°C). This resulted in suitable regeneration because of the thermodynamically favorable backward reaction ($\Delta G > 0$ at above 224°C).

TABLE 15. The chemical composition of the olivine sample

Compound	Composition %
MgO	49.3
SiO ₂	42.1
Fe ₂ O ₃	8.3
Al ₂ O ₃	0.15
Na ₂ O	0.04
K ₂ O	0.04
CaO	0.01

The bulk chemical composition of the studied sample is shown in Table 15. Olivine is composed of mainly MgO and SiO₂. Since in nature, magnesium is rarely found as a binary oxide and has a high tendency to be bound to a silicate mineral, MgO generally exists as a form of magnesium silicate.

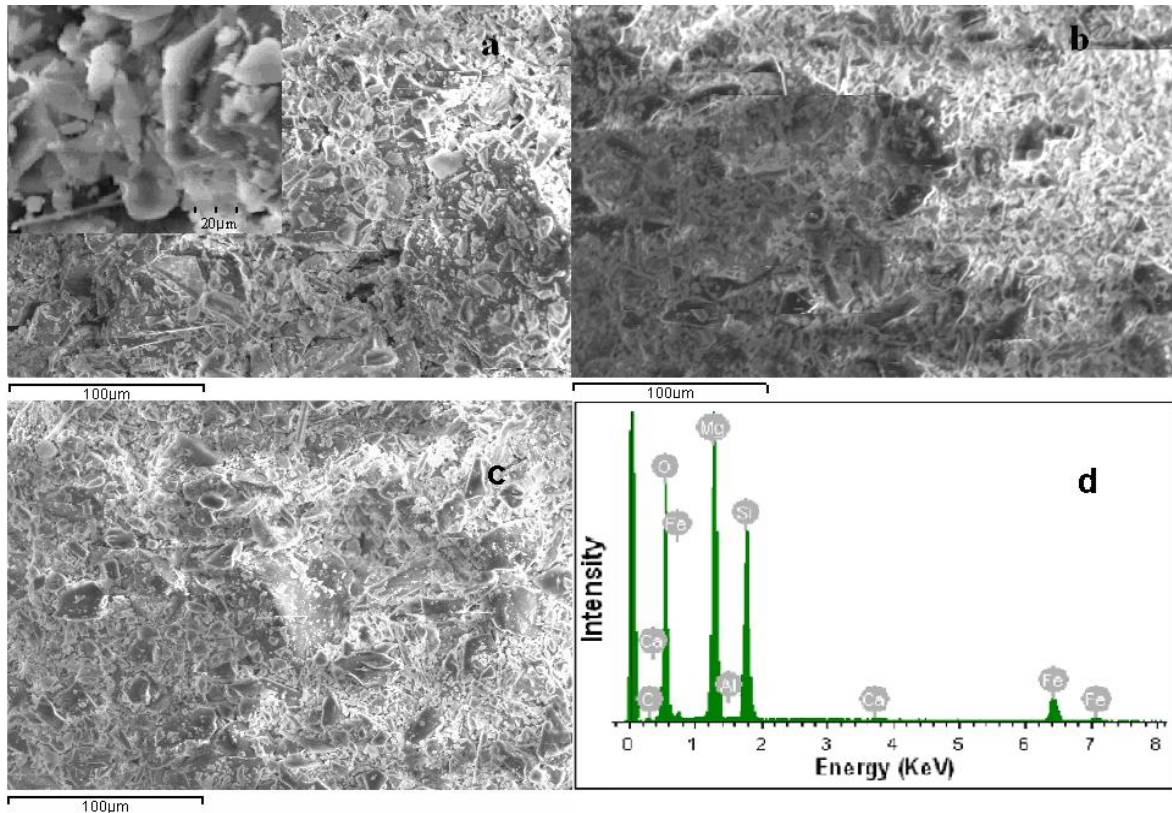


Figure 46. SEM images of (a) Fresh olivine sample, (b) After olivine carbonation in the absence of water vapor at 200°C, (c) After olivine carbonation without the presence of water vapor at 200°C, and (d) EDS spectra of the fresh olivine sample.

The SEM images of the non-carbonated and carbonated olivine samples indicate morphological differences between them (Figure 46). In Figure 46a, the fresh olivine is in the form of irregular and polyhedral polycrystalline particles in linking ingrown groups. The polyhedral structures display the main contributors of Mg and O for MgO, and the irregular and laminar fragments indicate Si and O for SiO₂ as another major mineral in the multi-mixture mineral [170]. After carbonation, slight abrasion and erosion occurred due to interactions between the particles and other particles as well as between the particles and the polyhedral clusters of mineral crystals, resulting in the agglomeration of particle crystallites

and the formation of product fragments. The fracture and desquamation of fragmentary materials with irregular structures are attributed to the phase transformation of amorphous minerals with CO₂ under chemical sorption. The textural modification of the olivine sorbent after the carbonation step was shown because of the formation of carbonates. In addition, during the carbonation in the presence of water vapor (Figure 46c), filling and pluggage of the pores was observed more significantly than in the absence of water vapor (Figure 46b), indicating that water vapor plays a key role in the enhancement of the carbonation reaction. Peak intensities in energy-dispersive X-ray spectroscopy (EDS) also indicate that the olivine material consists of the high Si, Mg and O contents (Figure 46d).

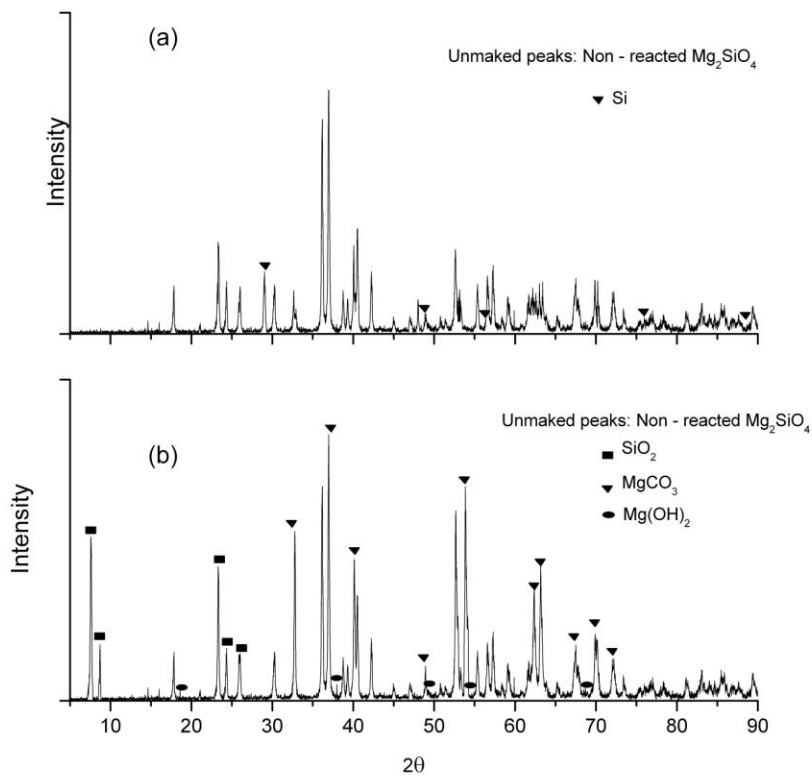


Figure 47. XRD patterns of the fresh (a) and (b) carbonated product samples with 10% vol CO₂, ~8.3% vol H₂O at 200°C.

Figure 47 shows the XRD patterns of the olivine sample after carbonation in the presence of water vapor at 200°C. The XRD pattern of carbonated material shows magnesite (MgCO₃), silica (SiO₂), and non-reacted olivine (non-carbonated region of olivine). In addition, the XRD results do not show a high quantity of hydrogen linked materials, indicating that the silicon dioxide-rich compounds are not associated with hydrogen bonding, but with Si-O-Si formation [171].

4.3.2 Thermodynamics of olivine carbonation

Carbonates are highly stable under ambient conditions because the Gibbs free energy of MgCO₃ (-1028kJ/mol) is significantly higher than CO₂ (-394kJ/mol). The enthalpy and Gibbs free energy of olivine carbonation dependent on the temperature were calculated to determine the thermodynamically feasible conditions for this process (Figure 48). Gibbs free energy of formation can be estimated by using the formulation of the free energy of reaction:

$$\Delta G_T = \Delta H_T - T\Delta S_T \quad (52)$$

$$\Delta G_T = (\Delta H_T + \int_{T_0}^T \Delta C_p dT) - T(\Delta S + \int_{T_0}^T \frac{\Delta C_p}{T} dT) \quad (53)$$

$$\Delta G_T^{Carbonation} = \left(\sum_i v_i \Delta G_{T,i} \right)_{\text{products}} - \left(\sum_i v_i \Delta G_{T,i} \right)_{\text{reactants}} \quad (54)$$

where ΔG : Gibbs free energy, ΔH : enthalpy, ΔS : entropy, v is the stoichiometric coefficient of species i , $C_p = a + bT + cT^2$ in which a, b, and c are empirical constants [172]. Note that these empirical constants are obtained by interpolation of the data at 298K, 400K, and 600K.

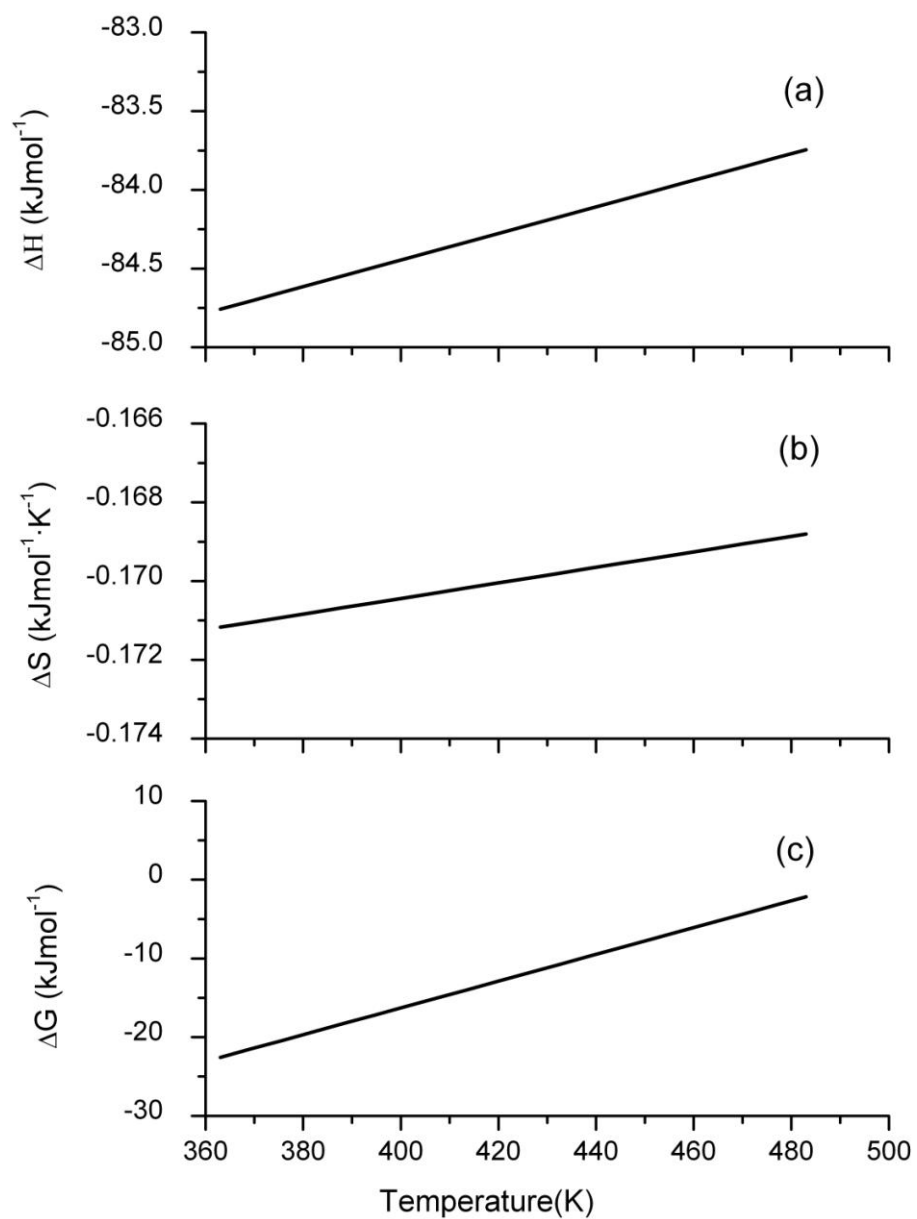


Figure 48. Thermodynamic properties of olivine carbonation reaction. (a) Enthalpy change ($\Delta H_T^{\text{Carbonation}}$), (b) Entropy ($\Delta S_T^{\text{Carbonation}}$), and (c) Gibbs free energy change ($\Delta G_T^{\text{Carbonation}}$).

Since forsterite ($(\text{Mg}_{0.92}, \text{Fe}_{0.08})_2\text{SiO}_4$) is present in most olivine samples where $\text{Mg}/(\text{Mg}+\text{Fe})$ is greater than 0.9, and the reaction between Fe^{2+} and CO_2 is neglected due to the low tendency of reaction process, the thermodynamic properties of olivine is approximated from those of magnesium silicate (Mg_2SiO_4). The heat yielded during the olivine carbonation reaction is used as the energy for heating the reactant to the desired experimental temperature (423K to 473K). The highly exothermic carbonation leads to the heat generation, which strongly implies that olivine carbonation is a feasible reaction since the change in enthalpy retains a negative value in the experimental temperature range.

The plot of entropy change also supports the idea that olivine carbonation capacity declines as temperature increases because when a system is heated to higher temperatures, the entropy of reaction is smaller. This result suggests that this mineral carbonation reaction depends on a temperature effect, which is compatible with the experiment results.

As temperature increases, the enthalpy for olivine carbonation slightly increases, and Gibbs free energy change gradually increases. This confirms that the process tendency of olivine carbonation gradually decreases with an increase in temperature. In the lower than 200°C (473K) temperature range, the values of $\Delta G_T^{\text{Carbonation}}$ are still negative since the increases of $\Delta H_T^{\text{Carbonation}}$ are smaller than $\Delta S_T^{\text{Carbonation}}$, so olivine carbonation spontaneously proceeds to form the carbonate products. For this carbonation reaction, the optimal temperature is known to be between 150°C and 200°C [153, 168, 169]. Thus, we decided to perform olivine mineralization at an experimental temperature below 200°C.

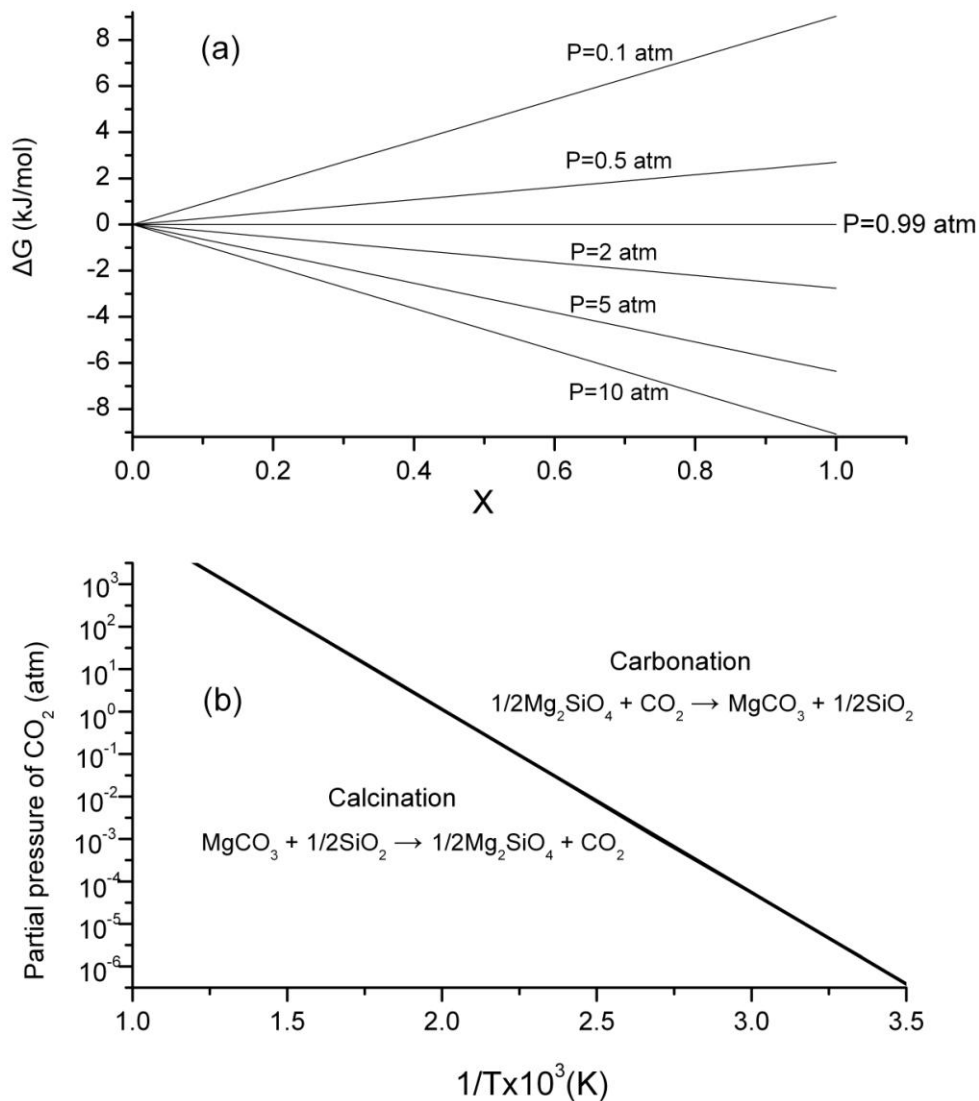


Figure 49. Gibbs free energy change as a function of extent of carbonation at $T=473\text{K}$ (a); Carbonation pressure of Mg_2SiO_4 – MgCO_3 – CO_2 equilibrium (b).

We carried out experiments of olivine carbonation at temperatures below 200°C as shown in Figure 49. The change in Gibbs free energy can be seen as a function of the CO_2 partial pressure and the equilibrium state of the magnesium silicate–magnesite (carbonate)–carbon dioxide system. Above 0.99 atm of CO_2 partial pressure at 200°C (473K), the Gibbs energy change of reaction decreases as the chemical reaction proceeds (Figure 49a),

indicating that full carbonation is highly favorable under these conditions. Below 0.99 atm, on the other hand, the Gibbs free energy change of the reaction increases as the molar extent of the chemical reaction increases. However, at 0.99 atm of CO₂ partial pressure at 473K, the Gibbs free energy change is zero along the entire reaction coordinate and the material is fully carbonated, indicating that a partial or full forward reaction can still occur without driving forces to produce carbonates. The equilibrium partial pressure of carbon dioxide results from a balance between calcination and the formation of carbonates (Figure 49b). The carbonate formation pressure changes significantly with temperature, varying by 9 orders of magnitude in the temperature range studied. In the range of the experimental temperatures (423K to 473K), the carbonation spontaneously proceeds when CO₂ partial pressure is above 0.37 atm.

4.3.3 Effect of the temperature on CO₂ separation

Figure 50 illustrates the carbonation and regeneration profiles on 0.5g of olivine adsorbent for CO₂ sequestration with/without water vapor in the range of 150°C to 200°C at intervals of 25°C. At temperatures above 150°C, the reactions for the surface carbonation occur quickly (in minutes, not days). The CO₂ concentration in the effluent gas stream decreased noticeably within less than 1 minute and then gradually increased to the initial inlet CO₂ concentration level (10% v/v CO₂).

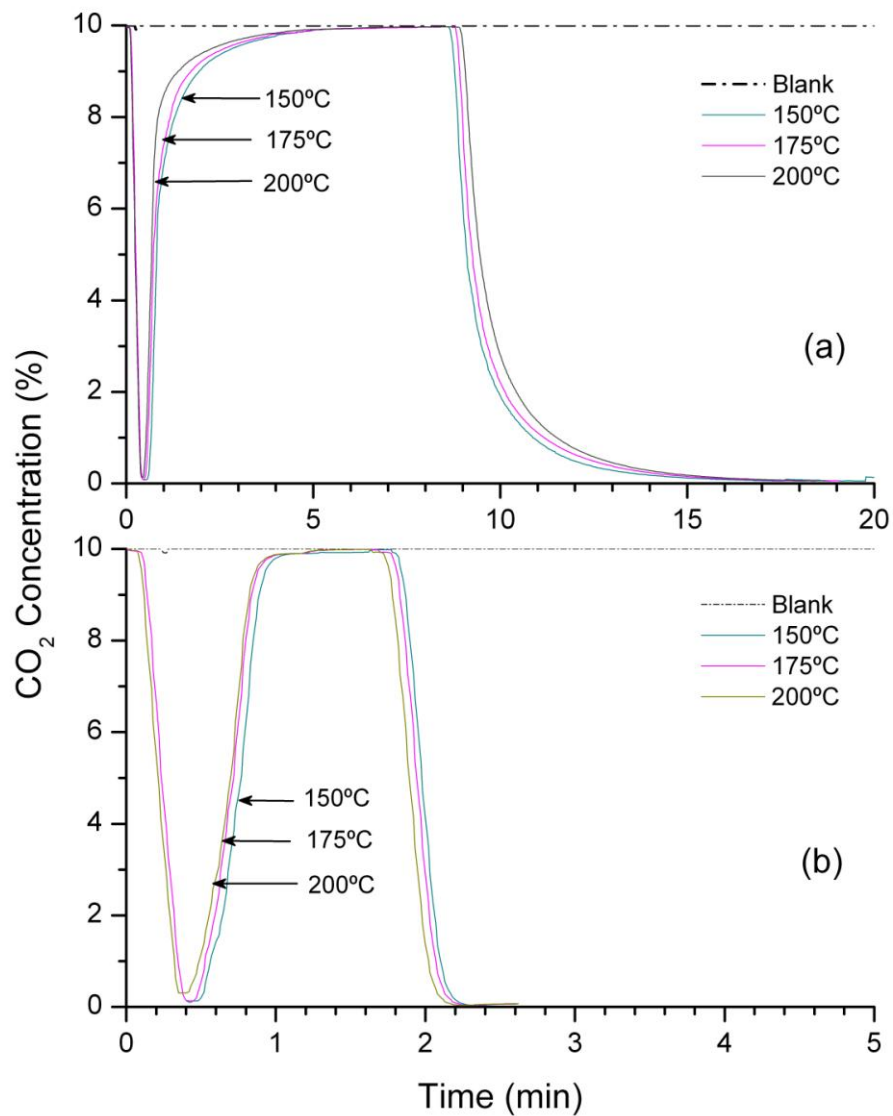


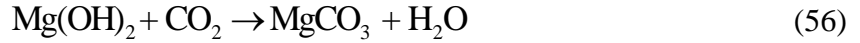
Figure 50. CO₂ carbonation and regeneration profile with water vapor (a) and without water vapor (b) as a function of temperature while employing an inlet flow rate of 0.5L/min, weight of 0.5g magnesium silicate adsorbent, and feed composition of 10% vol CO₂, ~8.3% vol H₂O, balanced with N₂. The blank test is performed without sorbent at 200°C.

The lowest concentration reached is 0.3% v/v (97% removal), indicating a higher capture capacity for olivine adsorbents than for conventional materials (0.03 g CO₂/g to 0.13 g CO₂/g) [8, 14, 15, 46, 51, 57, 70, 71, 77, 83, 93, 111]. Figure 50 shows that as temperature increases the adsorption capacities of CO₂ obtained with olivine decrease, following a bell-shaped curve regardless of the presence of water vapor. In spite of this trend, the sorption rate at high temperature was faster than that at low temperature, as observed by the higher slope of the higher temperature curve. This behavior is the results of thermal effects, which enhance the energy of the species and increase thermal motions, both of which lead to a higher carbonation rate.

CO₂ adsorption on olivine is likely to be a surface-limited phenomenon since the amount of CO₂ adsorbed per unit weight of olivine is relatively small. In the initial period, the CO₂ is linked to the surface of the olivine adsorbent. Then, the carbonation reaction quickly proceeds with the heterogeneous surface adsorption process to form a stable surface carbonate instead of the bulk carbonate. During the carbonation reaction, the MgCO₃ surface layer thickens, inhibiting CO₂ adsorption into the unreacted pore regions of materials. Thus, the chemical process rate is reduced even if the Mg₂SiO₄ sample keeps reacting at the pores of the sorbents, indicating that the extent of mineralization for CO₂ sequestration is mainly dependent on the carbonation rate.

To determine the effect of water vapor, we performed a series of experiments using 0.5g olivine sorbent without water vapor. The breakthrough curve of CO₂ adsorption in the presence of water vapor indicates a considerable effect of water vapor on CO₂ capture capacity, indicating that the presence of moisture promotes the CO₂ carbonation reaction with olivine sorbents.

It is believed that the role of water vapor is that it activates the olivine surface by producing hydroxide ($\text{Mg}(\text{OH})_2$) as an intermediate and carbonate (MgCO_3) as a final formation on the surface by the following equation:



These processes increase reaction rate on the surface according to the following steps:

1) adsorbed water desorbs at a temperature above 100°C ; 2) a hydroxide dissociates at a temperature above 150°C and Mg^{2+} and O^{2-} reacts with CO_2 to form MgCO_3 [173, 174]. The observation of a small amount of $\text{Mg}(\text{OH})_2$ in the preceding XRD pattern of the olivine sample after carbonation also supports this mechanism (Figure 47b).

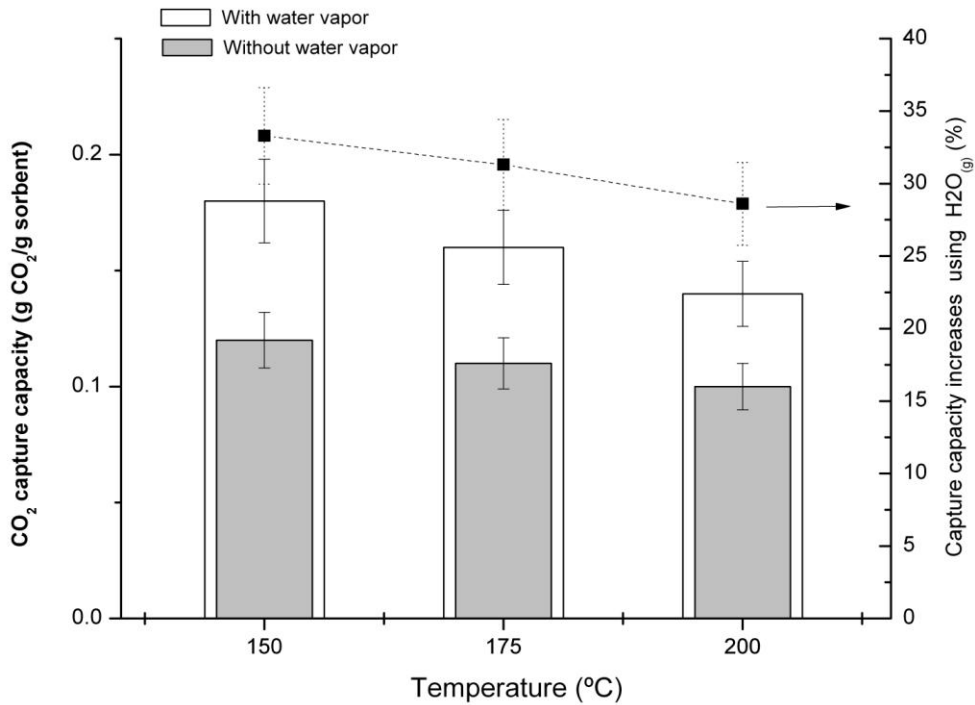


Figure 51. CO_2 capture capacities without and with water vapor dependent on the temperature. Uncertainty results from 5 time multiple tests.

In the entire range of temperatures, the partial regeneration process at constant high temperature was carried out after mineral carbonation was completed, indicating that the partial recovery process of the sorbent proceeded relatively forthrightly. In the isothermal desorption process, due to the yield of thermal energy from desorption of the adsorbed species, the adsorption becomes equilibrium state between a reacting olivine surface and an adsorbed CO₂ gas phase. Finally, the adsorbed CO₂ on the surface of the sorbents can be partially recovered and return to the surrounding mobile gas phase via purging with N₂.

Figure 51 shows the qualitative total and 90% capture capacities in the temperature range of 150°C to 200°C. Compared to commercially available sorbents with CO₂ capture capacities between 0.08 and 0.088g CO₂/g sorbent as well as currently researched adsorbents with a range of 0.1 to 0.3g CO₂/g adsorbent, olivine adsorbents in this temperature range are noticeably better performing than commercial sorbents [8, 14, 15, 46, 51, 57, 70, 71, 77, 83, 93, 111]. In the entire temperature range, the total capture capacity of 0.5g of olivine is more than 0.14g CO₂/g olivine and even the 90% capture capacity is considerably larger than those of other adsorbents. When using water vapor, the capacities increase more than 28%, indicating that the capture capacity of carbon dioxide in the presence of water vapor is actually improved over that in the absence of water vapor. Olivine carbonation without water vapor always trailed carbonation with water vapor, so a much higher temperature is required in dry carbonation processes to achieve the same carbonation capacities of CO₂ as were achieved with water vapor.

In addition, the CO₂ capture capacity of olivine sorbents is slightly greater than that of pure Mg₂SiO₄ [175], which could be due to multiple effects, involving (1) the catalytic function of other olivine components, especially Fe₂O₃, known as a feasible catalyst, (2) the

vigorous abrasion and erosion of particles and clusters, and (3) the high adsorption affinity related to the tridimensional structure of olivine. Under the optimized operational conditions, the higher conversion rates and lower energy consumption of the olivine based olivine based CO₂ capture technology could lead to its feasible applications in practical power plants [175, 176].

4.3.4 Regeneration of spent sorbent

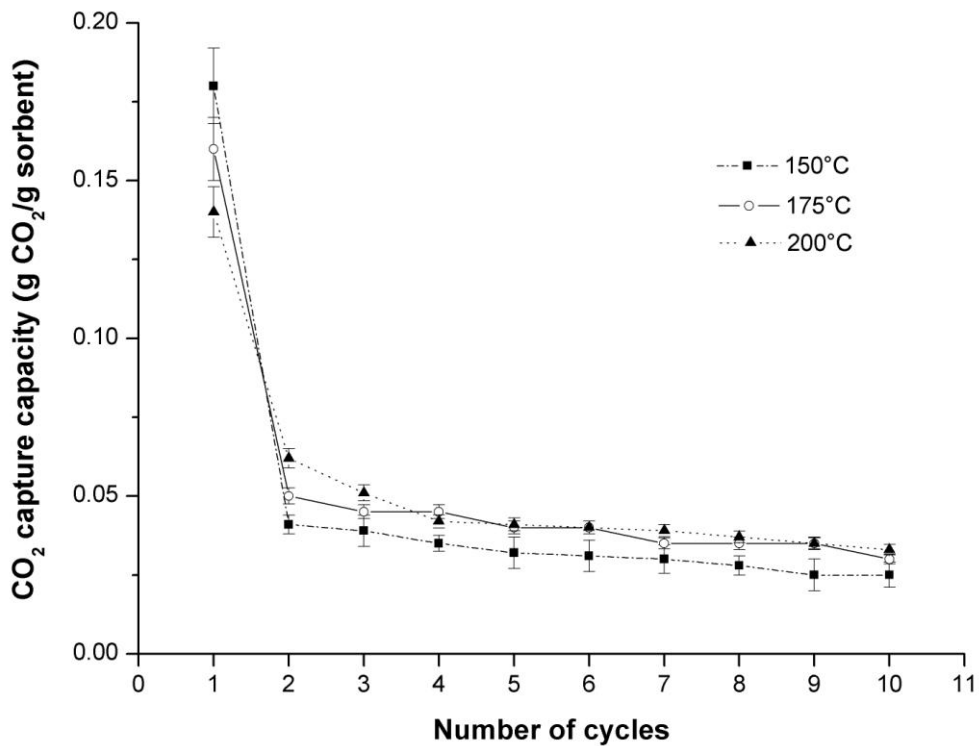


Figure 52. Cyclic CO₂ adsorption and desorption processes in the different temperatures (Inlet flow rate of 0.5 L/min, weight of 0.5 g magnesium silicate adsorbent, and feed composition of 10% vol CO₂, ~8.3% vol H₂O, and balanced with N₂). Uncertainty results from 5 time multiple tests.

Another series of tests shows that the regeneration capacities of olivine adsorbent after ten carbonation and regeneration cycles using the same sorbent with two main steps: carbonation for 30 minutes and partial regeneration, as shown in Figure 52. Overall, CO₂ capture capacities dramatically decrease during cyclic regeneration due to the textural modification of the solid sorbent surface after the fast carbonation step, increasing the formation of stable surface carbonates during CO₂ reduction. Additionally, the isothermal desorption could not fully regenerate the sample because the dissociation of the chemisorbed species is a slow process that requires a high temperature. Above 175°C, where the chemical reaction is more favorable, regeneration capacities decrease even more abruptly. During the recycle process, olivine mostly forms products that fill the pores, cover the surface, and thicken the product layers of the sorbents, causing a slow carbonation rate and reducing the CO₂ sorption capacities. These phenomena result from a lower energy of activated coordinative chemisorption (weak interaction), indicated by the low heat of adsorption, since the dissociative strong chemisorption is a slow process and these species must be desorbed at a higher temperature [177].

4.3.5 Effect of residence time

To evaluate the effect of reactor throughput or the time of contact with the heterogeneous adsorbent, another series of tests was conducted in which total gas feed rate was varied under constant inlet concentration and temperature, determining residence time. The experimental results were analyzed by observation of how carbonation was affected by residence time, or the time expended in processing a unit mass of feed by a unit mass of

adsorbent in the tubular flow reactor, because space time is defined by the mass instead of the surface area of the sorbent as follows:.

$$\text{Residence time} = \frac{V - \frac{W}{\rho_{\text{olivine}}}}{\nu} \quad (57)$$

where V is the volume of reactor; W is the mass of olivine (mg); ν is the feed rate, cm^3/min ; and ρ is the olivine density, mg/cm^3 . The experimental results were analyzed by observing how carbonation was affected by space time or the time expended in processing a unit mass of feed by a unit mass of adsorbent in the tubular flow reactor.

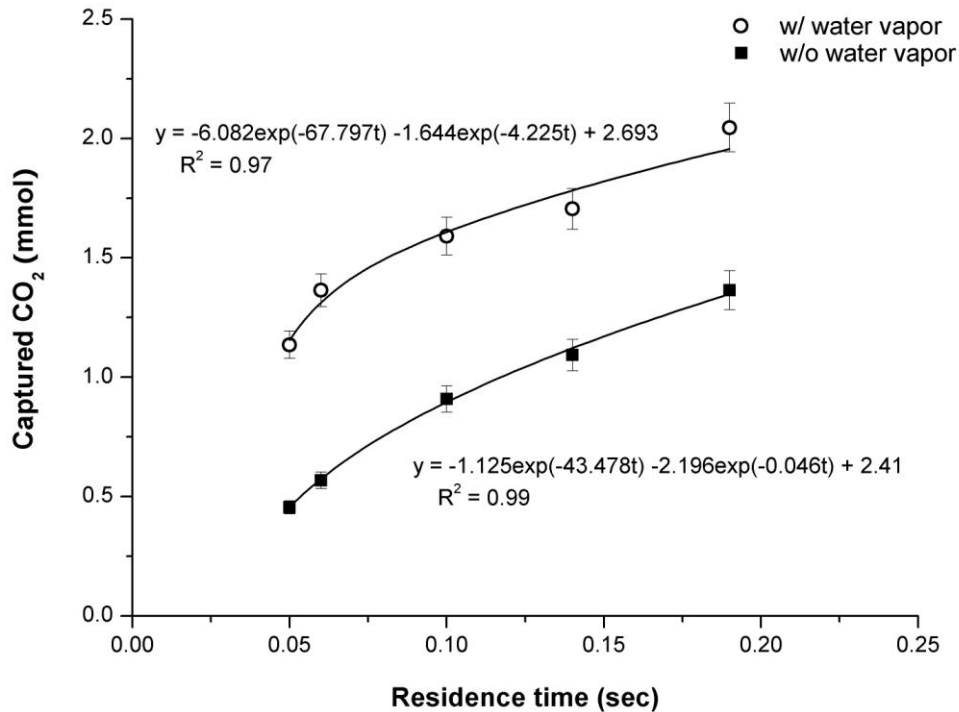


Figure 53. CO₂ capture capacities as a function of residence time (Experimental temperature of 200 °C, weight of 0.5 g olivine adsorbent, and feed composition of 10% vol CO₂, ~8.3% vol H₂O, and balanced with N₂). Uncertainty results from 5 time multiple tests.

We performed experiments at five different flow rates (0.25, 0.35, 0.5, 0.75, and 1L/min) of the inlet gas mixture for magnesium silicate adsorbent at 200°C. The effects of space time on the CO₂ adsorption capacity are illustrated in Figure 53. It is apparent that CO₂ adsorption on the olivine sorbent was significantly influenced by changes in the employed space time. The carbonation reaction is seen to be limited by space time since the lower flow rate provides a longer contact time between adsorbates and adsorbents in a heterogeneous system. In other words, the final extent of carbonation was determined by the reaction rate because in a very short contact time mass transfer became limiting and the total mass transfer of carbon dioxide was smaller than that in a long space time.

4.3.6 Effect of initial concentration

We also performed additional experiments to determine the activity of the olivine sorbent as we varied CO₂ concentrations (5% v/v, 10% v/v, and 20% v/v) and water vapor concentrations at 200°C (Table 16). The concentration in the inlet gas stream was the only parameter changed during the tests while the rest of the experimental conditions remained unchanged (0.5 g of olivine, 0.5 mL/min of flow rate). At a high initial CO₂ concentration (20% v/v), the carbonation capacity was reduced as a large amount of carbon dioxide molecules were adsorbed in certain large sites of the adsorbent's surface through valence bonds, limiting additional adsorption.

TABLE 16. The capture capacities of mineral carbonation as a function of the initial CO₂ concentration. (Experimental temperature of 200°C, weight of 0.5 g olivine adsorbent and feed flow rate of 0.5 L/min). Uncertainty results from 5 time multiple tests.

Concentration (vol %)		CO ₂ capture capacity (g CO ₂ /g olivine)
5% CO ₂	w/o H ₂ O(g)	0.10±0.011
	~8.3% H ₂ O(g)	0.11±0.012
10% CO ₂	w/o H ₂ O(g)	0.10±0.010
	~8.3% H ₂ O(g)	0.14±0.014
20% CO ₂	~8.3% H ₂ O(g)	0.06±0.005
	~17.2% H ₂ O(g)	0.08±0.007

Typically, CO₂ capture capacities increases when CO₂ concentration decreases. However, at a lower CO₂ concentration (5% v/v), the capture capacity was reduced in comparison to the one obtained at a concentration of 10% v/v CO₂. There is also no significant enhancement in carbonation capacity in the presence of water vapor compared to the same process in the absence of water vapor. This was probably limited by the fact that the CO₂ concentration (5% v/v) was smaller than that of the water vapor (~8.3% v/v), so that the adsorption of the water molecules onto the olivine's surface, instead of CO₂ molecules, is likely to increase.

4.3.7 Water sensitivity

The mineral carbonation and regeneration as a function of water vapor concentration was also investigated, as shown in Table 17. Three water vapor concentrations were sampled ~5.6% v/v, ~8.3% v/v, ~17.2% v/v H₂O with a constant concentration of 10% v/v CO₂. The breakthrough curve of CO₂ indicates a significant effect of water vapor on CO₂ capture capacity.

TABLE 17. Olivine carbonation processes for CO₂ sequestration as a function of water vapor concentration (Experimental temperature of 200°C, weight of 0.5 g olivine adsorbent, feed flow rate of 0.5 L/min and 10% vol CO₂ concentration). Uncertainty results from 5 time multiple tests.

Concentration (vol %)	CO ₂ capture capacity (g CO ₂ /g olivine)
w/o H ₂ O (g)	0.10±0.010
~5.6% H ₂ O(g)	0.13±0.015
~8.3% H ₂ O(g)	0.14±0.014
~17.2% H ₂ O(g)	0.12±0.013

It was observed that increasing in water vapor concentration to ~8.3% v/v H₂O, which was a smaller concentration than that of the CO₂ inlet gas, enhanced the CO₂ capture capacity. However, increasing the water vapor concentration to ~17% v/v H₂O, above the initial CO₂ concentration of 10% v/v CO₂, results in a loss of CO₂ capture capacity due to the wet agglomeration of the adsorbent as well as competition between H₂O molecules and CO₂ for adsorption on olivine. For the conditions of 5% v/v CO₂ and ~8.3% v/v H₂O shown in Table 16, the same pattern of carbonation and regeneration, with the material losing its capacity, is seen.

To verify the effect of water vapor concentrations, an additional CO₂ adsorption experiment was performed with a CO₂ concentration of 20% v/v and a high water vapor concentration of ~17.2% v/v. At these conditions, the ratio of CO₂ and H₂O is approximately double that of the original conditions represented in Table 16, which indicated that the capture capacity increased as water vapor concentration increased. It is apparent that the lower capture capacity of olivine at high H₂O concentration is caused not just by being

exposed to a high water vapor level, but also by overexposing H₂O molecules to sorbents. Since these molecules have an affinity to adsorb, the first filling of water vapor adsorbed can reduce the amount of CO₂ adsorbed and its condensation may lead to a pressure drop in the column and corrosive products by mixing with the CO₂.

These results support the premise that CO₂ adsorption is considerably limited by H₂O(g) concentration while H₂O(g) adsorption is insignificantly affected by the presence of CO₂, which has relatively low affinity and slow reaction rate to the olivine surface compared with H₂O(g). This evidence supports that the existence of active adsorption regions for water vapor on the surface of olivine samples. Thus, it is necessary to determine the level of water vapor injection to avoid losing capture capacities caused by overexposure of water vapor in order to improve the carbonation rate [7].

4.3.8 Effect of SO₂ and NO

Since CO₂ separation systems in the power plants are placed after additional pretreatments such as electrostatic precipitation and flue gas desulfurization to remove the toxic compounds such as fly ash, SO_x, and NO_x, SO₂ concentration in the flue gas mixture is lower than 5 ppm. However, even small concentration of SO₂ may affect on CO₂ capture capacity in the olivine carbonation. Thus, I performed an additional experiment using 2 ppmv SO₂ concentration to determine the effect of SO₂ for CO₂ capture (Table 18).

SO₂ doesn't affect the CO₂ capture although SO₂ is introduced since SO₂ concentration (2 ppmv) is significantly small and SO₂ adsorption on the olivine surface is not considerable.

TABLE 18. Effect of SO₂ concentration for olivine carbonation processes (Experimental condition: 10 % vol CO₂; 8.3 % vol H₂O; 2 ppm vol SO₂ balanced with N₂; Flow rate, 0.5 L/min; Temperature 200°C)

Capture capacity (CO ₂ g/g sorbent)	w/o H ₂ O	w/ H ₂ O
w/o SO ₂	0.10±0.010	0.14±0.014
w/ SO ₂	0.10±0.007	0.14±0.012

I used 5ppmv NO concentration to evaluate the effect of NO_x since flue gas stream consists of NO_x (Table 19). The difference of CO₂ capture capacity with and without NO is ignorable; NO doesn't affect CO₂ adsorption on the olivine surface since NO concentration is small, which does not make the reaction between NO and olivine at a faster rate.

TABLE 19. Effect of NO concentration for olivine carbonation processes (Experimental condition: 10% vol CO₂; 8.3% vol H₂O; 5ppm vol NO balanced with N₂; Flow rate, 0.5 L/min; Temperature 200°C)

Capture capacity (CO ₂ g/g sorbent)	w/o H ₂ O	w/ H ₂ O
w/o NO	0.10±0.010	0.14±0.014
w/ NO	0.10±0.009	0.14±0.012

4.4 Conclusion

Olivine carbonation was performed as a laboratory scale demonstration for CO₂ sequestration directly out of exhaust streams without the need for previous CO₂ separation and/or pressurization. The reaction activity of olivine was carried out by varying the temperature and the inlet concentration. The capture capacity of carbon dioxide with the appropriate concentration of water vapor was comparable to that without water vapor, and

CO₂ could be disposed of in a stable form. The thermodynamic parameters for olivine carbonation reaction indicate that substantial heat energy is released during carbonation, so additional energy for a reaction is not required. Olivine carbonation depends on residence time; it is controlled by reaction kinetics. The fast initial adsorption rate triggers the phenomenon whereby chemisorption on olivine predominantly takes place. This study basically lays the groundwork for the mechanism of mineral carbonation with carbon dioxide in the presence of water vapor and provides relevant information for the practical application of CO₂ sequestration by stable adsorption on mineral silicates.

CHAPTER 5

DENSITY FUNCTIONAL THEORY (DFT) STUDY OF CO₂ ADSORPTION ON THE CALCIUM OXIDE (100) SURFACE

SOONCHUL KWON,[†] JI IL CHOI,[‡] ARMISTEAD G. RUSSELL,[†] WANG RO LEE,[§]
SEUNG GEOL LEE,[‡] MAOHONG FAN,[†] AND SEUNG SOON JANG^{‡,*}

School of Civil and Environmental Engineering, School of Materials Science and Engineering, Georgia Institute of Technology, Atlanta, GA 30332-0245, U.S.A., and Faculty of Liberal Education, Chonbuk National University, Jeonju, Jeonbuk 561-756, Korea

Since surface adsorption using mineral sorbents has the potential to capture CO₂, more fundamental understanding of the molecular reaction mechanism of CO₂ adsorption on the metal oxide surface is necessitated. Chapter 5 shows a quantum calculation of CO₂ adsorption on the CaO surface which provides higher reactivity than MgO to determine the molecular chemical reactivity of multiple CO₂ molecules on CaO for CO₂ sequestration.

We investigated the adsorption configurations of multi-CO₂ molecules on the CaO (100) surface using density functional theory (DFT) in order to understand the CO₂ adsorption mechanism on the CaO (100) surface. In the formation of a monolayer, CO₂ molecules were chemi-sorbed due to the charge reorganization between the CaO surface and CO₂ molecules. The adsorbed CO₂ molecules got together rather than distributing uniformly over the CaO surface. Through calculating the monolayer formation energy, the optimal coverage of the CO₂ adsorption is found to be 1 molecules/unit cell (4.211Å × 4.211Å) with

* *Corresponding author:* SeungSoon.Jang@mse.gatech.edu (S. S. Jang),
Phone)404-385-3356, Fax)404-894-9140

[†] School of Civil and Environmental Engineering, Georgia Institute of Technology.

[‡] School of Materials Science and Engineering, Georgia Institute of Technology.

[§] Faculty of Liberal Education, Chonbuk National University.

the most stable adsorption energy ($-0.506 \text{ kcal/mol/ \AA}^2$). The multi-layer adsorption of CO_2 is also investigated and resulted in $-0.017 \text{ kcal/mol/ \AA}^2$ for the second layer and $-0.015 \text{ kcal/mol/ \AA}^2$ for the third layer, implying that the second layer adsorption can take place at ambient condition and characterized as the physi-sorption.

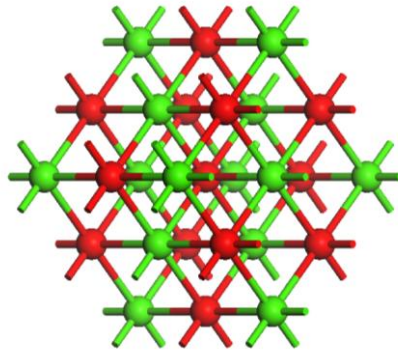
5.1 Introduction

The global environment has experienced significant changes in the climate due to the increasing emission of the greenhouse gases in the atmosphere. Among the greenhouse gases, the carbon dioxide emissions account for 94% of the total emissions, and over 80% of the anthropogenic CO_2 emissions in the world are generated through energy production [32]. Thus, in order to mitigate climate change, researchers have focused much of their attention on the reduction of CO_2 emissions from power generation facilities which are the most serious sources of CO_2 emissions in the form of a flue gas mixture, accounting for about 41% of the total [2, 6]. Therefore, many separation technologies for CO_2 sequestration have been developed and widely used [8, 18, 51, 57, 71, 77, 83, 98, 108, 109]. Among various CO_2 separation processes, the CO_2 adsorption technology using solid state sorbents such as minerals have been intensively studied due to its low operating costs and low energy demands resulting from its stable recycle capacity and high CO_2 selectivity [3, 10, 37, 38]. In addition, solid state sorbents are relatively easy to handle compared to liquid sorbents [11, 12] since the former has much less corrosion problems than the latter. Of all the CO_2 adsorption processes for the CO_2 sequestration, particularly, the mineral carbonation using alkaline-earth metal oxide minerals such as calcium oxide (CaO , Figure 54a) and magnesium (MgO) seems to be promising since they can form stable carbonates, which have very low

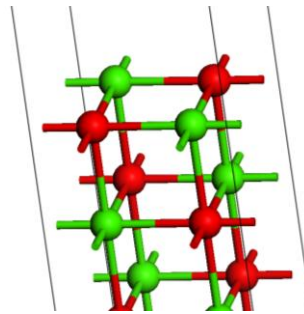
CO₂ leakage after sequestration. Furthermore, such stable carbonates produced by the carbonation process could be treated through environmentally friendly ways such as the mine reclamation and the soil amendments [18]. In the carbonation process, the alkaline-earth oxides (i.e., CaO and MgO) react with CO₂ exothermically to produce CaCO₃ and MgCO₃, respectively, in which the basicity of metal oxides mainly determines the reaction with CO₂ [147]. For instance, CO₂ molecules are bound at oxygen atoms of CaO surface to form calcium carbonate (CaCO₃), which occurs through the charge transfer from the CaO surface to the CO₂ molecule [40].

In this study, we investigated the CO₂ adsorption on mineral oxide surface, particularly CaO (100) surface (i.e., CaO surface is exposed along x-axis) (Figures 54b and 54c), using density functional theory (DFT). Although a few theoretical studies have reported that the adsorption of a single CO₂ molecule on the CaO surface on the surface [147, 178-182], there has been no study on the multiple-CO₂ adsorption, which would be critical to assess the adsorption capacity of the CaO.

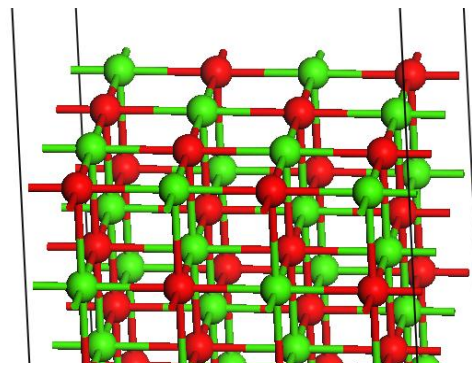
In this DFT study, therefore, we calculated various configurations of the multiple-CO₂ adsorption on the CaO (100) surface in an attempt to determine the optimal number of CO₂ molecules and the charge transfer between CO₂ and CaO surface, and analyzed the charge transfer and the entailed changes in electronic properties such as density of states and surface charge redistribution [148, 149].



(a)



(b)



(c)

Figure 54. Structure of CaO crystal: (a) unit cell; (b) (100) unit surface; (c) (100) 2×2 surface. The green ball and the red ball denote calcium and oxygen, respectively.

5.2 Computation details

In this study, we used quantum mechanical density functional theory (DFT) which is a method for electronic structures and properties of materials [183], and has been widely used to study condensed matter systems including surfaces. The goal of each computation is to solve the Kohn-Sham equations:

$$\left[-\frac{\nabla^2}{2} + v_{KS}[n](r) \right] \phi_i(r) = \varepsilon_i \phi_i(r) \quad (1)$$

$$v_{KS}[n](r) = v_{external}(r) + v_{Hartree}[n](r) + v_{XC}[n](r) \quad (2)$$

where $v_{KS}[n]$ is the Kohn-Sham potential that has a functional dependence on the electronic density (n), and $v_{external}$, $v_{Hartree}[n]$ and $v_{XC}[n]$ denotes the external potential, the Hartree term and the exchange-correlation term. By solving Equation (57), the most probable ground state electronics configuration and corresponding energy are obtained based on its atomic structure. Thus, we believe that DFT calculation can accurately describe interaction between CO₂ and CaO, which is essential to investigate the CO₂ adsorption.

Among various functionals for DFT, we used the generalized gradient approximation (GGA) method with the non-empirical local functional, Perdew-Burke-Ernzerhof correlation (PBE) [184, 185], which has been widely used in field of materials science as well as physics. And the DNP (double numerical basis plus polarization) basis set was used [186].

The structure of the CaO (100) surface was constructed as a four-layer slab (Figure 58). After the initial atomic positions were determined according to experimental structure, the geometry optimization was performed to refine the structure [187].

The CO₂ adsorption energy ($\Delta E_{adsorption}$) on the CaO (100) surface was calculated using Equation (56):

$$\Delta E_{adsorption} = \frac{E_{MgO+CO_2+H_2O} - (E_{MgO} + n \times E_{CO_2} + nE_{H_2O})}{n} \quad (56)$$

where E_{CaO-CO_2} is the energy of the whole system in which CO₂ molecules are adsorbed on CaO surface, E_{CaO} and E_{CO_2} are the energy of the bare CaO surface without CO₂ and the energy of the single CO₂ in the vacuum, respectively, and n denotes the number of CO₂ molecules.

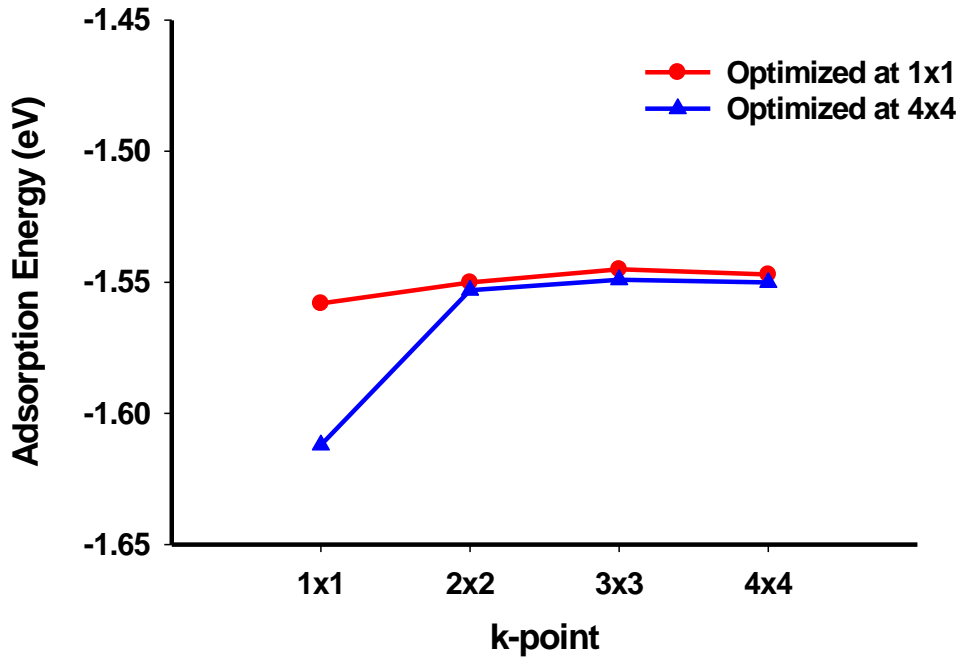


Figure 55. Coverage (θ) as a function of CO₂ adsorption energy

For this study, the (2×2) supercell (8.422Å ×8.422Å) of CaO (100) surface was employed as shown in Figure 54c. To analyze the electronic effect of k-point sampling on the structure and energy (i.e., The points in k-space can be defined to specify the grid dimensions in the three directions of the reciprocal space lattice vectors), various k-point samplings for the Brillouin zone were implemented using the Monkhorst-Pack k-point scheme [188]. To determine the suitable k-point set, we performed geometry optimization of a CO₂ adsorbed on the (2×2) CaO (100) surface at a gamma point (denoted by 1×1) and (4×4×1) k-point (denoted by 4×4), and then calculated the CO₂ adsorption energy as a function of k-point sets. As shown in Figure 55, the effect of k-point set on the adsorption energy is diminished beyond (2×2) k-point at both cases, so that the (2×2) k-point sampling was used to study all the characteristics of the CO₂-CaO system.

5.3 Results and discussion

5.3.1 Single CO₂adsorption on CaO

1) Adsorption Energy and Geometry

First, in order to investigate the nature of the CO₂ adsorption on the CaO (100) surface, we performed the geometry optimization of CO₂-CaO (100) surface. As summarized in Table 20, it is found that these calculated adsorption energy and geometry are in a good agreement with the experimental result as well as other computational result [147, 179], validating our calculations.

TABLE 20. The geometry and energy of the single CO₂ adsorption on CaO (100) surface

	Bond length ($C_{CO_2}-O_{CaO}$) (Å)	Bond length ($C_{CO_2}-O_{CO_2}$) (Å)	Bond angle ($O_{CO_2}-C_{CO_2}-O_{CO_2}$) (degree)	Adsorption energy (eV)
Experiment ^I [179]				-1.1
Theory ^{II} [147]	1.38	1.23	130.0	-1.0
This study ^{III}	1.47	1.25	134.1	-0.94
This study ^{IV}	1.39	1.27	129.4	-1.5

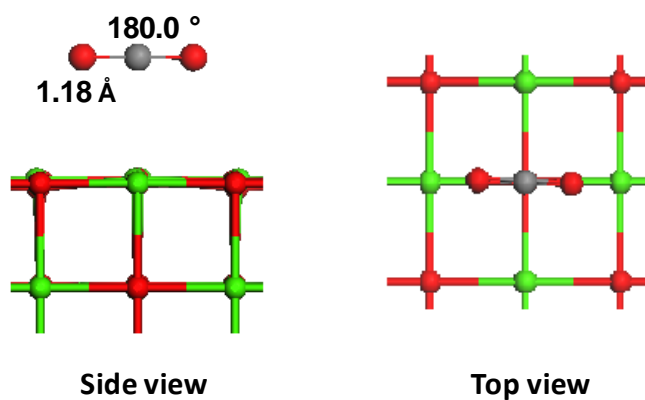
^I Adsorption energy obtained by thermal desorption method

^{II} Ab Initio Hartree-Fock calculation

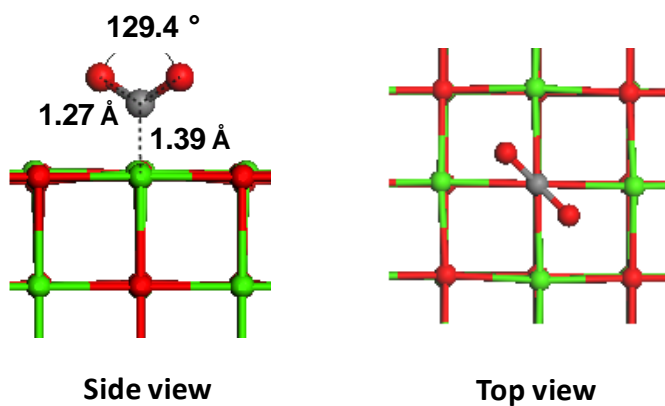
^{III} CO₂ adsorption on the (1×1) CaO surface

^{IV} CO₂ adsorption on the (2×2) CaO surface

The geometry of CO₂ is significantly changed before and after geometry optimization (Figure 56): the bond angle ($O_{CO_2}-C_{CO_2}-O_{CO_2}$) is substantially reduced from 180° to 134.1° on the (1×1) CaO surface and 129.4° on (2×2) CaO surface, and the $C_{CO_2}-O_{CO_2}$ bond length is increased from 1.18 Å to 1.25 Å and 1.27 Å for (1×1) and (2×2) CaO surface, respectively, which indicates that the hybridization of $C_{CO_2}-O_{CO_2}$ bonds are changed from sp_1 to sp_2 by forming a new chemical bond ($C_{CO_2}-O_{CaO}$) with the oxygen atom of the CaO surface. The calculated adsorption energy (-0.94 eV and -1.5 eV for (1×1) and (2×2) CaO surface, respectively) also supports a new bond formation. Thus, CO₂ adsorption on the CaO (100) surface is characterized as the chemi-sorption.



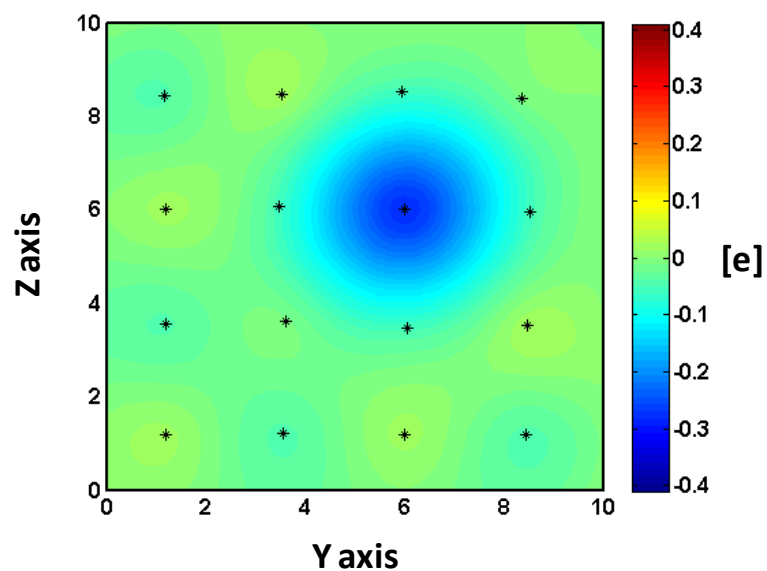
(a)



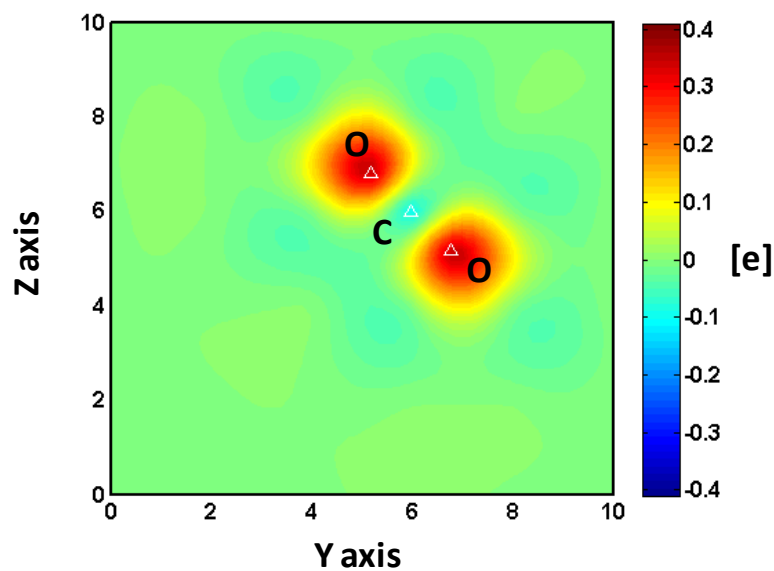
(b)



Figure 56. Geometries of the single CO₂ molecule on the (2×2) CaO (100) surface: (a) before geometry optimization; (b) after geometry optimization.



(a)



(b)

Figure 57. Charge reorganization of (a) the CaO (100) surface and (b) the CO₂ molecule. Note that positive value (red color) means the electron gain while negative value (blue color) means the electron loss compared to the original charge of CaO surface and CO₂ molecule.

2) Charge Reorganization

Pacchioni and his coworkers suggested that such strong adsorption can be understood by the low Madelung potential energy of CaO due to the larger cation-anion distance of the CaO matrix, which leads to the high basicity that provides active donation of a charge from the surface to the adsorbed molecule [40, 147]. In this study, in order to evaluate such charge transfer, we calculated the charge difference of each atom (Δq_i) of the CaO surface with and without the adsorbate CO₂ molecule using Equations (57) and (58)

$$\Delta q_i = q_{i, \text{CaO before adsorption}} - q_{i, \text{CaO after adsorption}} \quad (57)$$

$$\Delta q_i = q_{i, \text{CO}_2 \text{ before adsorption}} - q_{i, \text{CO}_2 \text{ after adsorption}} \quad (58)$$

where $q_{i, \text{CaO before adsorption}}$ and $q_{i, \text{CaO after adsorption}}$ denote the charges of the i -th atom in the CaO surface before and after the adsorption, respectively, and $q_{i, \text{CO}_2 \text{ before adsorption}}$ and $q_{i, \text{CO}_2 \text{ after adsorption}}$ denote the charges of the i -th atom of the CO₂ before and after the adsorption, respectively. Figure 57 visualizes the charge reorganization of the CaO surface and CO₂ via charge transfer between them. Since Δq_i will have a negative value (blue color) if the i -th atom loses charges, whereas it will have a positive value (red color) if the atom gains more charges, it is clear that the charge is transferred from the CaO surface to the CO₂ molecule whose amount is -0.7e calculated using Mulliken population analysis.

3) Effect of Surface Coverage

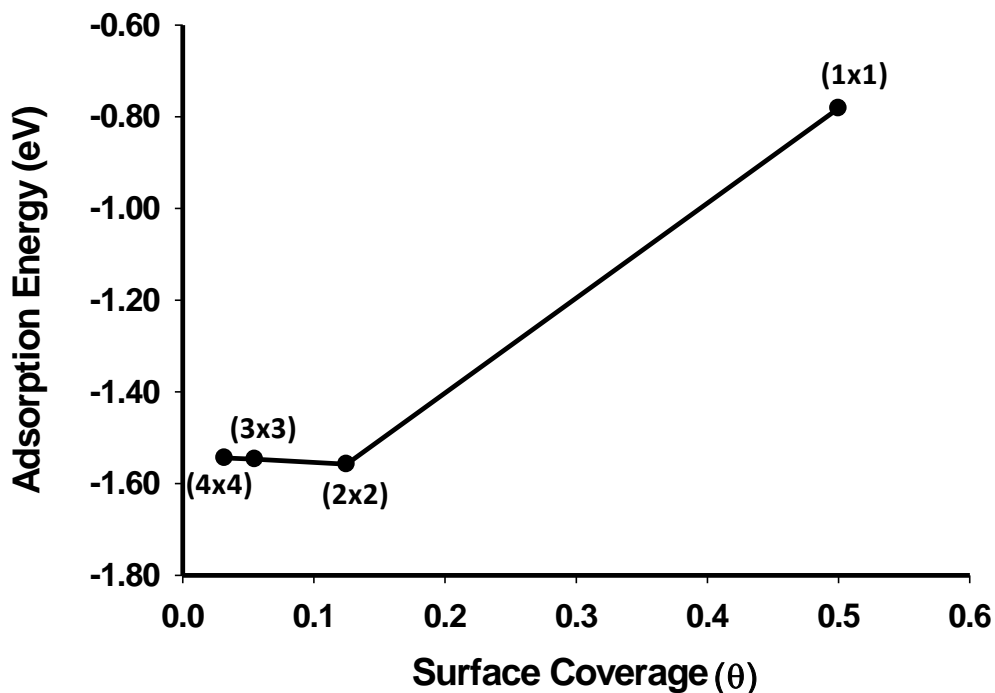


Figure 58. Change of CO₂ adsorption energy as a function of surface coverage (θ).

Here we investigate the single molecular adsorption of CO₂ on various sizes of CaO (100) surface such as (1×1), (2×2), (3×3) and (4×4) supercells (corresponding surface coverages (θ) are 0.5, 0.125, 0.055 and 0.032, respectively) was simulated via geometry optimization in an attempt to investigate the effect of the interaction between neighboring CO₂ molecules on the adsorption energy. At $\theta=1.0$, every oxygen atom of CaO (100) surface is occupied by adsorbed CO₂ molecule. As clearly shown in Figure 58, the adsorption energy depends on the surface coverage of CO₂, indicating that the adsorbed CO₂ is influenced by neighboring adsorbed CO₂ molecules. Furthermore, it should be noticed that the adsorption energy shows a minimum point at a specific surface coverage, $\theta=0.125$ at (2×2) supercell where the electrostatic attraction between adsorbed CO₂ molecules stabilizes the adsorption.

It seems that the adsorbed molecules may not obtain such electrostatic attractive interaction at low coverage and thus the adsorption energy becomes slightly higher, whereas at high coverage, the adsorbed molecules become too close to each other and thereby the electrostatic repulsion destabilizes the adsorption. This effect of surface coverage will be discussed further in the next section.

5.3.2 Multiple CO₂ adsorption on CaO

1) Formation of Monolayer

Although multiple CO₂ molecules can be adsorbed on the CaO (100) surface in the model system due to the presence of the multiple adsorption sites (oxygen atoms) of CaO surface, the corresponding simulation study has not been performed yet to the best of our knowledge. Thus, the formation of CO₂ monolayer was simulated using DFT in order to understand the CO₂ adsorption mechanism on the CaO (100) surface. From the study on the single CO₂ adsorption in the previous section (Figure 57), we already saw that the adsorption energy is affected by the surface coverage and the optimal surface coverage is 0.125.

TABLE 21. Adsorption energy (E_a) of CO₂ on CaO (100) surface

Size	1×1		2×2							
Number of CO ₂	1	2	1	2	3	4	5	6	7	8
Coverage (θ)	0.5	1	0.125	0.25	0.375	0.5	0.625	0.75	0.875	1
E_a (eV)	-0.78	-0.49	-1.56	-1.24	-1.31	-1.08	-0.69	-0.60	-0.61	-0.65

Here the surface coverage is scrutinized in more depth using multiple CO₂ molecules. In order to determine the optimal surface coverage, various systems were built (Table 21) with multiple CO₂ molecules. These CO₂ molecules were initially attached on the oxygen atoms of the CaO and geometry-optimized. For example, since the (1×1) CaO (100) surface has two oxygen atoms (Figure 58b), we can put one CO₂ molecule on either of two oxygen atoms and also two CO₂ molecules on both oxygen atoms.

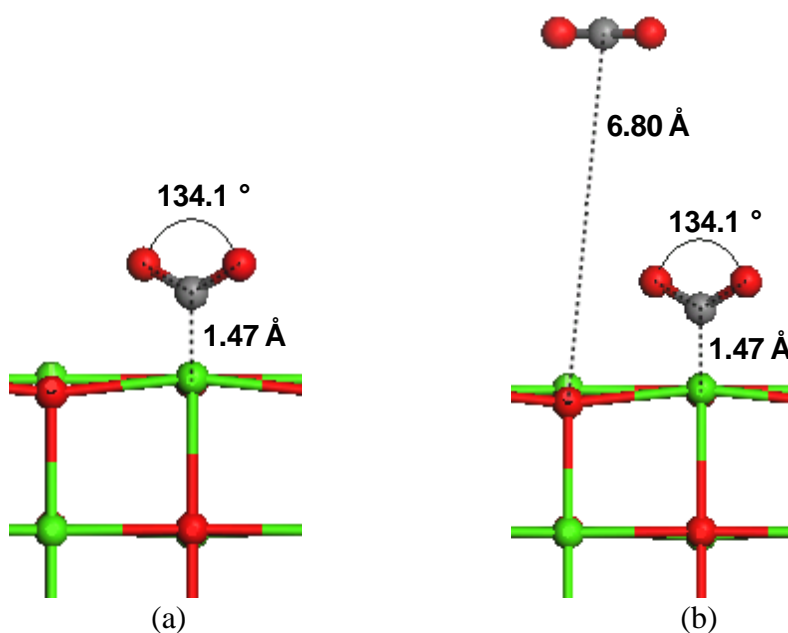
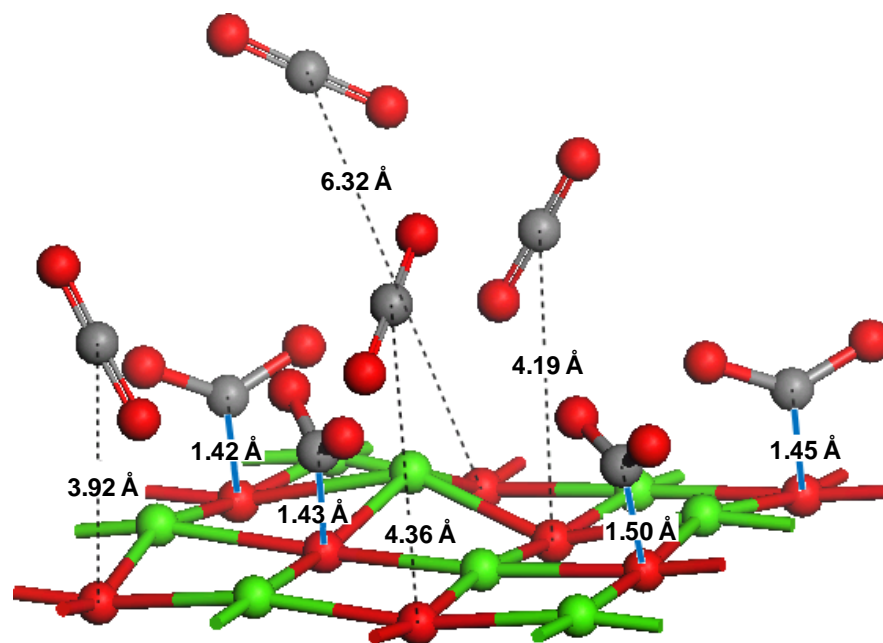
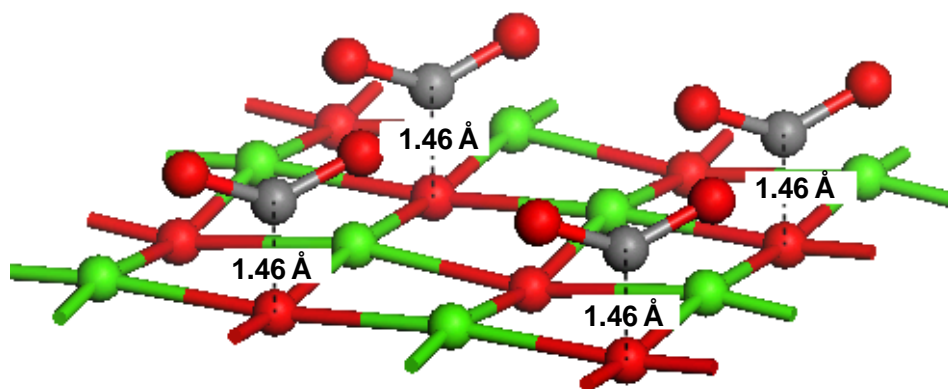


Figure 59. Optimized geometries of (a) single CO₂ molecule and (b) a pair of CO₂ molecules on the (1×1) CaO (100) surface. The color code is the same with Figure 60.

Figure 59 shows the optimized geometries for these two cases, showing that the (1×1) CaO (100) surface can accommodate only one CO₂ molecule. Although two CO₂ molecules are attached on the oxygen atoms at the beginning, only one CO₂ molecule can make chemi-sorption with an oxygen atom while another CO₂ molecule flies away from the surface.



(a)



(b)

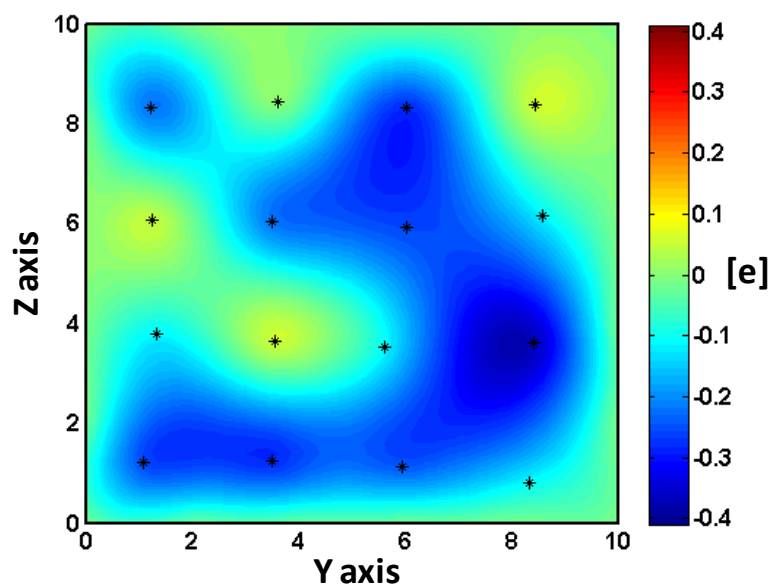
Figure 60. Optimized geometry of the eight CO₂ molecules on the (2×2) CaO (100) surface: (a) non-uniform adsorption; (b) uniform adsorption. The color code is the same with Figure 60.

For the (2×2) CaO (100) surface, we attached up to eight CO₂ molecules and performed geometry optimization. As shown in Figure 60a, however, only four CO₂ molecules were chemisorbed on the CaO surface and the rest of them were detached, and any attempt to put CO₂ molecules more than four was failed.

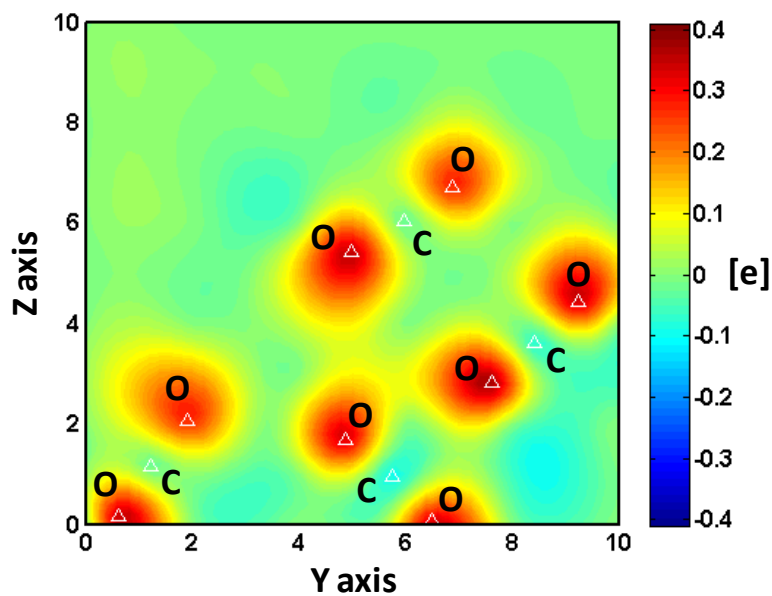
The adsorption energy was calculated as a function of surface coverage using the (2×2) CaO (100) surface with multiple CO₂ molecules. From Table 19, it is confirmed again that the adsorption energy becomes higher with increasing the number of molecules, meaning that the adsorption is destabilized as a function of surface coverage. Thus, from our study, the optimal surface coverage was found at $\theta=0.125$, corresponding to 70.93 Å²/CO₂ for the formation of CO₂ monolayer.

2) Charge Reorganization

In the previous section, it was discussed that the charge reorganization of the CaO surface takes place due to the charge transfer from CaO surface to CO₂ molecule. We think this charge reorganization should be the essential factor to determine the optimal surface coverage of CO₂ since the atomic charges on CO₂ provided from the CaO surface are distributed onto the oxygen atoms of adsorbed CO₂ molecule, and hence as the adsorbed CO₂ molecules become closer, they would repel each other due to these negative charges of oxygen atoms.



(a)



(b)

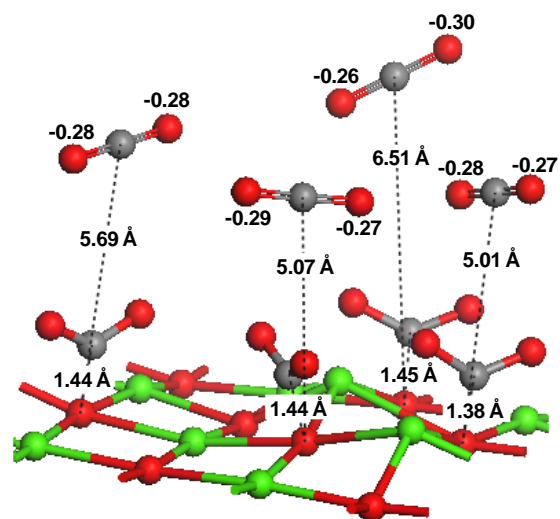
Figure 61. Charge reorganization of (a) the CaO (100) surface and (b) four CO₂ molecules. Note that positive value (red color) means the electron gain while negative value (blue color) means the electron loss compared to the original charge of CaO surface and CO₂ molecule.

In Figure 61, the charge reorganizations of the CaO surface and the adsorbed CO₂ molecules are presented. As expected, the charges are transferred from CaO surface to CO₂ molecules, which is the same feature we observed in Figure 57. The amount of charge transfer is -0.66e/CO₂ in average. However, it is worthwhile to note that the adsorbed CO₂ molecules get together rather than spreading out uniformly over the CaO surface. This can be rationalized that since the adsorbed CO₂ molecule has positively charged carbon atom (0.56e in average), the CO₂ molecules obtain the inter-molecular electrostatic attraction between negatively charged oxygen atoms (-0.58e in average) and positively charged carbon atoms. Therefore, there should be a balanced inter-molecular distance to attain the stable adsorption which is around 1.46 Å in average. Indeed, by simulating an independent system which has an uniform CO₂ adsorption for comparison, it was found that the adsorption energy from the non-uniform CO₂ adsorption (-1.08 eV from Figure 60a) is lower than that from the uniform adsorption (-0.83 eV from Figure 60b), which means that the non-uniform adsorption is more stable than the uniform adsorption.

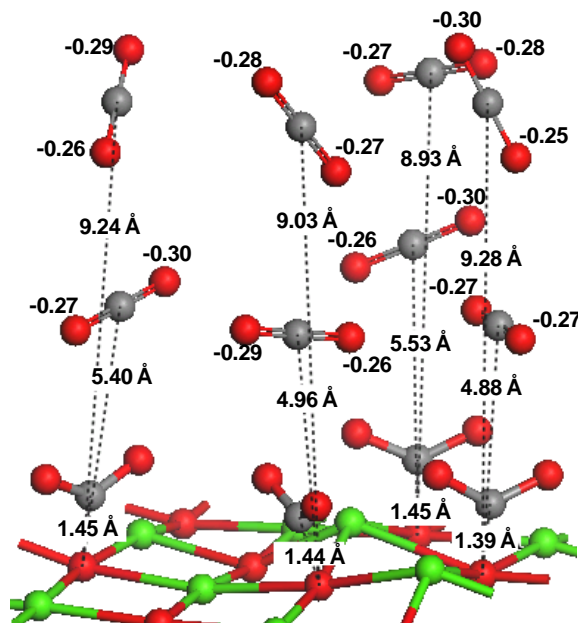
3) Formation of Multilayer

It is expected that after the monolayer formation from the multiple CO₂ adsorption, more CO₂ molecules interact with given adsorbed CO₂ monolayer to form multilayer adsorption (Figure 62). As observed in Figures 62a and 62b, the four CO₂ molecules in the second and another four CO₂ molecules in the third layer retain the same molecular geometry with free CO₂ molecule with weak adsorption energies such as -0.210 eV and -0.179 eV for the second layer and the third layer, respectively, indicating that the CO₂ molecules in the second and the third layer are physisorbed on top of the previous layer. From the adsorption

energy, it is expected that the stability of the second and the third layer would be similar to various molecular self-assemblies mediated by non-bonded interactions such as van der Waals and hydrogen bonding interaction.



(a)



(b)

Figure 62. Optimized geometries of the multilayer CO₂ adsorption on the (2×2) CaO (100) surface: (a) bilayer; (b) trilayer. Note that the numbers at oxygen atoms of CO₂ molecules are the atomic charges (unit: e).

5.4 Conclusion

This study investigated various configurations of the multiple-CO₂ adsorption on the CaO (100) surface using density functional theory (DFT) in order to determine the optimal number of CO₂ molecules and the charge transfer between CO₂ molecules and the CaO surface. It is clear that the charge reorganization from the CaO surface to CO₂ molecules causes the formation of CO₂ monolayer on the surface. The adsorbed CO₂ molecules get together rather than distributing uniformly over the CaO surface, but the adsorption is destabilized as the number of CO₂ molecules increases. It was also found that the non-uniform adsorption is more stable than the uniform adsorption on the surface. In the formation of CO₂ multi-layers, CO₂ molecules are physisorbed on top of the previous layer. Consequently, this study enhances the understanding of the adsorption mechanism of CO₂ molecules on CaO and provides a basis of CO₂ adsorption on Ca-based minerals such as wollastonite (CaSiO₃) and diopside (CaMgSi₂O₆).

CHAPTER 6

SUMMARY AND FUTURE STUDIES

6.1 Summary of this study

The surface carbonation of olivine, the most abundant mineral in the upper mantle, in the presence of water vapor was investigated to determine its potential for CO₂ sequestration. This study discussed the technologies and concepts that have already been investigated and then evaluated effective improvements of CO₂ sequestration using mineral sorbents. This thesis primarily described fundamental and applied studies of olivine carbonation in the presence of water vapor to provide a better understanding of direct CO₂ sequestration using natural minerals. Olivine carbonation was performed as a laboratory scale demonstration for direct CO₂ sequestration without the need for previous CO₂ separation and/or pressurization. The molecular mechanism and adsorption properties of multiple CO₂ molecules on the mineral surface were investigated. To conclude this study, each chapter is briefly summarized.

• CO₂ adsorption: A review

This chapter provides a literature view of various CO₂ capture technologies and an evaluation of their performance. The review also presents current research of CO₂ adsorption on many solid sorbents, including mineral carbonation. It mainly focused on the various separation procedures and the different CO₂ adsorbents and evaluates the factors affecting their performance. Many adsorbents provide the highly stable and highly cyclic capture capacities of CO₂ and low energy consumption for regeneration. In terms of adsorption

kinetics, high efficiency of CO₂ capture depends on the temperature and pressure used in the reaction system, the interaction energy between the sorbent and the CO₂, and the pore size or the surface area of the adsorbents. Thus, multiple parameters affect the capture capacity, the operation cost, and the process efficiency.

• **Reaction kinetics of Mg₂SiO₄-based CO₂ sorption**

This chapter presented results from experiments used to determine the reaction properties, temperature effects, and cyclic adsorption of pure Mg₂SiO₄ carbonation in the presence of water vapor and evaluated a reaction kinetics model. It was found that the CO₂ interaction with water on the sorbent surface is the rate controlling step of the CO₂ capture process. The fast initial adsorption rate predominantly is derived by chemisorption on the olivine surface. Based on changes in the CO₂ concentration with sorption time, a kinetic model of the reaction of pure Mg₂SiO₄ was developed. Kinetic parameters such as the reaction order and apparent activation energy in the empirical Arrhenius form of the pure magnesium silicate reaction were derived from the relationship between temperatures with respect to their obtained reaction rate coefficient. The reaction order was found to be approximately 1 for CO₂. The activation energy derived for the Arrhenius equation of Mg₂SiO₄-based carbonation is 76.2±4.8 kJ/mol based on the changes in the reaction rates with temperature in the range of 150-200°C. This kinetic study evaluates the adsorption properties of CO₂ for CO₂ sequestration resulting from the formation of stable MgCO₃ on the olivine surface.

- **Mineral carbonation using natural olivine sorbents in the presence of water vapor**

To evaluate the application of natural olivine for CO₂ sequestration, we carried out natural olivine mineralization in the presence/absence of water vapor under variable conditions of temperature, concentration, and residence time. Based on thermodynamics, the olivine carbonation is thermodynamically favorable. The thermodynamic parameters for olivine carbonation also indicate that substantial heat energy is released during the carbonation so that additional energy input is not required for a reaction. The capture capacity of carbon dioxide with water vapor was comparable to that without water vapor under the appropriate concentration. This finding indicates that water vapor plays a role in accelerating the carbonation rate. The extent of carbonation depends on residence time; it is controlled by reaction kinetics. According to the analysis of residence time, CO₂ adsorption on the olivine surface tends to be a surface-limited phenomenon, limiting the diffusion process. These results provide evidence that CO₂ could be disposed in a stable form.

Within this temperature range, the maximum total capture capacity is over 0.13 g CO₂/g pure Mg₂SiO₄ (chapter 3), indicating its capacity is similar or larger than other commercial sorbents (0.03 g CO₂/g sorbent to 0.13 g CO₂/g sorbent) [8, 14, 15, 46, 51, 57, 70, 71, 77, 83, 93, 111]. Compared to the study using natural olivine in chapter 4 [189], which is mostly composed of Mg₂SiO₄ (92% Mg₂SiO₄), natural olivine has slightly higher capture capacity (>0.14 g CO₂/g Mg₂SiO₄). Such a difference could be due to the cumulative effects of: (1) catalytic activity of other olivine components; (2) active abrasion and erosion of particles; and (3) adsorption due the tridimensional structure of olivine. These results confirm that magnesium silicate itself plays an important role in the CO₂ adsorption.

•A Density Functional Theory (DFT) Study of competitive CO₂ Adsorption on CaO (100) for CO₂ capture

Since surface adsorption using mineral sorbents has the potential to capture CO₂, more fundamental understanding of the molecular reaction mechanism of CO₂ adsorption on the metal oxide surface is desired. We performed a quantum chemistry calculation of CO₂ adsorption on the CaO (100) surface to determine the molecular chemical reactivity of many CO₂ molecules on the oxygen site of CaO for CO₂ sequestration. This study evaluated the adsorption energies and geometries of CO₂ molecules on the CaO (100) surface using a density functional theory (DFT) study. To determine the characteristics of CO₂ molecule capture, the adsorption properties of fully-loaded CO₂ molecules on the surface was investigated. These results show that CO₂ molecules strongly react with the CaO surface due to its high reactivity and high basicity. Based on the DFT calculation, molecular structures and the reaction mechanism of CO₂ molecules on the CaO surface are derived, which can help lead to the determination of the CO₂ adsorption activity on the calcium-based mineral surface. Consequently, this study will help lay the groundwork for the chemical mechanism of mineral carbonation with carbon dioxide and provide relevant information for the practical application of CO₂ sequestration by stable adsorption on mineral silicates.

6.2 Recommendations for Future Study

6.2.1 The investigation of molecular CO₂ adsorption on the Mg-based silicate mineral surface

Although calcium carbonation is more highly reactive than magnesium carbonation, magnesium-containing minerals are also affordable for use in the carbonation process because large deposits with relatively high purity are available worldwide. Since igneous rocks are particularly appropriate for CO₂ capture due to the stable nature of free carbonates, the feasible adsorbents of magnesium-rich minerals for CO₂ carbonation are olivine and serpentine due to their abundance and their high molar proportion of the alkaline earth oxides in Mg-based minerals. To determine the molecular reaction mechanism of these minerals, future study should investigate the molecular CO₂ adsorption property on MgO, olivine, and serpentine surfaces using a DFT quantum chemistry study.

Such a DFT study should perform calculations of the multi-layer adsorption of CO₂ molecules on a specific surface to determine the molecular surface transition between the CO₂ molecules and the mineral surface. In addition, to evaluate the adsorption properties of CO₂ multi-layers, the geometry optimization of CO₂ multi-layers on the strongly-adsorbed monolayer on the mineral surface should be determined. Therefore, the study can evaluate the feasible molecular properties of Mg-based mineral carbonation and the competitive interaction of CO₂ molecules.

Based on the adsorption properties obtained, one can investigate partially substituting magnesium for other alkali/alkaline-earth metals such as potassium, calcium, and barium to improve carbonation efficiency. In addition, such a study can investigate grafting polymer

chains such as amine branches on the mineral surface. The proposed approaches can provide basic information about the molecular structure and the mechanism of modified sorbents. These results will provide a better understanding of the experimental reactivity of modified adsorbents and thus benefit those conducting the experiments of CO₂ adsorption on modified adsorbents.

6.2.2 The process development of the large scale reactor for mineralization

In the future, to derive a cost-effective demonstration of a commercial operation of mineral carbonation, further research should investigate scale-up applications following the lab-scale experiments. First, the study would involve the design of a large-scale system that can use a larger reactor. For the thermal stability of the reaction temperature for the reactor, the thermal system requires the highly stable capacity of a thermo-controller. To introduce the gas mixture with a high flow rate, this study also requires the highly stable flow controller.

Secondly, for the optimization of the system, an appropriate flow rate of a gas mixture should be investigated according to the size of the reactor. In addition, the loading direction (i.e., vertical or horizontal loading) of the reactors in the thermal system should be studied. In the study, the amount of sorbents depending on the reactor size will have to be determined because of the effect of the sorbent weight, which may cause the gravitational packing in the lower part of the reactor.

REFERENCES

1. IEA, *World Energy Outlook*. OECD/IEA, Paris., 2002a.
2. EPA, *Inventory of U.S. Greenhouse Gas Emissions and sinks: 1990-2006*. 2008.
3. Plaza, M.G., C. Pevida, A. Arenillas, F. Rubiera, and J.J. Pis, *CO₂ capture by adsorption with nitrogen enriched carbons*. *Fuel*, 2007. **86**(14): p. 2204-2212.
4. Yamasaki, A., *An overview of CO₂ mitigation options for global warming - Emphasizing CO₂ sequestration options*. *Journal of Chemical Engineering of Japan*, 2003. **36**(4): p. 361-375.
5. Carapellucci, R. and A. Milazzo, *Membrane systems for CO₂ capture and their integration with gas turbine plants*. *Proceedings of the Institution of Mechanical Engineers Part a-Journal of Power and Energy*, 2003. **217**(A5): p. 505-517.
6. IEA, *CO₂ emissions from fuel combustion*. International Energy Agency (IEA) Statistics Data 2009.
7. Li, G., P. Xiao, P. Webley, J. Zhang, R. Singh, and M. Marshall, *Capture of CO₂ from high humidity flue gas by vacuum swing adsorption with zeolite 13X*. *Adsorption-Journal of the International Adsorption Society*, 2008. **14**(2-3): p. 415-422.
8. Na, B.K., K.K. Koo, H.M. Eum, H. Lee, and H.K. Song, *CO₂ recovery from flue gas by PSA process using activated carbon*. *Korean Journal of Chemical Engineering*, 2001. **18**(2): p. 220-227.
9. Riahi, K., E.S. Rubin, M.R. Taylor, L. Schrattenholzer, and D. Hounshell, *Technological learning for carbon capture and sequestration technologies*. *Energy Economics*, 2004. **26**(4): p. 539-564.
10. Meisen, A. and X.S. Shuai, *Research and development issues in CO₂ capture*. *Energy Conversion and Management*, 1997. **38**: p. S37-S42.
11. Niswander, R.H., D.J. Edwards, M.S. Dupart, and J.P. Tse, *A More Energy-Efficient Product for Carbon-Dioxide Separation*. *Separation Science and Technology*, 1993. **28**(1-3): p. 565-578.
12. Veawab, A., P. Tontiwachwuthikul, and A. Chakma, *Corrosion behavior of carbon steel in the CO₂ absorption process using aqueous amine solutions*. *Industrial & Engineering Chemistry Research*, 1999. **38**(10): p. 3917-3924.
13. Davini, P., *Flue gas treatment by activated carbon obtained from oil-fired fly ash*. *Carbon*, 2002. **40**(11): p. 1973-1979.
14. Gray, M.L., K.J. Champagne, D. Fauth, J.P. Baltrus, and H. Pennline, *Performance of immobilized tertiary amine solid sorbents for the capture of carbon dioxide*. *International Journal of Greenhouse Gas Control*, 2008. **2**(1): p. 3-8.
15. Ko, D., R. Siriwardane, and L.T. Biegler, *Optimization of pressure swing adsorption and fractionated vacuum pressure swing adsorption processes for CO₂ capture*. *Industrial & Engineering Chemistry Research*, 2005. **44**(21): p. 8084-8094.
16. Seo, Y., S.H. Jo, C.K. Ryu, and C.K. Yi, *Effects of water vapor pretreatment time and reaction temperature on CO₂ capture characteristics of a sodium-based solid sorbent in a bubbling fluidized-bed reactor*. *Chemosphere*, 2007. **69**(5): p. 712-718.
17. Ziock, H., *Zero emissions coal to hydrogen*. <http://www.lanl.gov/energy/ziock.html>, 2000. Zero emissions coal to hydrogen. Retrieved 2010-01-14

18. Maroto-Valer, M.M., D.J. Fauth, M.E. Kuchta, Y. Zhang, and J.M. Andresen, *Activation of magnesium rich minerals as carbonation feedstock materials for CO₂ sequestration*. Fuel Processing Technology, 2005. **86**(14-15): p. 1627-1645.
19. Herzog, H.J., *Carbon Sequestration via Mineral Carbonation: overview and assessment*. MIT Laboratory for Energy and the Environment, Cambridge, Massachusetts, 2002.
20. Seifritz, W., *CO₂ Disposal by Means of Silicates*. Nature, 1990. **345**(6275): p. 486-486.
21. Rochon, E., J. Kuper, E. Bjureby, P. Johnston, R. Oakley, D. Santillo, N. Schulz, and G. von Goerne, *False Hope: Why carbon capture and storage won't save the climate*. Greenpeace, 2008.
22. *Carbon dioxide: IDLH Documentation*. National Institute for Occupational Safety and Health (<http://www.cdc.gov/niosh/idlh/124389.html>). Retrieved 2009-05-08
23. Suehiro, Y., M. Nakajima, K. Yamada, and M. Uematsu, *Critical parameters of $\{x\text{CO}_2 + (1 - x)\text{CHF}_3\}$ for $x = (1.0000, 0.7496, 0.5013, \text{ and } 0.2522)$* . J. Chem. Thermodyn., 1996. **28** p. 1153-1164.
24. *Common Questions about Climate Change*. US Global Change Research Information Office (<http://www.gcric.org/ipcc/qa/05.html>). Retrieved 2010-02-04
25. *Schematic diagram of the general carbon capture and storage*. http://www-static.shell.com/static/chemicals/imgs/general/ccs_graphic_544px.jpg. Retrieved 2009-09-04
26. Yang, H.Q., Z.H. Xu, M.H. Fan, R. Gupta, R.B. Slimane, A.E. Bland, and I. Wright, *Progress in carbon dioxide separation and capture: A review*. Journal of Environmental Sciences-China, 2008. **20**(1): p. 14-27.
27. Goodell, J., *Big Coal*. 2006, New York: Houghton Mifflin. 214.
28. Gupta, M., I. Coyle, and K. Thambimuthu, *CO₂ capture technologies and opportunities in Canada*, in *1st Canadian CC&S Technology Roadmap Workshop*. 2003, CANMET Energy Technology Centre, Natural Resources Canada: Calgary, Alberta, Canada.
29. Aaron, D. and C. Tsouris, *Separation of CO₂ from flue gas: A review*. Separation Science and Technology, 2005. **40**(1-3): p. 321-348.
30. *CRC Handbook of Chemistry & Physics*, ed. D.R. Lide. Vol. 89th. 2008, New York: CRC Press.
31. Parfomak, P.W. and P. Folger, *CRS Report for Congress: Carbon Dioxide (CO₂) Pipelines for Carbon Sequestration: Emerging Policy Issues*. Congressional Research Service, 2008.
32. IPCC, *IPCC special report on carbon dioxide capture and storage 2005*.
33. Sciencedaily.com, *Deep-Sea Disposal Of Fossil-Fuel CO₂: First Ocean Observations*, in <http://www.sciencedaily.com/releases/1999/05/990507071858.htm>. Retrieved 2010-07-12.
34. Goldberg, P., Z.Y. Chen, W. O'Connor, R. Walters, and H. Ziock, *CO₂ mineral sequestration situation in US*. Journal of Energy and Environmental Research 1, 2001. **1**: p. 117.
35. Oelkers, E.H., S.R. Gislason, and J. Matter, *Mineral Carbonation of CO₂*. elements, 2008. **4**: p. 333-337.

36. Walters, R.P., Z.Y. Chen, P. Goldberg, K. Lackner, M. McKelvy, and H. Ziock, *Mineral Carbonation: A Viable Method for CO₂ Sequestration*. The National Energy Technology Laboratory, Morgantown, West Virginia, 1999.
37. Khatri, R.A., S.S.C. Chuang, Y. Soong, and M. Gray, *Carbon dioxide capture by diamine-grafted SBA-15: A combined Fourier transform infrared and mass spectrometry study*. *Industrial & Engineering Chemistry Research*, 2005. **44**(10): p. 3702-3708.
38. Khatri, R.A., S.S.C. Chuang, Y. Soong, and M. Gray, *Thermal and chemical stability of regenerable solid amine sorbent for CO₂ capture*. *Energy & Fuels*, 2006. **20**(4): p. 1514-1520.
39. [http://www.rwe.com/web/cms/en/2756/rwe/innovations/power-generation/clean-coal/CO₂-removal-uk/](http://www.rwe.com/web/cms/en/2756/rwe/innovations/power-generation/clean-coal/CO2-removal-uk/), *Model of 1 MWe Post Combustion CO₂ Capture Pilot Plant at Aberthaw Power Station*. Retrieved 2010-03-04
40. Freund, H.J. and M.W. Roberts, *Surface chemistry of carbon dioxide* *Surface Science Reports*, 1996. **25**: p. 225-273.
41. Chakma, A. and P. Tontiwachwuthikul, *CO₂ Separation from Combustion Gas Streams by Chemical Reactive Solvents*. Online Library: Combustion Canada, 1999.
42. O'onnor, W.K., D.C. Dahlin, G.E. Rush, S.J. Gerdemann, L.R. Penner, and D.N. Nilsen, *Aqueous Mineral Carbonation: Mineral Availability, Pretreatment, Reaction Parametrics, and Process Studies* DOE/ARC-TR-04-002, 2004.
43. Atkin, P., *Physical Chemistry*. 6th Ed. Freeman, New York, 1998.
44. Engineered Gas Systems Worldwide, I., *Schematic diagram of swing adsorption process*. www.enggas.com/non_cryo/psa.htm, 2003. Retrieved 2009-02-21
45. Gomes, V.G. and K.W.K. Yee, *Pressure swing adsorption for carbon dioxide sequestration from exhaust gases*. *Separation and Purification Technology*, 2002. **28**(2): p. 161-171.
46. Reynolds, S.P., A.D. Ebner, and J.A. Ritter, *New pressure swing adsorption cycles for carbon dioxide sequestration*. *Adsorption-Journal of the International Adsorption Society*, 2005. **11**: p. 531-536.
47. Ho, M.T., G.W. Allinson, and D.E. Wiley, *Reducing the cost of CO₂ capture from flue gases using pressure swing adsorption*. *Industrial & Engineering Chemistry Research*, 2008. **47**(14): p. 4883-4890.
48. Park, J.H., J.N. Kim, S.H. Cho, J.D. Kim, and R.T. Yang, *Adsorber dynamics and optimal design of layered beds for multicomponent gas adsorption*. *Chemical Engineering Science*, 1998. **53**(23): p. 3951-3963.
49. Reynolds, S.P., A.D. Ebner, and J.A. Ritter, *Carbon dioxide capture from flue gas by pressure swing adsorption at high temperature using a K-promoted HTlc: Effects of mass transfer on the process performance*. *Environmental Progress*, 2006. **25**(4): p. 334-342.
50. Chue, K.T., J.N. Kim, Y.J. Yoo, S.H. Cho, and R.T. Yang, *Comparison of Activated Carbon and Zeolite 13x for CO₂ Recovery from Flue-Gas by Pressure Swing Adsorption*. *Industrial & Engineering Chemistry Research*, 1995. **34**(2): p. 591-598.
51. Ochoa-Fernandez, E., M. Ronning, X.F. Yu, T. Grande, and D. Chen, *Compositional effects of nanocrystalline lithium zirconate on its CO₂ capture properties*. *Industrial & Engineering Chemistry Research*, 2008. **47**(2): p. 434-442.

52. Kikkinides, E.S. and R.T. Yang, *Concentration and Recovery of CO₂ from Flue-Gas by Pressure Swing Adsorption*. Industrial & Engineering Chemistry Research, 1994. **33**(11): p. 2881-2881.
53. Diagne, D., M. Goto, and T. Hirose, *Experimental-Study of Simultaneous Removal and Concentration of CO₂ by an Improved Pressure Swing Adsorption Process*. Energy Conversion and Management, 1995. **36**(6-9): p. 431-434.
54. Reynolds, S.P., A. Mehrotra, A.D. Ebner, and J.A. Ritter, *Heavy reflux PSA cycles for CO₂ recovery from flue gas: Part I. Performance evaluation*. Adsorption-Journal of the International Adsorption Society, 2008. **14**(2-3): p. 399-413.
55. Park, J.H., H.T. Beum, J.N. Kim, and S.H. Cho, *Numerical analysis on the power consumption of the PSA process for recovering CO₂ from flue gas*. Industrial & Engineering Chemistry Research, 2002. **41**(16): p. 4122-4131.
56. Choi, W.K., T.I. Kwon, Y.K. Yeo, H. Lee, H.K. Song, and B.K. Na, *Optimal operation of the Pressure Swing Adsorption (PSA) process for CO₂ recovery*. Korean Journal of Chemical Engineering, 2003. **20**(4): p. 617-623.
57. Ko, D., R. Siriwardane, and L.T. Biegler, *Optimization of a pressure-swing adsorption process using zeolite 13X for CO₂ sequestration*. Industrial & Engineering Chemistry Research, 2003. **42**(2): p. 339-348.
58. Chang, D., J. Min, K. Moon, Y.K. Park, J.K. Jeon, and S.K. Ihm, *Robust numerical simulation of pressure swing adsorption process with strong adsorbate CO₂*. Chemical Engineering Science, 2004. **59**(13): p. 2715-2725.
59. Liu, X.W., L. Zhou, X. Fu, Y. Sun, W. Su, and Y.P. Zhou, *Adsorption and regeneration study of the mesoporous adsorbent SBA-15 adapted to the capture/separation of CO₂ and CH₄*. Chemical Engineering Science, 2007. **62**(4): p. 1101-1110.
60. Wright, A.D., M.A. Kalbassi, and T.C. Golden, *Prepurification of Air Using an Advanced Thermal-Pressure Swing Adsorption (Tpsa) Cycle*. AlchE, The Preliminary Program for 2005 Annual Meeting (Cincinnati, OH), 2005.
61. Zhang, J. and P.A. Webley, *Cycle development and design for CO₂ capture from flue gas by vacuum swing adsorption*. Environmental Science & Technology, 2008. **42**(2): p. 563-569.
62. Zhang, J., P.A. Webley, and P. Xiao, *Effect of process parameters on power requirements of vacuum swing adsorption technology for CO₂ capture from flue gas*. Energy Conversion and Management, 2008. **49**(2): p. 346-356.
63. Yang, R.T., *Gas Separation by Adsorption Processes*. Butterworths, Boston, MA, 1987.
64. Ruthven, D.M., *Principles of Adsorption Processes*. Wiley&Sons Inc, New York, 1984.
65. Konduru, N., P. Lindner, and N.M. Assaf-Anad, *Curbing the greenhouse effect by carbon dioxide adsorption with zeolite 13X*. Aiche Journal, 2007. **53**(12): p. 3137-3143.
66. Fogler, H.S., *Elements of Chemical Reaction Engineering, 3rd Ed.* . Prentice Hall PTR, 2000.

67. Lee, J.S., J.H. Kim, J.T. Kim, J.K. Suh, J.M. Lee, and C.H. Lee, *Adsorption equilibria of CO₂ on zeolite 13X and zeolite X/Activated carbon composite*. Journal of Chemical and Engineering Data, 2002. **47**(5): p. 1237-1242.
68. Yong, Z., V. Mata, and A.E. Rodrigues, *Adsorption of carbon dioxide at high temperature - a review*. Separation and Purification Technology, 2002. **26**(2-3): p. 195-205.
69. Hiyoshi, N., K. Yogo, and T. Yashima, *Adsorption of carbon dioxide on amine modified SBA-15 in the presence of water vapor*. Chemistry Letters, 2004. **33**(5): p. 510-511.
70. Yong, Z., V. Mata, and A.E. Rodrigues, *Adsorption of carbon dioxide on basic alumina at high temperatures*. Journal of Chemical and Engineering Data, 2000. **45**(6): p. 1093-1095.
71. Yong, Z., V. Mata, and A.E. Rodriguez, *Adsorption of carbon dioxide onto hydrotalcite-like compounds (HTlcs) at high temperatures*. Industrial & Engineering Chemistry Research, 2001. **40**(1): p. 204-209.
72. Siriwardane, R.V., M.S. Shen, and E.P. Fisher, *Adsorption of CO₂ on zeolites at moderate temperatures*. Energy & Fuels, 2005. **19**(3): p. 1153-1159.
73. Li, P.Y. and F.H. Tezel, *Adsorption separation of N₂, O₂, CO₂ and CH₄ gases by beta-zeolite*. Microporous and Mesoporous Materials, 2007. **98**(1-3): p. 94-101.
74. Lee, S.C., B.Y. Choi, T.J. Lee, C.K. Ryu, Y.S. Soo, and J.C. Kim, *CO₂ absorption and regeneration of alkali metal-based solid sorbents*. Catalysis Today, 2006. **111**(3-4): p. 385-390.
75. Gray, M.L., Y. Soong, K.J. Champagne, J. Baltrus, R.W. Stevens, P. Toochinda, and S.S.C. Chuang, *CO₂ capture by amine-enriched fly ash carbon sorbents*. Separation and Purification Technology, 2004. **35**(1): p. 31-36.
76. Chakma, A., *CO₂ capture processes - Opportunities for improved energy efficiencies*. Energy Conversion and Management, 1997. **38**: p. S51-S56.
77. Hicks, J.C., J.H. Drese, D.J. Fauth, M.L. Gray, G.G. Qi, and C.W. Jones, *Designing adsorbents for CO₂ capture from flue gas-hyperbranched aminosilicas capable of capturing CO₂ reversibly*. Journal of the American Chemical Society, 2008. **130**(10): p. 2902-2903.
78. Seo, Y., S.H. Jo, H.J. Ryu, D.H. Bae, C.K. Ryu, and C.K. Yi, *Effect of water pretreatment on CO₂ capture using a potassium-based solid sorbent in a bubbling fluidized bed reactor*. Korean Journal of Chemical Engineering, 2007. **24**(3): p. 457-460.
79. Kierzkowska-Pawlak, H., *Enthalpies of absorption and solubility of CO₂ in aqueous solutions of methyldiethanolamine*. Separation Science and Technology, 2007. **42**(12): p. 2723-2737.
80. Fauth, D.J., E.A. Frommell, J.S. Hoffman, R.P. Reasbeck, and H.W. Pennline, *Eutectic salt promoted lithium zirconate: Novel high temperature sorbent for CO₂ capture*. Fuel Processing Technology, 2005. **86**(14-15): p. 1503-1521.
81. Pannocchia, G., M. Puccini, M. Seggiani, and S. Vitolo, *Experimental and modeling studies on high-temperature capture of CO₂ using lithium zirconate based sorbents*. Industrial & Engineering Chemistry Research, 2007. **46**(21): p. 6696-6706.

82. Merel, J., M. Clausse, and F. Meunier, *Experimental investigation on CO₂ post-combustion capture by indirect thermal swing adsorption using 13X and 5A zeolites*. Industrial & Engineering Chemistry Research, 2008. **47**(1): p. 209-215.
83. Gray, M.L., Y. Soong, K.J. Champagne, H. Pennline, J.P. Baltrus, R.W. Stevens, R. Khatri, S.S.C. Chuang, and T. Filburn, *Improved immobilized carbon dioxide capture sorbents*. Fuel Processing Technology, 2005. **86**(14-15): p. 1449-1455.
84. Yi, K.B. and D.O. Eriksen, *Low temperature liquid state synthesis of lithium zirconate and its characteristics as a CO₂ sorbent*. Separation Science and Technology, 2006. **41**(2): p. 283-296.
85. Shigemoto, N., T. Yanagihara, S. Sugiyama, and H. Hayashi, *Material balance and energy consumption for CO₂ recovery from moist flue gas employing K₂CO₃-on-activated carbon and its evaluation for practical adaptation*. Energy & Fuels, 2006. **20**(2): p. 721-726.
86. Ida, J. and Y.S. Lin, *Mechanism of high-temperature CO₂ sorption on lithium zirconate*. Environmental Science & Technology, 2003. **37**(9): p. 1999-2004.
87. Jadhav, P.D., R.V. Chatti, R.B. Biniwale, N.K. Labhsetwar, S. Devotta, and S.S. Rayalu, *Monoethanol amine modified zeolite 13X for CO₂ adsorption at different temperatures*. Energy & Fuels, 2007. **21**(6): p. 3555-3559.
88. Ochoa-Fernandez, E., M. Ronning, T. Grande, and D. Chen, *Nanocrystalline lithium zirconate with improved kinetics for high-temperature CO₂ capture*. Chemistry of Materials, 2006. **18**(6): p. 1383-1385.
89. Bretado, M.E., V.G. Velderrain, D.L. Gutierrez, V. Collins-Martinez, and A.L. Ortiz, *A new synthesis route to Li₄SiO₄ as CO₂ catalytic/sorbent*. Catalysis Today, 2005. **107-08**: p. 863-867.
90. Walton, K.S. and M.D. LeVan, *A novel adsorption cycle for CO₂ recovery: Experimental and theoretical investigations of a temperature swing compression process*. Separation Science and Technology, 2006. **41**(3): p. 485-500.
91. Siriwardane, R.V., C. Robinson, M. Shen, and T. Simonyi, *Novel regenerable sodium-based sorbents for CO₂ capture at warm gas temperatures*. Energy & Fuels, 2007. **21**(4): p. 2088-2097.
92. Wu, S.F., Q.H. Li, J.N. Kim, and K.B. Yi, *Properties of a nano CaO/Al₂O₃ CO₂ sorbent*. Industrial & Engineering Chemistry Research, 2008. **47**(1): p. 180-184.
93. Bibara, P.J., T.P. Filburn, and T.A. Nalette, *Regenerable Solid Amine Sorbent*. US Patent 5,876,488, 1999.
94. Li, X.N., E. Hagaman, C. Tsouris, and J.W. Lee, *Removal of carbon dioxide from flue gas by ammonia carbonation in the gas phase*. Energy & Fuels, 2003. **17**(1): p. 69-74.
95. Rodriguez, M.T. and H. Pfeiffer, *Sodium metasilicate (Na₂SiO₃): A thermo-kinetic analysis of its CO₂ chemical sorption*. Thermochemica Acta, 2008. **473**(1-2): p. 92-95.
96. Ochoa-Fernandez, E., H.K. Rusten, H.A. Jakobsen, M. Ronning, A. Holmen, and D. Chen, *Sorption enhanced hydrogen production by steam methane reforming using Li₂ZrO₃ as sorbent: Sorption kinetics and reactor simulation*. Catalysis Today, 2005. **106**(1-4): p. 41-46.
97. Balaz, P., E. Turianicova, M. Fabian, R.A. Kleiv, J. Briancin, and A. Obut, *Structural changes in olivine (Mg,Fe)₂SiO₄ mechanically activated in high-energy mills*. International Journal of Mineral Processing, 2008. **88**(1-2): p. 1-6.

98. Hutson, N.D., S.A. Speakman, and E.A. Payzant, *Structural effects on the high temperature adsorption of CO₂ on a synthetic hydrotalcite*. Chemistry of Materials, 2004. **16**(21): p. 4135-4143.
99. Ji, D.F., X.B. Lu, R. He, X.L. Zhan, and Y.R. Yang, *Studies on chemical fixation of CO₂ and syntheses of alkylene carbonates*. Chemical Journal of Chinese Universities-Chinese, 2001. **22**(10): p. 1720-1723.
100. Schladt, M.J., T.P. Filburn, and J.J. Helble, *Supported amine sorbents under temperature swing absorption for CO₂ and moisture capture*. Industrial & Engineering Chemistry Research, 2007. **46**(5): p. 1590-1597.
101. Veliz-Enriquez, M.Y., G. Gonzalez, and H. Pfeiffer, *Synthesis and CO₂ capture evaluation of Li_{2-x}K_xZrO₃ solid solutions and crystal structure of a new lithium-potassium zirconate phase*. Journal of Solid State Chemistry, 2007. **180**(9): p. 2485-2492.
102. Ochoa-Fernandez, E., M. Ronning, T. Grande, and D. Chen, *Synthesis and CO₂ capture properties of nanocrystalline lithium zirconate*. Chemistry of Materials, 2006. **18**(25): p. 6037-6046.
103. Ida, J., R.T. Xiong, and Y.S. Lin, *Synthesis and CO₂ sorption properties of pure and modified lithium zirconate*. Separation and Purification Technology, 2004. **36**(1): p. 41-51.
104. Li, Z.S., N.S. Cai, Y.Y. Huang, and H.J. Han, *Synthesis, experimental studies, and analysis of a new calcium-based carbon dioxide absorbent*. Energy & Fuels, 2005. **19**(4): p. 1447-1452.
105. Tokuyama, H., K. Yanagawa, and S. Sakohara, *Temperature swing adsorption of heavy metals on novel phosphate-type adsorbents using thermosensitive gels and/or polymers*. Separation and Purification Technology, 2006. **50**(1): p. 8-14.
106. Lee, S.C. and J.C. Kim, *Dry potassium-based sorbents for CO₂ capture*. Catalysis Surveys from Asia, 2007. **11**(4): p. 171-185.
107. Sakadjian, B.B., M.V. Iyer, H. Gupta, and L.S. Fan, *Kinetics and structural characterization of calcium-based sorbents calcined under subatmospheric conditions for the high-temperature CO₂ capture process*. Industrial & Engineering Chemistry Research, 2007. **46**(1): p. 35-42.
108. Miura, K., H. Nakagawa, and H. Okamoto, *Production of high density activated carbon fiber by a hot briquetting method*. Carbon, 2000. **38**(1): p. 119-125.
109. Millward, A.R. and O.M. Yaghi, *Metal-organic frameworks with exceptionally high capacity for storage of carbon dioxide at room temperature*. Journal of the American Chemical Society, 2005. **127**(51): p. 17998-17999.
110. Walton, K.S., A.R. Millward, D. Dubbeldam, H. Frost, J.J. Low, O.M. Yaghi, and R.Q. Snurr, *Understanding inflections and steps in carbon dioxide adsorption isotherms in metal-organic frameworks*. Journal of the American Chemical Society, 2008. **130**(2): p. 406-+.
111. Xu, X.C., C.S. Song, B.G. Miller, and A.W. Scaroni, *Adsorption separation of carbon dioxide from flue gas of natural gas-fired boiler by a novel nanoporous "molecular basket" adsorbent*. Fuel Processing Technology, 2005. **86**(14-15): p. 1457-1472.

112. Chaffee, A.L., G.P. Knowles, Z. Liang, J. Zhany, P. Xiao, and P.A. Webley, *CO₂ capture by adsorption: Materials and process development*. International Journal of Greenhouse Gas Control, 2007. **1**(1): p. 11-18.
113. Ahn, H. and C.H. Lee, *Effects of capillary condensation on adsorption and thermal desorption dynamics of water in zeolite 13X and layered beds*. Chemical Engineering Science, 2004. **59**(13): p. 2727-2743.
114. Feron, P.H.M. and C.A. Hendriks, *CO₂ capture process principles and costs*. Oil & Gas Science and Technology-Revue De L Institut Francais Du Petrole, 2005. **60**(3): p. 451-459.
115. Rueiner, P., H. Audus, and A.R. Smith, *Carbon Dioxide Capture from Fossil Fuel Power Plants*. IEA Greenhouse Gas R&D Programme 1994. **Report SR2**(CHeltenham, U.K.).
116. Reddy, M.K.R., Z.P. Xu, G.Q. Lu, and J.C.D. Da Costa, *Layered double hydroxides for CO₂ capture: Structure evolution and regeneration*. Industrial & Engineering Chemistry Research, 2006. **45**(22): p. 7504-7509.
117. Sharma, S. and G.P. Agarwal, *Interactions of proteins with immobilized metal ions: A comparative analysis using various isotherm models*. Analytical Biochemistry, 2001. **288**(2): p. 126-140.
118. Weissermel, H., H. Arpe, C.R. Lindley, and S. Hawkins, *Chap. 7. Oxidation Products of Ethylene*. Industrial Organic Chemistry. Wiley-VCH, 2003: p. 159-161. ISBN 3527305785.
119. Caplow, M., *Kinetics of Carbamate Formation and Breakdown*. Journal of the American Chemical Society, 1968. **90**(24): p. 6795-&.
120. Mahajani, V.V. and J.B. Joshi, *Kinetics of reactions between carbon dioxide and alkanolamines* Gas Separation & Purification 1988. **2**: p. 50-64.
121. Vaidya, P.D. and E.Y. Kenig, *Acceleration of CO₂ reaction with N,N-diethylethanolamine in aqueous solutions by piperazine*. Industrial & Engineering Chemistry Research, 2008. **47**(1): p. 34-38.
122. Sartori, G. and D.W. Savage, *Sterically Hindered Amines for CO₂ Removal from Gases*. Industrial & Engineering Chemistry Fundamentals, 1983. **22**(2): p. 239-249.
123. Donaldson, T.L. and Y.N. Nguyen, *Carbon-Dioxide Reaction-Kinetics and Transport in Aqueous Amine Membranes*. Industrial & Engineering Chemistry Fundamentals, 1980. **19**(3): p. 260-266.
124. Resnik, K.P., J.T. Yeh, and H.W. Pennline, *Aqua ammonia process for simultaneous removal of CO₂, SO₂ and NO_x*. International Journal of Environmental Technology and management, 2004. **4**(1-2): p. 89-104.
125. Yeh, J.T., K.P. Resnik, K. Rygle, and H.W. Pennline, *Semi-batch absorption and regeneration studies for CO₂ capture by aqueous ammonia*. Fuel Processing Technology, 2005. **86**(14-15): p. 1533-1546.
126. Idem, R., M. Wilson, P. Tontiwachwuthikul, A. Chakma, A. Veawab, A. Aroonwilas, and D. Gelowitz, *Pilot plant studies of the CO₂ capture performance of aqueous MEA and mixed MEA/MDEA solvents at the University of Regina CO₂ capture technology development plant and the Boundary Dam CO₂ capture demonstration*. Industrial & Engineering Chemistry Research, 2006. **45**(8): p. 2414-2420.

127. Aboudheir, A., P. Tontiwachwuthikul, A. Chakma, and R. Idem, *Kinetics of the reactive absorption of carbon dioxide in high CO₂-loaded, concentrated aqueous monoethanolamine solutions*. Chemical Engineering Science, 2003. **58**(23-24): p. 5195-5210.
128. Lawal, A.O. and R.O. Idem, *Kinetics of the oxidative degradation of CO₂ loaded and concentrated aqueous MEA-MDEA blends during CO₂ absorption from flue gas streams*. Industrial & Engineering Chemistry Research, 2006. **45**(8): p. 2601-2607.
129. Ramachandran, N., A. Aboudheir, R. Idem, and P. Tontiwachwuthikul, *Kinetics of the absorption of CO₂ into mixed aqueous loaded solutions of monoethanolamine and methyldiethanolamine*. Industrial & Engineering Chemistry Research, 2006. **45**(8): p. 2608-2616.
130. Zhang, X., C.F. Zhang, and Y. Liu, *Kinetics of absorption of CO₂ into aqueous solution of MDEA blended with DEA*. Industrial & Engineering Chemistry Research, 2002. **41**(5): p. 1135-1141.
131. Oyekan, B.A. and G.T. Rochelle, *Energy performance of stripper configurations for CO₂ capture by aqueous amines*. Industrial & Engineering Chemistry Research, 2006. **45**(8): p. 2457-2464.
132. Supap, T., R. Idem, P. Tontiwachwuthikul, and C. Saiwan, *Analysis of monoethanolamine and its oxidative degradation products during CO₂ absorption from flue gases: A comparative study of GC-MS, HPLC-RID, and CE-DAD analytical techniques and possible optimum combinations*. Industrial & Engineering Chemistry Research, 2006. **45**(8): p. 2437-2451.
133. Tanthapanichakoon, W., A. Veawab, and B. McGarvey, *Electrochemical investigation on the effect of heat-stable salts on corrosion in CO₂ capture plants using aqueous solution of MEA*. Industrial & Engineering Chemistry Research, 2006. **45**(8): p. 2586-2593.
134. Migita, H., K. Soga, and Y.H. Mori, *Gas absorption in a wetted-wire column*. Aiche Journal, 2005. **51**(8): p. 2190-2198.
135. Battjes, K.P., A.M. Barolo, and P. Dreyfuss, *New Evidence Related to Reactions of Aminated Silane Coupling Agents with Carbon-Dioxide*. Journal of Adhesion Science and Technology, 1991. **5**(10): p. 785-799.
136. Drese, J.H., S. Choi, R.P. Lively, W.J. Koros, D.J. Fauth, M.L. Gray, and C.W. Jones, *Synthesis-Structure-Property Relationships for Hyperbranched Aminosilica CO₂ Adsorbents*. Advanced Functional Materials, 2009. **19**(23): p. 3821-3832.
137. Chujo, Y. and T. Saegusa, *Organic Polymer Hybrids with Silica-Gel Formed by Means of the Sol-Gel Method*. Advances in Polymer Science, 1992. **100**: p. 11-29.
138. Chujo, Y., I. Tomita, and T. Saegusa, *Allylboration Polymerization .I. Synthesis of Boron-Containing Polymers by the Reaction between Triallylborane and Dicyano Compounds*. Macromolecules, 1992. **25**(11): p. 3005-3006.
139. Saegusa, T. and Y. Chujo, *Macromolecular Engineering on the Basis of the Polymerization of 2-Oxazolines*. Makromolekulare Chemie-Macromolekulare Symposia, 1991. **51**: p. 1-10.
140. Bilba, D., D. Bejan, and L. Tofan, *Chelating sorbents in inorganic chemical analysis*. Croatica Chemica Acta, 1998. **71**(1): p. 155-178.

141. Li, H., M. Eddaoudi, M. O'Keeffe, and O. Yaghi, *Design and synthesis of an exceptionally stable and highly porous metal-organic framework*. *Nature*, 1999. **402**(6759): p. 276-279.
142. Rouquerol, F., J. Rouquerol, and K. Sing, *Adsorption by Powders and Porous Solids*. . Academic Press: London 1999.
143. Lin, Y.S., K.J. Devries, H.W. Brinkman, and A.J. Burggraaf, *Oxygen semipermeable solid oxide membrane composites prepared by electrochemical vapor deposition*. *Journal of Membrane Science*. 1992. **66**(2-3): p. 211-226.
144. Spedding, P.L., *Densities and Molar Volumes of Molten Alkali Carbonate Binary Mixtures*. *Journal of the Electrochemical Society*, 1970. **117**(2): p. 177.
145. Ulibarri, M.A., I. Pavlovic, C. Barriga, M.C. Hermosin, and J. Cornejo, *Adsorption of anionic species on hydrotalcite-like compounds: effect of interlayer anion and crystallinity*. *Applied Clay Science*, 2001.
146. Vaccari, A. and M. Gazzano, *Hydrotalcite-type anionic clays as precursors of high-surface-area Ni/Mg/Al mixed oxides*. *Preparation of Catalysts Vi*, 1995. **91**: p. 893-902.
147. Pacchioni, G., J.M. Ricart, and F. Illas, *Ab-Initio Cluster Model-Calculations on the Chemisorption of CO₂ and SO₂ Probe Molecules on MgO and CaO (100)Surfaces - a Theoretical Measure of Oxide Basicity*. *Journal of the American Chemical Society*, 1994. **116**(22): p. 10152-10158.
148. Tutuianu, M., O.R. Inderwildi, W.G. Bessler, and J. Warnatz, *Competitive adsorption of NO, NO₂, CO₂, and H₂O on BaO(100): A quantum chemical study*. *Journal of Physical Chemistry B*, 2006. **110**(35): p. 17484-17492.
149. Gronbeck, H., *Mechanism for NO₂ charging on metal supported MgO*. *Journal of Physical Chemistry B*, 2006. **110**(24): p. 11977-11981.
150. Pacchioni, G., A.M. Ferrari, A.M. Marquez, and F. Illas, *Importance of Madelung potential in quantum chemical modeling of ionic surfaces*. *Journal of Computational Chemistry*, 1997. **18**(5): p. 617-628.
151. Yanagisawa, Y., K. Takaoka, and S. Yamabe, *Exchange of Strong Carbon-Dioxide O = C Bonds on an Mgo Surface*. *Journal of the Chemical Society-Faraday Transactions*, 1994. **90**(17): p. 2561-2566.
152. Trabelsi, M. and J.P. Coulomba, *Thermodynamic study of ethane thin films adsorbed on MgO(100) powder*. *Surface Science*, 1992. **272**(1-3): p. 352-357.
153. Lackner, K.S., C.H. Wendt, D.P. Butt, E.L. Joyce, and D.H. Sharp, *Carbon-Dioxide Disposal in Carbonate Minerals*. *Energy*, 1995. **20**(11): p. 1153-1170.
154. NETL, *Proceeding of workshop NETL mineral CO₂ sequestration*. 2001.
155. Lackner, K.S., *Carbonate chemistry for sequestering fossil carbon*. *Annual review of energy and the environment*, 2002. **27**: p. 193-232.
156. O'Connor, W.K., D.C. Dahlin, G.E. Rush, S.J. Gerdemann, and L.R. Penner, *Energy and Economic Considerations for Ex Situ Aqueous Mineral Carbonation*. . Proc. 29th International Technical Conference on Coal Utilization and Fuel Systems, Coal Technology Association, Clearwater, FL., 2004.
157. Gerdemann, S.J., D.C. Dahlin, W.K. O'Connor, L.R. Penner, and G.E. Rush, *Ex-Situ and In-Situ Mineral Carbonation as a Means to Sequester Carbon Dioxide*

- Conference: 21st Annual International Pittsburgh Coal Conference, Osaka, Japan, 2004.
158. *Diagram of carbonation for CO₂ sequestration*.
http://www.columbia.edu/~ap2622/research_carbon.html. Retrieved 2009-003-16
 159. O'Connor, W.K., D.C. Dahlin, D.N. Nilsen, R.P. Walters, and P.C. Turner, *Carbon dioxide sequestration by direct mineral carbonation with carbonic acid*, . Proceedings, 25th international technical conference on coal utilization and fuel systems, Clearwater, Florida, 2000.
 160. O'Connor, W.K., D.C. Dahlin, D.N. Nilsen, G.E. Rush, R.P. Walters, and P.C. Turner, *CO₂ storage in solid form: a study of direct mineral carbonation, 5th international conference on greenhouse gas technologies, Cairns, Australia*. 2000.
 161. O'Connor, W.K., D.C. Dahlin, P.C. Turner, and R. Walters, *Carbon dioxide sequestration by ex-situ mineral carbonation, Second Dixy Lee Memorial Symposium: Utilization of fossil fuel-generated carbon dioxide in agriculture and industry, Washington DC*. 1999.
 162. Newall, P.S., S.J. Clarke, H.M. Haywood, H. Scholes, N.R. Clarke, and P.A. King, *CO₂ storage as carbonate minerals*. IEA, Cheltenham, UK., 1999.
 163. Lackner, K.S., D.P. Butt, and C.H. Wendt, *Progress on binding CO₂ in mineral substrates*. Energy Conversion and Management, 1997. **38**: p. S259-S264.
 164. Kakizawa, M., A. Yamasaki, and Y. Yanagisawa, *A new CO₂ disposal process using artificial rock weathering of calcium silicate accelerated by acetic acid*. Energy, 2001. **26**: p. 341-354.
 165. Metz, B., O.R. Davidson, P.R. Bosch, R. Dave, and L.A. Meyer, *Contribution of Working Group III to the Fourth Assessment Report of the Intergovernmental Panel on Climate Change, 2007* Cambridge University Press, Cambridge, United Kingdom and New York, NY, USA, 2007.
 166. Rubin, E.S., *CO₂ capture and transport*. Elements, 2008. **4**: p. 311-317.
 167. Metz, B., O.R. Davidson, P.R. Bosch, R. Dave, and L.A. Meyer, *IPCC Special Report on Carbon Dioxide Capture and Storage. Working Group III to the Fourth Assessment Report of the Intergovernmental Panel on Climate Change*. Cambridge University Press, Cambridge, United Kingdom and New York, NY, USA, 2005.
 168. O'connor, W.K., C.L. Dahlin, G.E. Rush, S.J. Gerdemann, L.R. Penner, and D.N. Nilsen, *Aqueous mineral carbonation; mineral availability, pretreatment, reaction parametrics, and process studies*. Tech Rep. DOE/ARC-TR-04-002, Albany Research Center, 2004.
 169. Hanchen, M., V. Prigiobbe, G. Storti, T.M. Seward, and M. Mazzotti, *Dissolution kinetics of fosteritic olivine at 90-150 degrees C including effects of the presence of CO₂*. Geochimica Et Cosmochimica Acta, 2006. **70**(17): p. 4403-4416.
 170. Bearat, H., M.J. McKelvy, A.V.G. Chizmeshya, D. Gormley, R. Nunez, R.W. Carpenter, K. Squires, and G.H. Wolf, *Carbon sequestration via aqueous olivine mineral carbonation: Role of passivating layer formation*. Environmental Science & Technology, 2006. **40**(15): p. 4802-4808.
 171. Weissbart, E.J. and J.D. Rimstidt, *Wollastonite: Incongruent dissolution and leached layer formation*. Geochimica Et Cosmochimica Acta, 2000. **64**(23): p. 4007-4016.

172. Dean, J.A., *Lange's handbook of chemistry*. McGRAW-HILL INC., 1992. 14th edition.
173. Demirbas, A., *Carbon dioxide disposal via carbonation*. Energy Sources Part a-Recovery Utilization and Environmental Effects, 2007. **29**(1): p. 59-65.
174. Ward, S.M., J. Braslaw, and R.L. Gealer, *Carbon-Dioxide Sorption Studies on Magnesium-Oxide*. Thermochemica Acta, 1983. **64**(1-2): p. 107-114.
175. Kwon, S.C., M.H. Fan, H.F.M. DaCosta, A.G. Russell, and J. Mulholland, *Reaction kinetics for magnesium silicate carbonation in the presence of steam for carbon dioxide sequestration*. Submitted to Environmental Science & Technology, 2011.
176. DaCosta, H.F.M., M.H. Fan, and A.G. Russell, *Caterpillar pending patent, U.S. P.T.O.* 2009.
177. Demirbas, A., *Carbon dioxide disposal via carbonation*. . Energy Sources Part a-Recovery Utilization and Environmental Effects, 2007. **29**(1): p. 59-65.
178. Jensen, M.B., L.G.M. Pettersson, O. Swang, and U. Olsbye, *CO₂ sorption on MgO and CaO surfaces: A comparative quantum chemical cluster study*. Journal of Physical Chemistry B, 2005. **109**(35): p. 16774-16781.
179. Cazorlaamoros, D., J.P. Joly, A. Linaressolano, A. Marcillagomis, and C.S. Delecea, *CO₂-CaO Surface and Bulk Reactions - Thermodynamic and Kinetic Approach*. Journal of Physical Chemistry, 1991. **95**(17): p. 6611-6617.
180. Karlsen, E.J., M.A. Nygren, and L.G.M. Pettersson, *Comparative study on structures and energetics of NO_x, SO_x, and CO_x adsorption on alkaline-earth-metal oxides*. Journal of Physical Chemistry B, 2003. **107**(31): p. 7795-7802.
181. Plane, J.M.C. and R.J. Rollason, *Kinetic study of the reactions of CaO with H₂O, CO₂, O₂, and O₃: Implications for calcium chemistry in the mesosphere*. Journal of Physical Chemistry A, 2001. **105**(29): p. 7047-7056.
182. Nygren, M.A. and L.G.M. Pettersson, *Theoretical Modeling of Metal-Oxides - Influence of Field-Strength on Atomic Oxygen-Adsorption and a Simple-Model Reaction - O-Ads+CO-JCO₂*. Chemical Physics Letters, 1994. **230**(4-5): p. 456-462.
183. Koch, W. and M.C. Holthausen, *A Chemist's Guide to Density Functional Theory*. 2nd ed. 2001, Weinheim: Wiley-VCH.
184. Perdew, J.P., K. Burke, and M. Ernzerhof, *Local and gradient-corrected density functionals*. Chemical Applications of Density-Functional Theory, 1996. **629**: p. 453-462.
185. Perdew, J.P., K. Burke, and M. Ernzerhof, *Generalized gradient approximation made simple*. Physical Review Letters, 1996. **77**(18): p. 3865-3868.
186. Delley, B., *An all-electron numerical method for solving the local*. Journal of Chemical Physics, 1990. **92**(1): p. 508-517.
187. Waltenburg, H.N. and P.J. Moller, *Growth of ultrathin Cu films on CaO(100)*. Surface Science, 1999. **439**(1-3): p. 139-145.
188. Monkhorst, H.J. and J.D. Pack, *Special points for Brillouin-zone integrations*. Physical review B 1976. **13**(12): p. 5188-5192.
189. Kwon, S.C., M.H. Fan, H.F.M. DaCosta, and A.G. Russell, *Mineralization for CO₂ sequestration using olivine sorbent in the presence of water vapor*. In preparation to submit to Industrial & Engineering Chemistry Research, 2011.

VITA

Soonchul Kwon

Soonchul Kwon was born in Pusan, Korea in October 1976. He earned a Bachelor of Science degree in Civil Engineering from Pusan National University, Korea in 2003. He earned a Master of Science degree in Environmental Engineering in August 2005 from Iowa State University where he was introduced to air quality experiment. Soonchul earned another M.S. and finished his Ph. D. program in Civil and Environmental engineering at Georgia Institute of Technology in the research group of Professor Armistead (Ted) G. Russell. Soonchul has worked on the mineral carbonation for CO₂ sequestration. Soonchul married Myunghwa Jung in 2003 and they have two sons (Brandon Kwon and Bryan Kwon).